Organic sensitizers for application in photonic and photovoltaic devices

Svitlana Karamshuk

Submitted for the degree of

Doctor of Philosophy

List of abbreviations

HOMO Highest Occupied Molecular Orbital

LUMO Lowest Unoccupied Molecular Orbital

CB: Conduction Band

λ: Wavelength

J_{sc}: Short-circuit photocurrent

V_{oc}: Open-circuit voltage

FF: Fill Factor

IPCE: Incident Photon to Current Efficiency

LHE: Light Harvesting Efficiency

APCE: Absorbed Photon to Current Efficiency

P_{in}: Power of incident light

NIR: Near-Infrared

CV: Cyclic Voltammetry

EDWA: erbium-doped waveguide amplifier

ISC: intersystem crossing

ICT: Intramolecular Charge Transfer

OPO: optical parametric oscillator

PL: photoluminescence

NBS: *N*-Bromosuccinimide

NCS: *N*-Chlorosuccinimide

DME: dimethoxyethane

DCM: dichloromethne

EtOH: ethanol

Pd(dppf)Cl$_2$: 1,1'-Bis(diphenylphosphino)ferrocene palladium(II) dichloride

DMF: N-N-dimethylformamide

DMSO: dimethyl sulfoxide

Table of Content

1. Introduction

1.1.   Organic sensitizers for application in devices

Organic sensitizers have recently attracted much interest in the research community and industry as eco-friendly, reliable and efficient materials for photoelectric devices. Indeed, physical properties of organic electronics, unlike those of more traditional inorganic materials, are more diverse and easier to tune or upgrade simply because the variety of possible molecular structures for small organic molecules and polymers is substantially richer than that of their inorganic counterparts. This flexibility also leads to economic benefits as it can potentially reduce production cost of organic-based materials.[89-91]

Not surprisingly, the recent decade has seen a surge of research activity in understanding photoelectric, optical, magnetic and electrical properties of organic materials including organic semiconductors, superconductors and photoconductors, organic photoactive materials for solar cells, organic non-linear optical materials, organic ferromagnets, resist materials, liquid crystals, etc. Many of them have found industrial applications in field-effect transistors, optical data storage, display devices, sensors, plastic batteries, organic electroluminescent and other devices. However a truly remarkable impact of organic photo-electronics, and in particularly due to their strong response and interaction with charged particles (e.g., photons of light), has recently become apparent for the design of solar cells and optoelectronic devices.

In more details, photons of light emitted on a material trigger a transition to an excited state in organic compound which, depending on particularities of its life cycle and motion of the excited electron within the molecule, defines various photo-physical and electrochemical properties of the organic sensitizer. Electronic motion, in its turn, considerably depends on the π-electron delocalization in conjugated systems, which occurs due to an overlap of the p-type atomic orbitals of the carbon. This property gives an opportunity to regulate electronic motion in one, two or multiple directions, by changing the shape of molecule from linear to rod-shaped or flat. Moreover, thanks to their significant polarizability, organic materials possess nonlinear optical properties allowing multiphoton absorption and, thus, formation of bigger population of excited states, increased amount of charge carriers etc.

Last but not least, it is typical for electronic devices to use organic materials in the form of thin films. This fabrication approach, due to variability of film growing conditions (e.g., vacuum vapour deposition, solvent cast from solution, spin coating, electrochemical deposition, molecular monolayer self-assembly techniques), allows a wide range of organic compounds, not limited by solubility or sublimation temperature regimes, to be used in devices. Naturally, it gives organic materials another level of flexibility over conventional inorganic photo-electronics.

Coming from these inspiring observations, the current study is dedicated to the design and further application of new generation organic sensitizers for solar cells and electronics.

1.2. Dye sensitized photovoltaic cells

Following a prominent work of Grätzel and O'Reganin1991[4], dye-sensitized solar cells (DSSCs) were recognized as a relatively cheap and easy-to-scale approach to harness solar-to-electrical power conversion. Furthermore, their transparency, versatile design and wide colour palette have offered unique structural and architectural possibilities in the emerging field of building integration,[5,6] for example through the design of photovoltaic windows and façades.

The key design principle behind DSSCs lies in sensitization of a porous wide-band-gap semiconductor thin film with a photoactive dye which, following excitation, is able to transfer either electrons (n-type sensitization) or holes (p-type sensitization) to a semiconductor substrate.
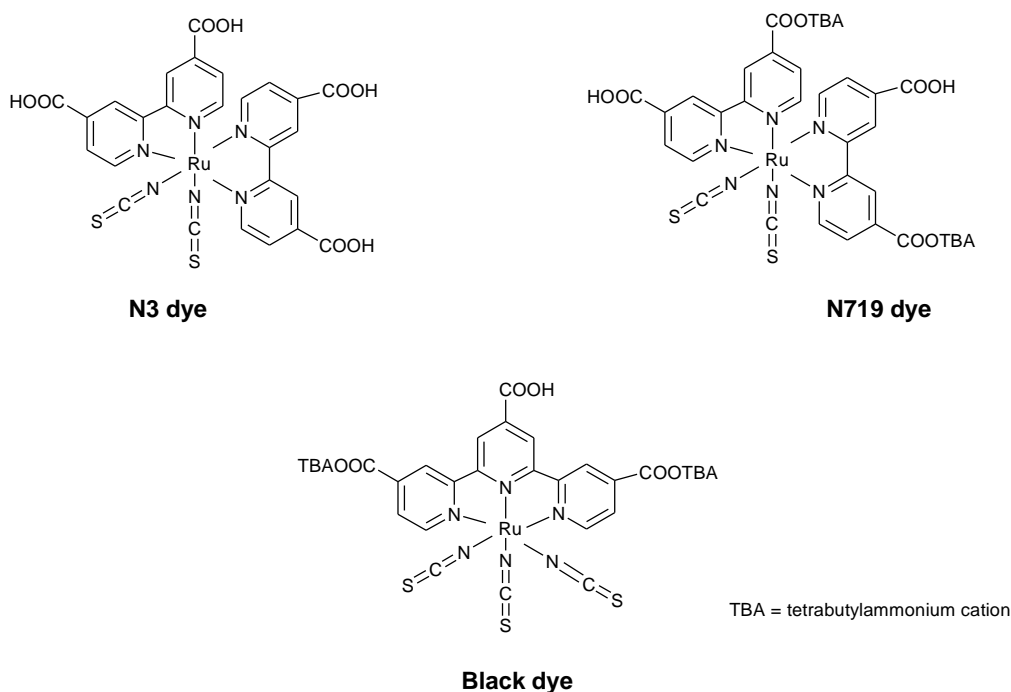
N3 dye

N719 dye

Black dye

TBA = tetrabutylammonium cation

Figure 1 Efficient Ru(III) complexes for n-type DSSCs.

n-Type DSSCs have been intensively investigated over the last two decades and have been reportedly reaching optimized power conversion efficiencies of up to 13% with a single photoactive junction (dye/n-TiO$_2$).[7] Organic sensitizers for n-Type devices significantly vary in structure and nature of separate units, but, can be in principle categorized into two main groups: metal based and metal-free compounds.

As far as organic metal-based sensitizers are concerned, the best result has been achieved with the complexes of ruthenium (Figure 1), whereas particularly high efficiency of corresponding devices was recorded in tandem with the I^-/I^{3-} redox couple.[8]

Fully organic sensitizers have been, on the other hand, appreciated by the research community due to their ability to easily tune the properties of the desired material through structural modification. Moreover, such compounds are easier to work with, less expensive and eco-friendly in comparison to their metal-based counterparts.[9] Coumarin,[10] indoline,[11] carbazole,[12] triphenylamine,[13,14] furan,[15] and thiophene and their derivatives, are some of the widely used building blocks for n-type dyes.

Nevertheless, and to a growing concern of the research community, power conversion efficiencies in n-type DSSCs have reportedly reached a plateau urging to look for new viable approaches to boost performance of DSSCs. One promising strategy to produce DSSCs with significantly enhanced power conversion efficiencies lies in connecting an n-type photoelectrode (n-dye/TiO$_2$) with a p-type photoelectrode(p-dye/NiO), therefore, achieving a tandem cell composed by two serially connected photoactive electrodes both contributing to the total photovoltage of a cell (Figure 2). This approach has a theoretical potential to achieve for up to 40% conversion efficiency in organic-based photovoltaic devices.[16]
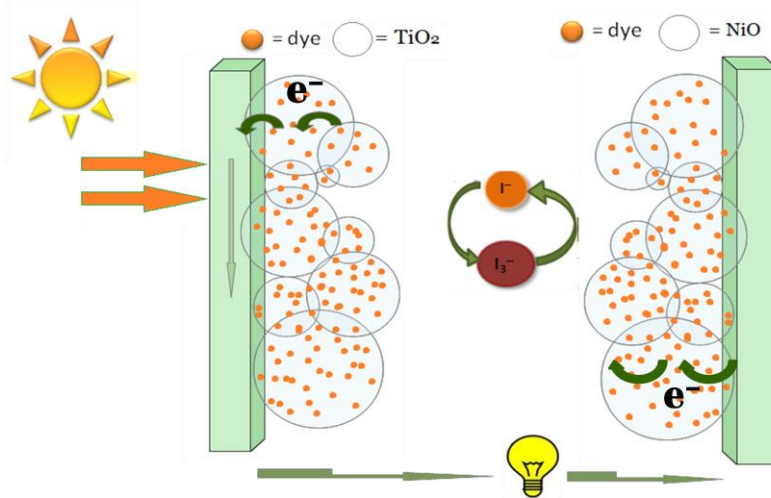

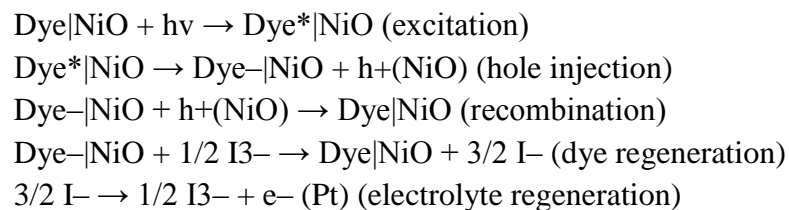**Figure 2.** Working principal of the tandem DSSC

The basic physical principle behind p-type DSSCs can be described as follows:

Dye|NiO + hv → Dye*|NiO (excitation)
Dye*|NiO → Dye–|NiO + h+(NiO) (hole injection)
Dye–|NiO + h+(NiO) → Dye|NiO (recombination)
Dye–|NiO + 1/2 I3– → Dye|NiO + 3/2 I– (dye regeneration)
3/2 I– → 1/2 I3– + e– (Pt) (electrolyte regeneration)

In more details, after absorption of the visible light by a p-type sensitizer, a hole injects from the excited organic molecule to the valence band of the semiconductor. The dye is then regenerated by electrolyte species (I^{3-}). By-process could take place in case if the reduced dye doesn't react with the electrolyte within the charge-separated lifetime. Then it recombines with the hole in NiO, or otherwise the hole moves from the semiconductor to the working electrode and the I^- species in the electrolyte diffuses to the Pt electrode. This charge collection gives rise to a cathodic photocurrent in the external circuit.

p-Type sensitized systems have been, so far, significantly less investigated and lower photocurrents, compared to their n-type counterparts, have been reported.[17] One of the main limitations in p-type systems, commonly based on NiO as a hole semiconductor,[18] arises from the fast charge recombination[19] between the photoinjected hole in NiO and the reduced dye. It can be explained by strong influences of the incorporated interfaces (like NiO-dye in our case), which change a lot the performance and characteristic parameters of the whole organic cell DSSCs.[20] If we assume that the interface of the p-type dye absorbed on the NiO semiconductor is described the same as of the n-type sensitizer on the TiO2 surface,[21-23] then the kinetics of charge recombination significantly relies on the distance between the semiconductor surface and the LUMO of the chemisorbed dye. Therefore, an efficient p-type chromophore should posses an electron poor moiety with a relatively exclusive contribution to the LUMO. Also electron acceptor must be located on the opposite end from the molecular fragment with an anchoring group. There are several claims also to the connecting linker between the donor and acceptor part of the molecule as it should be long and rigid, in order to maximize the distance between the generated hole and electron charges.

Clearly, there is still a number of open questions in the-state-of-the-art of organic p-type materials and, in particular, synthesis of new p-type chromophores with a long-lived charge separated state and minimized back recombination remains an interesting challenge.

1.3 Organic emitters for optical amplifiers

Optical amplifiers, as the name suggests, are electronic devices designed to amplify the power of light signal. Optical amplifiers are a crucial component of fiber-optic telecommunication networks which allow them to spread over hundred thousand kilometres across the globe and inter-connect all continents except Antarctica. In principle, optical amplifiers could be divided into several main groups according to the physical mechanisms which they operate on. The most commonly used amplifiers, and particularly as far as telecommunications industry is concerned, are semiconductor optical amplifiers (SOAs), Raman amplifiers and doped fibre laser amplifiers (DFAs).

SOAs are providing the gain of the signal by electron-hole recombination using a semoconductor,[24] usually based on III-V inorganic compound device such as GaAs/AlGaAs, InP/InGaAs, InP/InGaAsP and InP/InAlGaAs. This type of amplifiers are operating at 0.85 µm and 1.6 µm wavelengths performing the signal gain of around 20-25 dB. Slightly higher performance shows Raman and doped fibre amplifiers, though both of them need a high power pump laser to generate a signal gain in contradistinction from semiconductor devices. Raman amplification, though, requires around 500 mW more to achieve desired level of gain then the DFA amplifiers.[25] Taking into account fabrication peculiarities of these amplifying systems together with the possible rate of gain, doped fibre lasers turn out to be the most attractive technology for telecommunication networks.

DFAs are using optical fibers doped with ions, which are amplifying the signal passed through, as a gain medium (Figure 3). Lanthanides are currently the most typically used doping materials since they provide lower lost of the signal comparing to other types of doping compounds.[26-27]
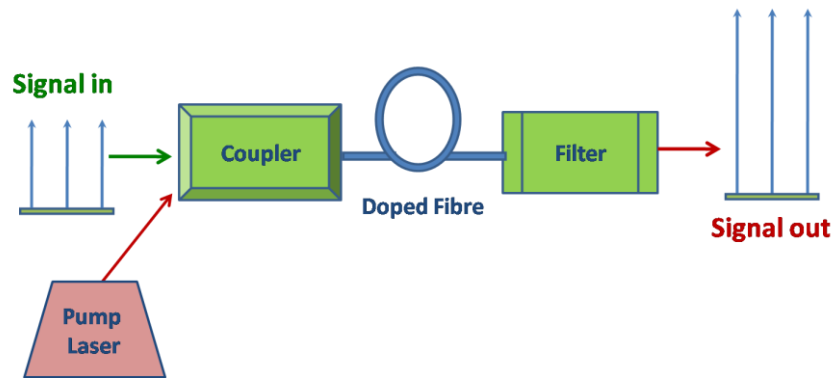

Figure 3. DFA working set up

Erbium has enjoyed much more attention as a doping compound than other lanthanides, because erbium doped waveguide amplifiers (EDWA) give signal gain at a wavelength of around 1550 nm perfectly suitable for telecommunication networks. While amplification in EDWA is achieved by laser stimulated emission of photons from Er (III), erbium still requires powerful pumping over comparably short distances and excitation at narrow wavelengths, therefore, complicating the setup and increasing the overall cost of the fiber-optic communication system.

As a promising alternative, systems of erbium together with organic chromophores have much more intense and broader absorption than lanthanide ions, therefore, suggesting a possibility for improving the pumping efficiency and broadening the range of light sources used for pumping.

Organic species are pumping Er(III) ions when the so-called "stimulated emission" happens. The physics of this process can be described with a Jablonski diagram (Figure 4).[28-30]
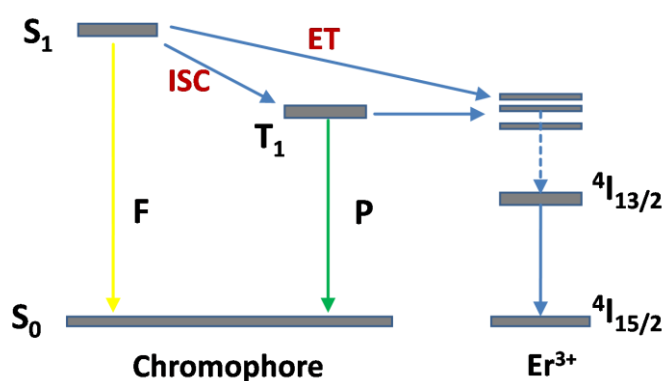
Figure 4 Jablonski diagram of Er^{3+} sensitazation with organic chromophore.

Because transitions between the states with equal total spin quantum number are forbidden, transition from the triplet state T_1 to S_0 is not allowed, in contrast to transition from the excited singlet state S_1 to the ground state S_0. Taking in account that only ¼ of the formed excited stated are singlets, in a typical situation only 25% of quantum efficiency can be achieved. However, due to various atomic structures and heaviness of the atoms in the organic molecule, the spin-orbit coupling and mixing of the singlet and the triplet state wave functions gives an opportunity for the triplet to relax in S_0 state. Thus, the overall quantum efficiency ideally can reach 100%.

In case of the organic chromophore-lanthanide ion system, it is energetically preferable for the excited triplets to populate the upper levels of the lanthanide ion via resonance energy transfer (RET).[31] Such transfer occurs following Dexter[32] or Förster[33] mechanisms and then the lanthanide ion may follow non-radiative or radiative deexcitation mechanisms. However, lanthanides in organic hosts have usually shorter emission lifetimes than in inorganic materials. It takes place due to the drastic quenching commonly assigned to the electric dipole-dipole interactions between lanthanides and the high-energy oscillators in the organics like O–H and C–H bonds.

Photoluminescence of erbium (III) ions is explained by the $^4I_{13/2} \rightarrow {}^4I_{15/2}$ transition, and since energy gap between $^4I_{13/2}$ and the ground state is small, the excited state is more likely to be quenched by the high energy O–H, N–H or C–H vibrations so typical for all organic materials and solvents. The emission decay time in this case decrease drastically from the value $\tau \approx 8$ ms in the isolated ion to values in the range of 1-2 μs in typical lanthanide complexes. Elimination of O–H and C–H oscillators will increase the non-radiative rates of the lanthanide excited states. Moreover, substitution of the C–H bonds with C–F bonds should considerably increase the overall triplet lifetime.[34] As it is shown on the Figure 5, only the 5th order of C-F bond vibrational frequencies could partially match the needed $^4I_{13/2} \rightarrow {}^4I_{15/2}$ of Er(III) making the influence of such bond on the Er(III) photoluminescence negligible.
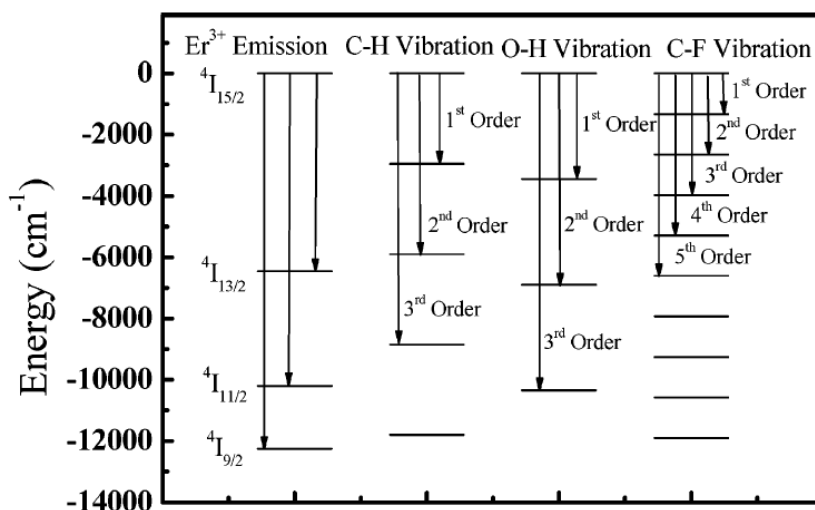
Figure 5 Energy levels of the vibrational modes.

1.4 Outline of the thesis

The aim of the current thesis is to perform a study of the novel photo and electro-active organic materials starting from the design of their molecular structure to fabrication of the corresponding materials.

We focus on the two most promising applications for organic sensitizers, namely, p-type sensitizers for dye synthesised solar cells (Chapter 2) and fully fluorinated organic materials for telecommunications networks (Chapter 3). For both studies, we provide a thorough justification of the design decisions with respect to the state-of-the-art in the field (Section 2.1-2.2 and Section 3.1-3.2) and develop synthetic approaches towards designed materials (Section 2.3 and Section 3.3). Finally, we provide a thorough characterization of photophysical and electrochemical properties of the obtained compounds (Section 2.4-2.7 and Section 3.4-3.8).

2 p-Type organic sensitizers

2.1 Introduction

Several families of dyes have been proposed in the recent literature for application in p-type DSSCs. Those based on coumarin and porphyrin scaffolds showed incident monochromatic photon-to-current conversion efficiencies (IPCE) of only up to 1.5% and overall efficiencies lower than 0.1%.[35-37]

A peryleneimide dye (**PI**) and the corresponding covalently linked peryleneimide-naphthalenediimide dyad (**NDI-PI**) were introduced in 2008 by the group of A. Hagfeld(Figure 6).[38]The latter (i.e., NDI-PI)showed much higher IPCE of 4% with respect to 1.3% of the former (i.e., PI) that can be explained by the presence of the long-lived charge-separated stat in NDI-PI and, therefore, lower charge recombination between the hole and the reduced dye.
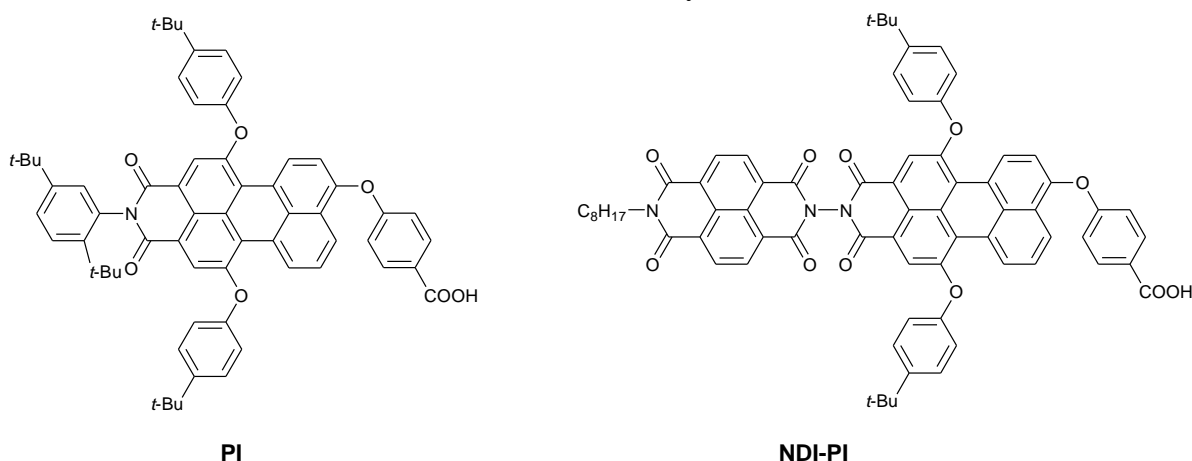

PI   **NDI-PI**

Figure 6 P-type dyes based on peryleneimide moiety.

Bach et al. in 2010 suggested an alternative approach for designing p-type dyes using triphenylamine as the donor, perylenemonoimide as the acceptor, and oligothiophene as the conjugated chain (Figure 7).[39]The resulting p-type cell was fabricated using a commercially available NiO nanopowder, which has been applied to produce NiO film. This approach allowed to design a device with Voc of 0.218 V and a Jsc of 5.35 mA cm^{-2} and the total η of 0.41% - the best efficiency recorded for a p-type DSSC. It is worth noting, that the tandem cell of the photoactive p-type cathode, n-type anode made of N719 dye andTiO$_2$ semiconductor featured an improvement for up to η = 2.42%, but still couldn't surpass the n-type N719|TiO$_2$ based solar cell with efficiency of η = 5.9%.
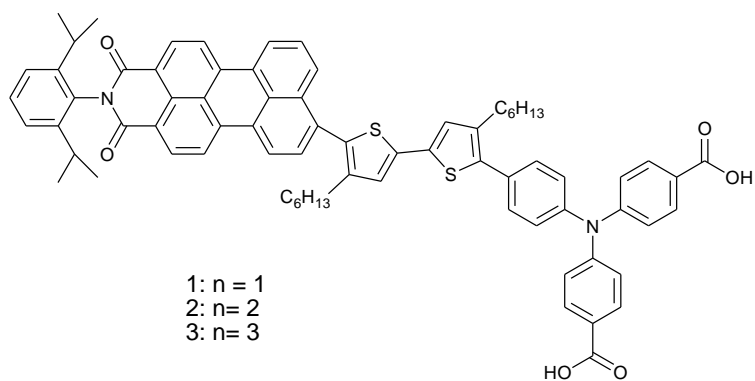
Figure 7. Molecular structure of dyes developed by Bach et al.

A remarkable example of an improved charge separation through the design of a dye is a push-pull systems based on a D-π-A (donor-π-spacer-acceptor) structures(Figure 8), such as P1introduced in 2008 by Sun et al.[40] This prototypical p-type dye had a carboxylic anchoring group on the triphenylamine donor part bridged to dicyanovinyl acceptor by thiophene acting as a π-linker.
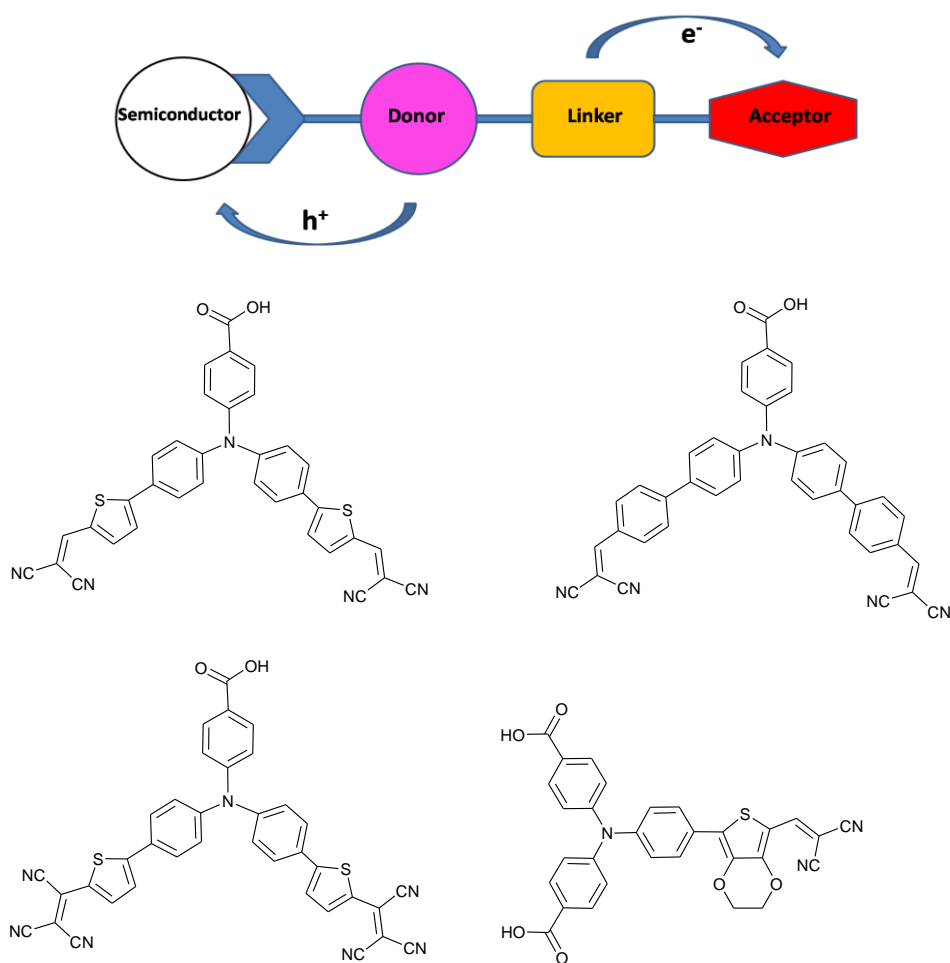

Figure 8D-π-A series of dyes.

The di-branched architecture, constituted by one donor and two π-spacer and acceptor units, follows a design approach common for recent n-type DSSC sensitizers.[41-43] Naturally, more complex compounds based on much more elaborated triphenylamine/oligothiophene dyes, but, sharing the same design principle has been recentlyproposed[44-45], whereas the best result has been achieved by the dyes based on the triphenyl amine donor groups connected via π-linkers to the acceptor groups.

Despite all recent advances, the power conversion efficiencies obtained by p-type sensitizers typically remains one order of magnitude lower than then the average efficiency delivered by n-type devices.

In this study we aim to explore new different structures for potentially efficient chromophores in p-type devices by considering that the intramolecular charge transfer, which constitutes the basis of efficient charge separation in donor-acceptor dyes, is strongly dependent on the electron-withdrawing ability of the acceptor and the length and tunnelling abilities of the π-spacer. To this end, we have designed and investigated new p-type dyes where P1-like structures have been optimized by inserting stronger and more efficient electron-acceptor groups compared to the conventional dicyanovinyl moiety.

2.2 Aim of the study

Taking in account all above-mentioned drawbacks of the state-of-the-art p-type dyes, in this study we focus on the design of new molecules which would consist of a) an efficient donating core directly connected to the semiconductor via the anchoring group; b) strong acceptor and a linker which could be easily incorporated in the resulting organic frame and c) would guarantee easy flow of electrons and holes through the dye volume (Figure 10).

Firstly, we chose a triphenylamine core (known as a highly efficient donor unit) which could be easily modified using common synthetic techniques and is economically affordable. [46-48]
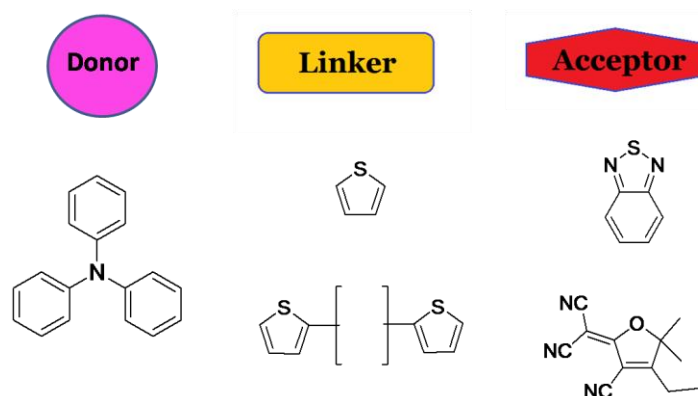

Figure 10 Building blocks for the designed p-type dyes.

After considering a wide range of currently used and industrially available π-spacers we decided for a thiophen group because it gives a lot of flexibility in the way it can be introduced into organic moiety but also in choosing a proper position for the group without causing additional synthetic obstructions. Particularly, a thiophene unit allowed us to study the influence of the position of a spacer group on charge separation which was one of the main goals behind this study.

Further, and taking in account strong donation abilities of the triphenylamine, the dye needs a stronger acceptorin order to reach sufficient charge separation. Therefore, the choice was made in favour of the strongest among currently known acceptors, namely, Dalton acceptor, and benzothiodiazole unit.
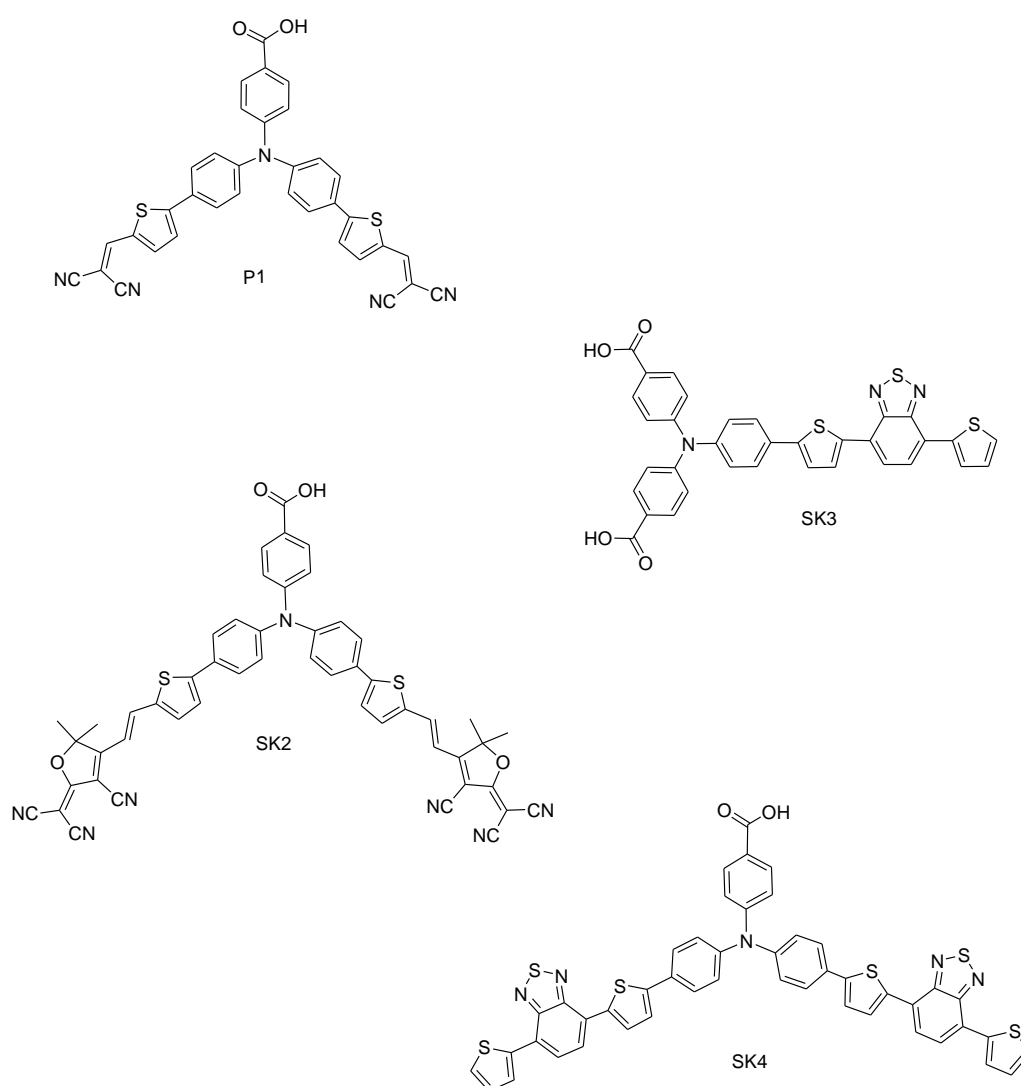

Figure 11 Designed SK series of dyes.

Different combinations of these units (Figure 11) should hypothetically give us an adequate picture on the chemical and physical properties of potentially promising materials for p-type dye sensitized solar cells.

2.3 Synthesis

Firstly, we have designed the SK2 dye, where the dicyanovinyl group of P1 has been replaced by the much stronger 3-cyano-2-(dicyanomethylene)-4,5,5-trimethyl-2,5-dihydrofuran (Dalton's acceptor) group, widely used in other materials science fields (Scheme 1).[49]
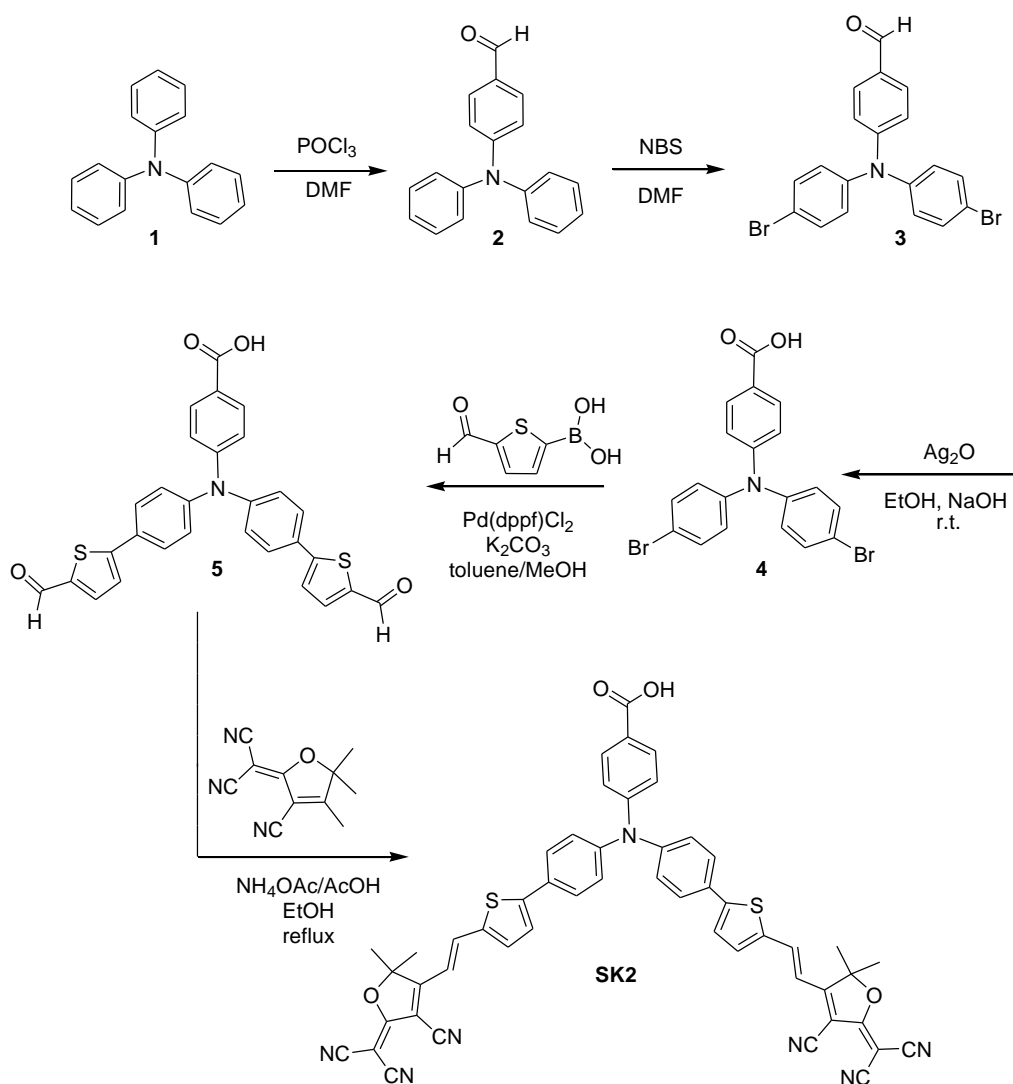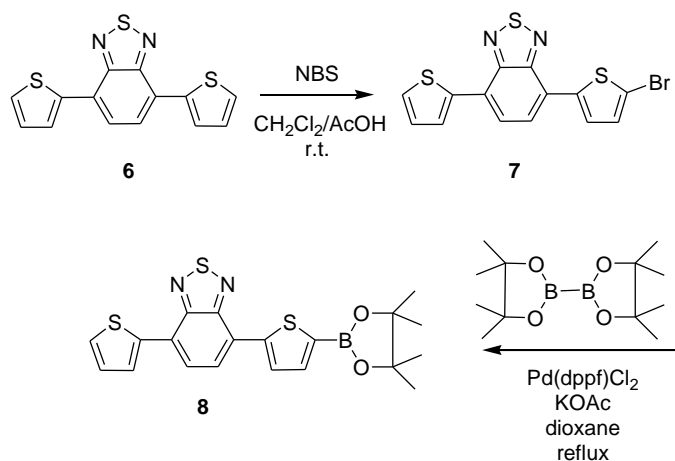

Scheme 1 Synthetic approach towards SK2 dye

Triphenylamine (**1**) was put in the conditions of Vilsmeier reaction to introduce an aldehyde group followed by bromination of the intermediate (**2**) with NBS in DMF

media. Obtained 4-[bis-(4-bromophenyl)amino]benzaldehyde (**3**) was oxidized to the corresponding benzoic acid (**4**) by standard silver mirror reaction and then submitted to the Suzuki coupling with 5-formyl-2-thienylboronic acid for introducing the two thienyl linkers. Knoevenagel reaction between the resulting bis-aldehyde (**5**) and 2-(3-cyano-4,5,5-trimethylfuran-2(5*H*)-ylidene)malononitrile afforded the desired chromophore SK2. It should be noted that the Knoevenagel condensation of (**5**) could be successfully accomplished only in acidic conditions at relatively high temperatures (>75 °C), while the reaction under conventional basic conditions (piperidine/EtOH) did not afford the condensation product, likely for the presence of the terminal COOH substituent on the donor core. Secondly, mono- and di-branched dyes (SK3 and SK4) characterized by a D- π-A- π architecture were realized. In the latter dyes, an additional benzothiadiazole-based acceptor-spacer unit was introduced both in linear (SK3) and branched (SK4) geometrical motifs for the manifold purpose of increasing the transition dipole moment, improving the spatial separation between hole and electron, and favouring the electron transfer to the electron mediator (I^-/I_3^-), resulting in improved interfacial charge separation.

Preparation of SK3 and SK4 started from bromination of 4,7-di(thiophen-2-yl)benzo[c][1,2,5]thiadiazole (**6**) to the mono-bromide (**7**) using *N*-bromosuccinimide (NBS) in presence of a 1:1 solution of CH_2Cl_2 and acetic acid.[50] Since such reaction gave mono- and di-substituted products possessing close polarities, the separation of these two compounds by column chromatography had to be performed with care in order to afford the mono-derivative in moderate yields. Borination of (**7**) with bis(pinacolato)diboron resulted in the key intermediate boronic ester (**8**) (Scheme 2).

Scheme 2 Synthetic approach towards boronic acid **8.**

Since presence of carboxylic group causes considerable difficulties during the essential purification of the crude product obtained after Suzuki condensation, of intermediate (**8**) was carried with previously obtained aldehyde (**3**). In order to obtain a bisaldehyde triphenylamine derivative the Vilsmeier reaction was carried on (**1**) under moderated conditions using 3 equivalents of $POCl_3$ and continuous reflux for 5 hours. Resulting product (**2**) was brominated without purification following the same

procedure used for (**3**) giving desired intermediate (**11).**
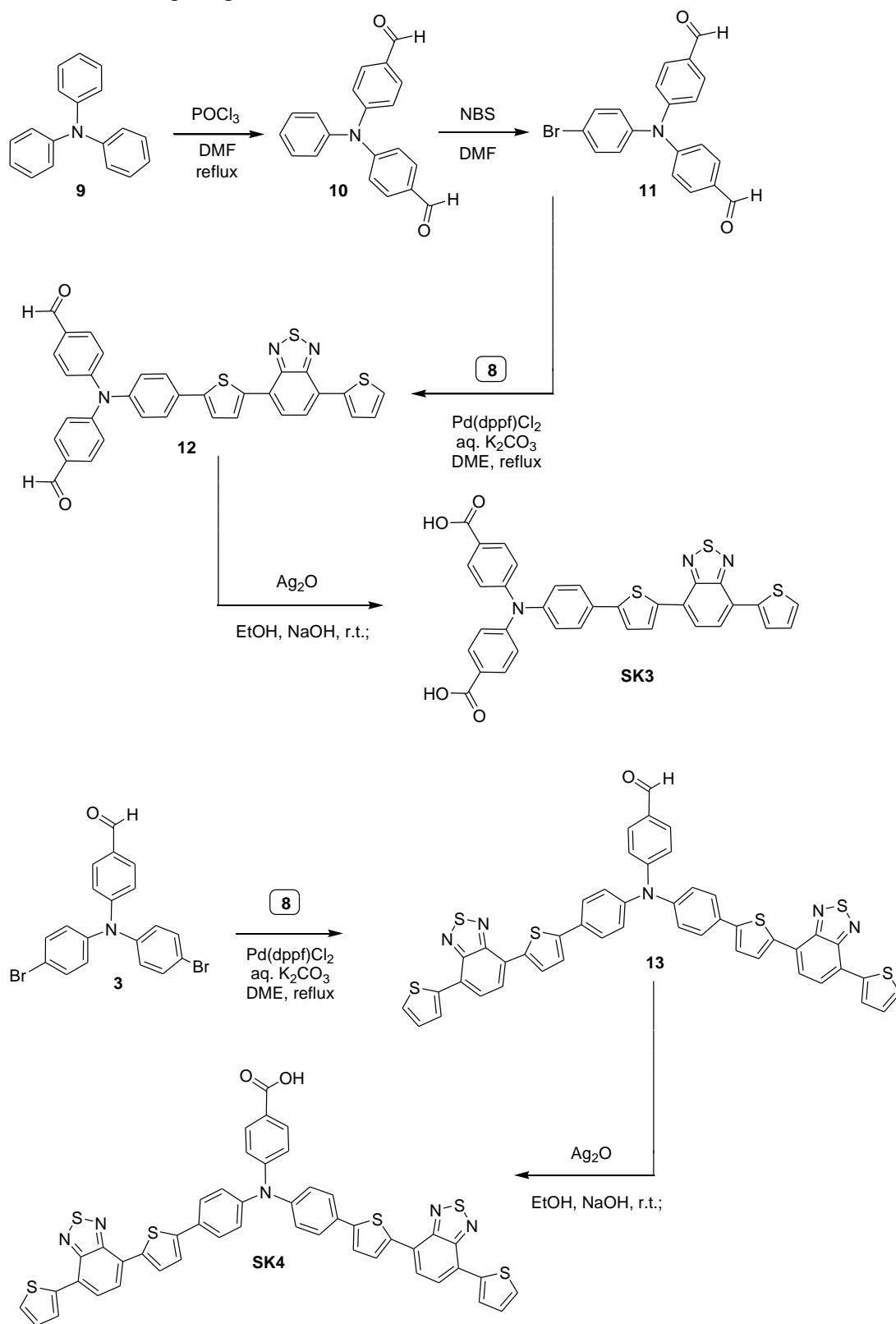
Scheme 3 Synthesis of SK3 and SK4 dyes.

Different reaction conditions (solvent, base, temperature) were investigated for the coupling of boronic ester (**8**) and triphenylamine derivatives (**3**) and (**11**). The best choice in both cases appears to be dimethoxyethane (DME) as a solvent and aqueous solution of K_2CO_3 as a base. Under these conditions the coupling reaction started immediately after mixing up the reagents and within a considerably short time afforded the desired targets (**12**) and (**13**) with fairly good yields.

SK3 and SK4 were then obtained by following the previously described procedure for silver mirror reaction (Scheme 3).

2.4. Characterization procedures, parameters and instruments

Structural characterization

The compounds synthesized in this thesis were characterized by 1H NMR, 13C NMR, IR spectroscopy and elemental analysis. NMR spectra were recorded with an instrument operating at 500.13 (^{1}H) and 125.77 MHz (^{13}C).

Optical characterization

Optical parameters (absorbance (*A*) of the sensitizer at corresponding wavelength (λ)of the light and e) of the dyes were measured using the absorption spectroscopy for both solution of the compound in the organic solvent and absorbed on the NiO film.

UV-Vis spectra of sensitized NiO thin films, collected in transmission mode, were recorded on a JASCO V570 UV-Vis-NIR spectrophotometer. UV-Vis spectra in solution were obtained with a V-570 JASCO spectrophotometer.

The molar extinction coefficient (ε) is particularly useful when comparing spectra of different compounds and determining the relative strength of light absorbing functions. ε is defined as equation:

$$\varepsilon = \frac{A}{c \times l} ,$$

where *A* is the absorbance, *c* is the sample concentration (mol L–1), and *l* is the length of light path through the sample (cm).

Emission spectra of light from the singlet excited state by a investigated dye that has absorbed light were recorded FP6200JASCO spectrofluorometer. TBAlClO$_4$ 0.1 DMSO. From the intersection of the normalized absorption and emission spectra, the 0–0 transition energy (*E*0–0) of the dye was calculated.

Electrochemical characterization

Electrochemical properties of the investigated dyes were studied using cyclic voltammetry (CV) potentiodynamic measurement. For this purpose sensitizers were dissolved in 0.1 M solution of tetrabutylammonium perchlorate (Fluka, electrochemical grade,99.0%) in anhydrous DMSO (Aldrich) as the supporting electrolyte and measurement was carried out at a glassy carbon working electrode

with a PARSTA2273 potentiostat in a two-chamber three-electrodeelectrochemical cell with a scan rate of 50 mVs^{-1}. Potentials are referred to the ferrocenium/ferrocene (Fc$^+$/Fc) couple as internal reference. The data were then plotted as current versus voltage.

Photovoltaic parameters characterizing the performance of p-type DSSCs

The main photovoltaic characteristics of DSSCs include the following parameters: open-circuit voltage (*V*oc), short-circuit photocurrent density (J_{sc}), fill factor (ff), incident photon to current efficiency (IPCE), light harvest efficiency (LHE) and the overall conversion efficiency (η).

An Ecochemie PGSTAT 302/N electrochemical workstation equipped with the FRA 2 Frequency Response Analyzer and running under either GPES or Nova software was used for collecting both the JV characteristics of the p-DSSCs. Solar cells were illuminated under simulated solar conditions (Am 1.5 G 100 mW/cm^2) generated by an ABET sun simulator. JV curves were recorded by linear scan voltammetry, using a scan rate of 5 mV/s. Every cell was left to equilibrate under illumination until a superimposable JV response was obtained upon subsequent scans. Curves reported in this work are those measured after steady state was achieved.

The measurement of a *J–V* curve was effectively used way for evaluation of the photovoltaic performance of a DSSC giving an opportunity to calculate the following parameters: *V*oc, *J*sc, ff and η (Figure 12).
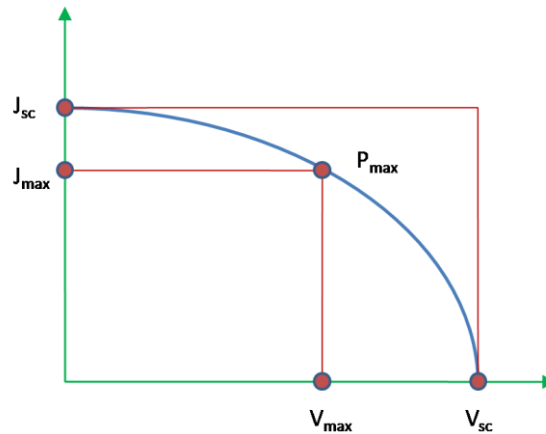

Figure 12. Current–voltage characteristics of DSSCs.

The *V*oc of a p-type DSSC corresponds to the difference between the *quasi*-Fermi level of the semiconductor and the redox potential of the electrolyte. In case of a p-type system, the *quasi*-Fermi level of a sensitizer should be situated close to the valence band of a semiconductor and also in the vicinity of the band gap.

*J*sc is the photocurrent per unit area under short-circuit condition. It is related to the optical properties of the dye and strongly depends on the dynamic processes in the cell.

The ff of a solar cell is in conjunction with V_{oc} and I_{sc}, determines the maximum power from a solar cell. The FF is defined as the ratio of the maximum power from the solar cell to the product of V_{oc} and I_{sc}.

Evaluation of the previously discussed photovoltaic parameters gives a way to calculate overall η of a solar cell as the ratio of the maximum output electrical power to the energy of incident sunlight (Is).

$$ff = \frac{Jmax \times Vmax}{Jsc \times Voc}$$

$$\eta = \frac{Jsc \times Voc \times ff}{Is}$$

The IPCE value corresponds to the photocurrent density produced in the external circuit under monochromatic illumination of the cell divided by the photon flux that strikes the cell. It is obtained by equation 2:

$$IPCE\,(\lambda) = \frac{1240 \times Jsc\,(\lambda)}{Pin\,(\lambda)} \times 100$$

Jsc (λ) is the short-circuit photocurrent density generated by the monochromatic light, λ and I are the wavelength and intensity of the monochromatic light.

The absorbed photon-to-current conversion efficiency (APCE) can be estimated from the ratio of IPCE and LHE. It is a better measure of the intrinsic light conversion efficiency.

$$APCE\,(\lambda) = IPCE\,(\lambda)\,LHE\,(\lambda)$$

Solar Cell Assembly.

NiO films were prepared by grounding 7.5 g of NiO nanoparticles (Inframat, nominal size 25 nm) in a mortar in the presence of 200 ìl of acetilacetone. 100 ml of terpineol were then added, followed by 10 g of ethlycellulose dissolved in 110 ml of absolute ethanol. The resulting mixture was homogenized by stirring and sonication in an ultrasonic bath. Ethanol was evaporated under reduced pressure leaving a dense paste constituted by terpineol, ethilcellulose and NiO nanoparticles. The resulting paste could be spread by blading onto well cleaned FTO glass to form, after drying and high temperature sintering, the NiO thin films. The temperature program adopted for drying and sintering in air was the following: 10 minutes at 120 °C, followed by a ramp (15 C°/min) to 450 C° which were maintained for 30 minutes. A subsequent ramp (10 C°/min) brought the temperature from 450 C° to 550 C° which were kept constant for further 20 minutes. Cooling occurred naturally, by interrupting the heating.

Sensitization of the resulting NiO electrodes, having an active surface of 0.25 cm^2, was carried out overnight, by immersion in the DMSO solutions of the selected sensitizers.

Solar cells were fabricated by clamping the sensitized NiO photocathode with a platinum coated FTO counter electrode (Chimet). The electrolyte was 1 M LiI/0.1 M I_2 in acetonitrile.

2.5. Optical and electrochemical characterization

The absorption spectra of SK2, SK3 and SK4 in DMSO are depicted in the Figure 13 together with that of the reference dye P1.All dyes under investigations exhibited similar general spectral features, summarized by two intense ($\varepsilon > 3 \times 10^4$ $M^{-1}cm^{-1}$) relatively broad absorption bands extending the light harvesting up to 700 nm in the case of SK2, where the presence of an efficient intramolecular charge transfer to the strong electron-withdrawing groups resulted in a significant bathochromic shift (ca. 70 nm) of the visible absorption maximum.
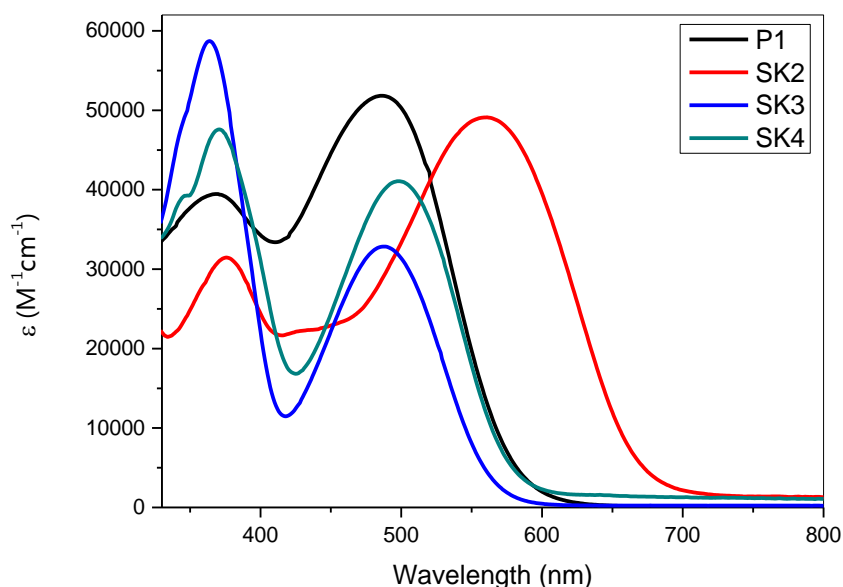

Figure 13. Absorption spectra of P1, SK2, SK3 and SK4 in DMSO.

SK3, SK4, and P1 are ca. 100 nm blue-shifted with respect to SK2, showing a visible absorption maximum at 480-490 nm and an absorption onset at ca. 600 nm. In all cases the second band is located in the UV region, with an absorption peak in the interval 350-370 nm, where SK3 and his di-branched analogue SK4, incorporating the same donor-acceptor side arm, showed the sharpest and most intense band. The main optical and electrochemical parameters together with HOMO/LUMO energies estimated by cyclic voltammetry in 0.1 M TBAClO$_4$ in DMSO are collected in Table 1.

Table 1.Optical and electrochemical parameters of the dyes.[a]

Dye	λ_{abs}(nm) (ε)(10^4 M^{-1}cm^{-1})	λem (nm)	E^{00}(eV)[b]	$E_{(HOMO)}$vs NHE(V) (vs vacuum) (eV)[c]	$E_{(LUMO)}$vs NHE (V) (vs vacuum) (eV)[d]
P1	372 (3.97) 489 (5.17)	611	1.91	1.16(-5.8)	-0.75(-3.8)
SK2	373 (3.12) 559 (4.90)	674	1.94	1.19(-5.8)	-0.75(-3.8)
SK3	357 (5.87) 488 (3.28)	609	2.43	1.14(-5.7)	-1.11(-3.3)
SK4	365 (4.76) 498 (4.11)	621	2.18	1.13(-5.7)	-1.05(-3.5)

[a] in DMSO. [b] Calculated from the intercept of the normalized absorption and emission spectra of the dyes. [c] Evaluated from the oxidation peak potential from cyclic voltammetry in the presence of ferrocene as an internal reference ($E_{1/2}$ Fc$^+$/Fc = 0.68 V vs NHE[51]and using a potential value of -4.6eVfor NHE vs. vacuum [d][52] Obtained from $E^{00} - E_{HOMO.}$[53]

As often observed with organic D-π-A dyes,[54-55] the electrochemical behaviour (Figure 14) of the series under investigation is dominated by irreversible processes which complicate a rigorous thermodynamic evaluation of the redox levels relevant to NiO sensitization. At anodic potentials, all chromophores presented a similar oxidation behaviour resulting in an irreversible wave having a peak potential at ca. 0.5 V vs Fc$^{+/0}$ which is related to the oxidation of the electron-rich TPA group.[56]
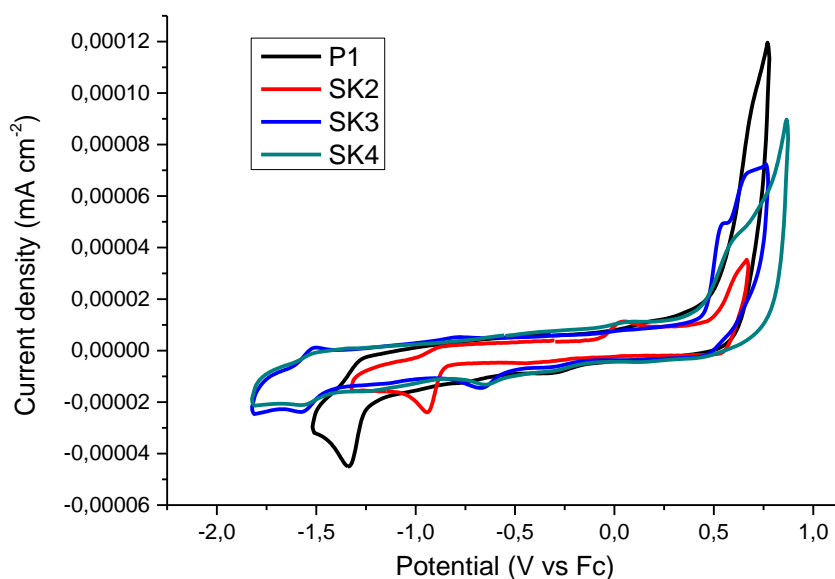

Figure 14. Cyclic voltammetry (vs. Fc) of P1, SK2, SK3 and SK4 in 0.1 M solution

19

of tetrabutylammonium perchlorate in anhydrous DMSO with a scan rate of 50 mVs^{-1}.

The reductive behaviour is generally more complex and not well defined, showing multiple weak irreversible waves probably originated by electrochemical-chemical processes. Therefore we preferred to estimate the LUMO energy by subtracting the HOMO energy from the spectroscopic energy gap (E^{00}) (Figure 15).[57] In agreement with the structural similarity of their acceptor group, SK3 and SK4 showed close LUMO energies at -3.3 and -3.5 eV correspondingly. This estimate is in reasonable agreement with the quasi-reversible wave observed at -1.55 V vs Fc$^{+/0}$. The reduction of SK2 dye, bearing a stronger acceptor group, is comparatively more anodically shifted with a lower energy LUMO at -3.8eV.
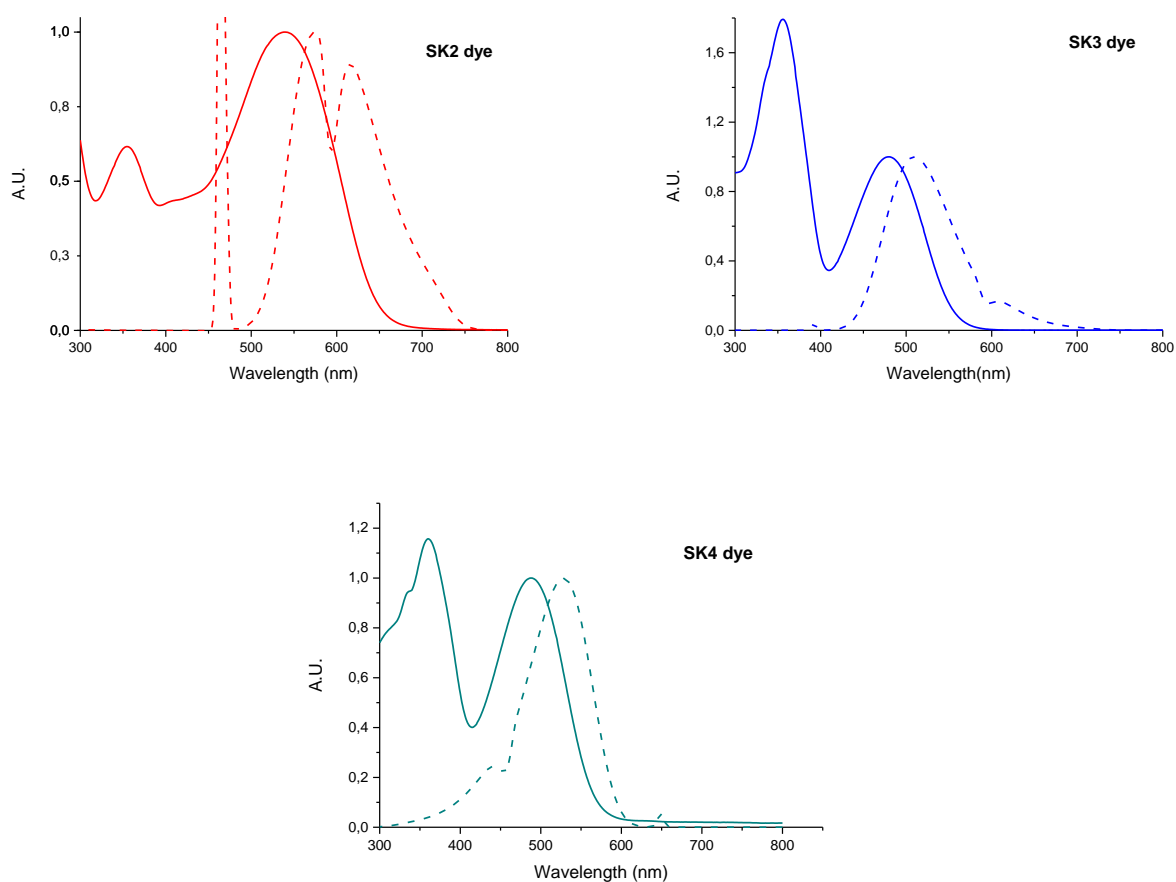

Figure 15. Evaluation of the spectroscopic energy gap E^{00}.

Thus, no thermodynamic limitation to hole transfer to NiO are expected: in all cases the HOMO energies are similar to the P1 dye and sufficiently lower than the upper valence band edge of NiO, located at $0.5 - 0.6$ V vs NHE.[58-59] Electron transfer to I_3^-, relevant to dye regeneration, is significantly exoergic, with ΔG^0 values > 1.2 eV, allowing to predict fast kinetics.

2.6 Computational characterization

To gain insights into the electronic and optical properties of the investigated sensitizers, we performed Density Functional Theory (DFT) calculations. All the calculations have been performed using the GAUSSIAN 09 program package.[60] The dye structures at the ground state were optimized at the B3LYP level employing the 6-31G* basis set, starting from a semi empirical PM3 pre-optimized geometry. Similar structural features were observed throughout the whole series. The nitrogen atom of the triphenylamine core gives rise to a distorted tetrahedral motif, resulting in a dihedral angle between the branches of the order of 40°. The π-A unit, constituted by thienylene bridges and dicyanovinly groups in P1 and SK2 and benzothiadiazole fragments in SK3 and SK4, is essentially planar in agreement with the presence of an extended π-electron delocalization. Each branch is linked to the electron donating group via a benzene ring, with a dihedral angle of about 20-27°. Such twisting angle is expected to be beneficial for decoupling holes and electrons, once the initial charge separation is achieved (Figure 16).
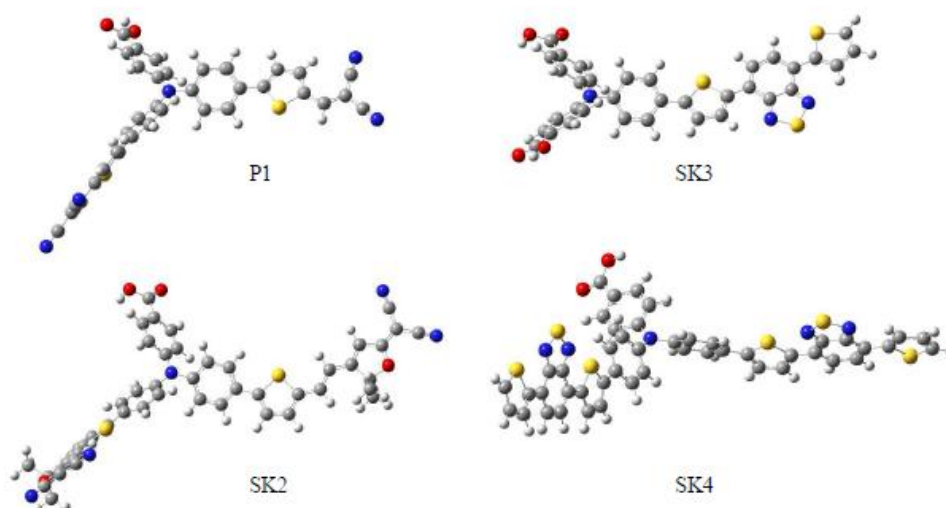

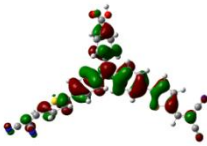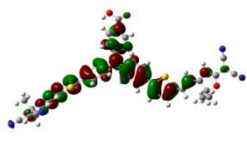**Figure 16.** Equilibrium geometries of the p-type dyes
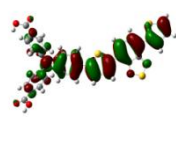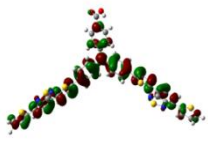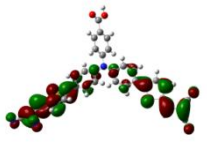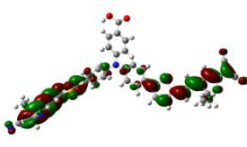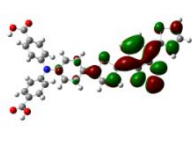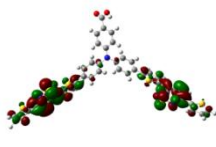
It is notoriously difficult for TimeDependent DFT (TDDFT) methods to reliably describe charge transfer states, particularly those involving spatially separated orbitals and long range excitations as in the case of our p-type systems.[61-62] Therefore, in the attempt to drive reasonable insights on the electronic structure and excited state energetics of the dye series under investigation, the excitation energies (Table 2), resulting from calculations with B3LYP [63] and BH&H (Half and Half) [64-65] functionals were compared. Frontier orbitals isodensity maps (isovalue of 0.02) of the selected dyes are reported on Table 3.

Table 2. Comparison of experimental and calculated lowest absorption maximum of the investigated dyes in DMSO.

Dye	E_{exp}(eV) [λ_{max}(nm)]	$E^{op}_{BH\&H}$(eV) [λ_{max}(nm)]	E^{op}_{B3LYP}(eV) [λ_{max}(nm)]	$|\Delta E_{BH\&H}|$(eV)	$|\Delta E_{B3LYP}|$(eV)
P1	2.53 [489]	2.79 [443]	2.30 [540]	0.26	0.23
SK2	2.22 [559]	2.86 [433]	2.08 [595]	0.64	0.14
SK3	2.54 [488]	2.62 [473]	2.14 [580]	0.08	0.40
SK4	2.49 [498]	2.48 [501]	1.92 [614]	0.01	0.57

The BH&H is considerably successful in predicting the optical transition energies of dyes SK3 and SK4, where deviations from the experimentally measured spectrum are as low as 0.08 and 0.01 eV, but less successful with dyes P1 and SK2, where the calculated E^{op} is higher than the experimental value by 0.26 and 0.64 eV respectively. The lowest transition has, in all cases, a major HOMO-LUMO component (55-87%) in the Kohn-Sham basis, with minor components arising from higher energy excitations, typically HOMO-1→LUMO, HOMO-1→LUMO+1 and HOMO→LUMO+2.

Table 3 Frontier orbitals isodensity maps

MO	P1	SK2	SK3	SK4
HOMO				
LUMO				

(**A**) Isodensity (0.02) plots of HOMOs and LUMOs calculated at the DFT 6311G,d,+ level employing the BH&H functional

MO	P1	SK2	SK3	SK4
HOMO				

LUMO				

(B) Isodensity (0.02) plots of HOMOs and LUMOs calculated at the DFT 6311G,d,+ level employing the B3LYP functional

The description of the lowest singlet state (S1) by the B3LYP calculation is roughly similar to that of the BH&H, although the HOMO-LUMO component to the excitation is largely predominating (> 93%). The lowest transition in P1 and SK2 is identified by B3LYP with a lower absolute error (0.21 and 0.11 eV) than the BH&H functional, whereas larger errors are found with SK3 and, particularly, with SK4, which shows long range charge transfers with a high degree of spatial charge separation, as indicated by Electron Density Difference Maps (EDDM) (Figure 17).Both the B3LYP and BH&H functional agree in the description of the EDDMs, showing a shift in electron density from the triphenylamine core to the electron acceptor branches, where the maximum density is localized in the proximity of the cyano groups (P1 and SK2) or on the benzothiadiazole acceptor (SK3 and SK4). It can be also appreciated that in branched dyes (P1, SK2, and SK4), the electronic excitation involves the two acceptor branches simultaneously. Thus, the electronic distribution resulting from the lowest, and usually most intense, electronic transition is favourable to a successful charge separation. The hole density is localized in the immediate proximity of the surface interacting with NiO via COOH groups. This causes photoexcitation of the electron to occur predominantly on the farthest from the NiO part of the molecule where scavenging of the electron by I_3^- is more favourable.

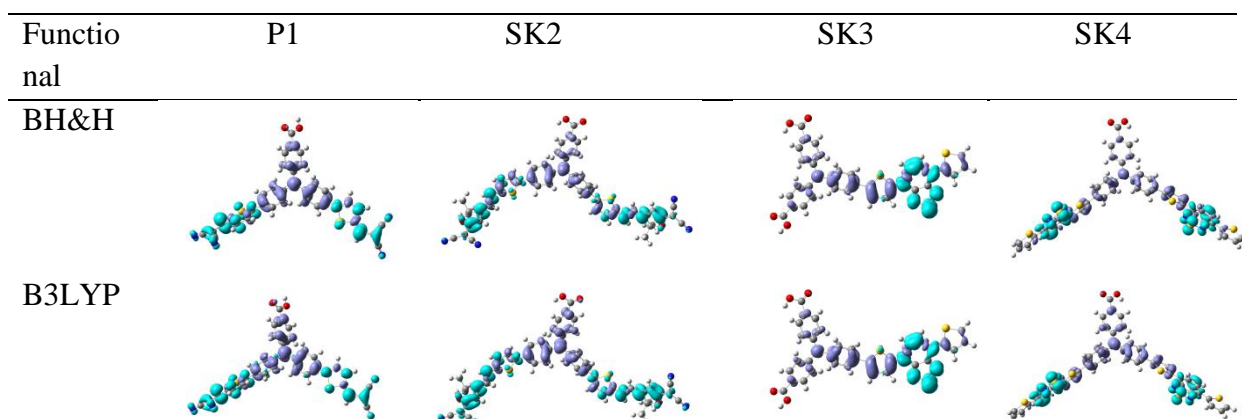| Functional	P1	SK2	SK3	SK4
BH&H				
B3LYP				

Figure 17. Electron Density Difference Maps (EDDMs) (isovalue = 0.001) of the main transition in the visible region calculated with a 6311 G,d,+ basis set obtained with the BH&H (top row) and B3LYP (bottom row) functionals. DMSO solvent was described as a polarisable continuum model (PCM). Light blue and violet indicate an increased and a depleted electron density respectively .

Table 4. HOMO-LUMO energy gap ($\Delta E_{(HOMO\text{-}LUMO)}$) and Exciton Binding Energy (EBE) calculated according to EBE = $\Delta E_{(HOMO\text{-}LUMO)}- E^{op}$ where E^{op} is the lowest vertical excitation energy calculated with the B3lyp and BH&H functionals.

Dye	$\Delta E_{(HOMO\text{-}LUMO)}$(eV) BH&H	$\Delta E_{(HOMO\text{-}LUMO)}$(eV) B3lyp	EBE BH&H	EBE B3lyp
P1	4.20	2.47	1.41	0.17
SK2	4.17	2.41	1.31	0.33
SK3	4.20	2.52	1.58	0.38
SK4	3.90	2.27	1.42	0.35

The exciton binding energy (EBE)[24] was calculated[25] from the B3LYP data set, since BH&H was found to give unrealistically high HOMO-LUMO gaps (Table 4) as well as binding energies (>1eV).

For the SK dyes, similar binding energies of the order of 0.33-0.38 eV are found, being comparable to that of some efficient n-type push pull charge separators[26] recently reported in the literature. P1 displays the smallest EBE within the series with a value as small as 0.17 eV, comparable to some of the best n-type charge separators reported.[27] Smaller EBE favour separation of the electron-hole pair, and, consequently, charge injection into the semiconductor. The largest binding energy value of 0.38 eV is found for the dye SK3, which means that a higher energy, usually provided by the local electric potential at the semiconductor/dye interface, or by collision with phonons, is needed in order to promote charge injection. The larger EBE of the SK series may constitute a disadvantage compared to the reference dye P1 for obtaining hole injection with high quantum yields.

2.7. Photovoltaic and Photoelectrochemical dependencies

The SK dyes together with reference compound P1 were tested as photosensitizers in p-type DSSCs. NiO photocathodes were fabricated by blading a NiO colloidal paste, obtained by dispersing commercial 25-nm NiO nanoparticles in terpineol, with ethylcellulose as an organic binder/densificating agent, followed by high temperature sintering on FTO (Fluorine-doped Tin Oxide) coated glass. The resulting photocurrent (*J*)/photovoltage (*V*) curves under AM 1.5 illumination (1 sun) are shown in Figure 4A and their main efficiency parameters are listed in Table 3.

Table 5. Photovoltaic parameters of investigated chromophores in p-type DSSC

Dye	J_{sc} (mA/cm^2)	V_{oc} (mV)	FF	PCE (%)
P1	1.14	95	0.32	0.035
SK2	0.51	81	0.33	0.014

|				
SK3	0.54	82	0.33	0.015
SK4	0.43	134	0.32	0.018

Several series of iodine-based I^-/I_3^- and Co (III)/(II) electrolytes with different concentration ratio were tested for the cells fabrication. However, the best average power conversion efficiencies were observed when using the *iodide/triiodide* redox couple (solution of 1.0 M LiI and 0.1 M I_2 in CH_3CN). Dye SK4 produces the highest open circuit voltage (133 mV), that is ca. 40 mV higher than that of device sensitized by the other reference and novel dyes. The SK2 and SK3 molecules produced comparable J_{sc} (ca. 0.5 mA/cm^2), which was however approximately half that of the reference P1 (ca. 1.1 mA/cm^2). In all cases the sloped *J/V* characteristic at reverse (negative) bias is consistent with a small shunt resistance of the NiO films, causing charge leaks and losses by recombination. For instance, in the case of P1 the photoinjected charge extracted from the photocathode under short circuit conditions (0 V) is roughly one half that available at -0.2 V. Such a photocurrent loss upon moving from negative to positive potential is less marked for the SK series, which, giving rise to a smaller extent of hole injection, result in fewer charge leaks to the electrolyte. The overall PCE of P1-sensitized cells is about twice as large as that of the SK-based devices, mainly due to their lower photocurrents. In general, although not optimized, the efficiencies of the NiO sensitized solar cells recorded in this work are in agreement with the average performances reported so far in the literature for similar types of sensitized p-type electrodes.

To understand the nature of photocathodic current, the IPCE spectra of the p-type cells, under short circuit conditions were measured (Figure 18 C). Consistent with their spectral properties, all dyes displayed a strongest response in the blue region of the spectrum for λ< 450 nm, reaching the best values of ca. 12-14% for P1 and SK2. The photoconversion then decreases by moving from the blue to the red region of the visible spectrum, showing a shoulder the 500-600 nm region, with values of 4-5% in the case of P1 and SK4.
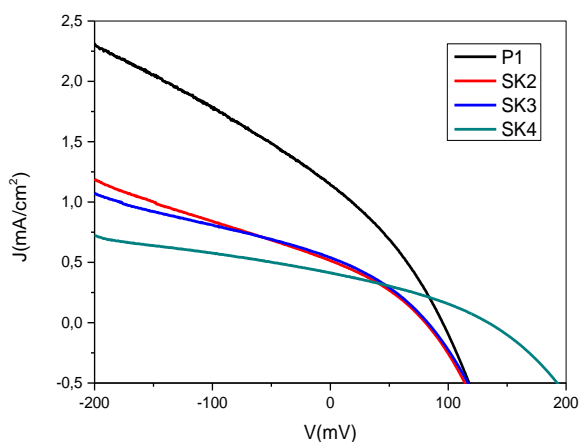
A
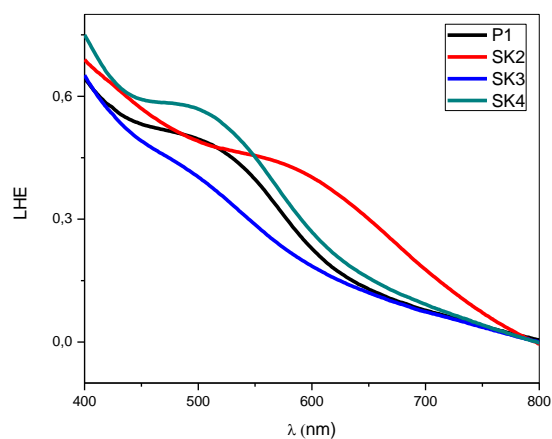
B
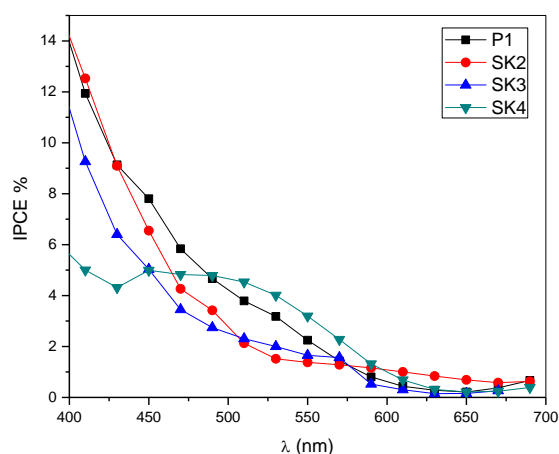
C
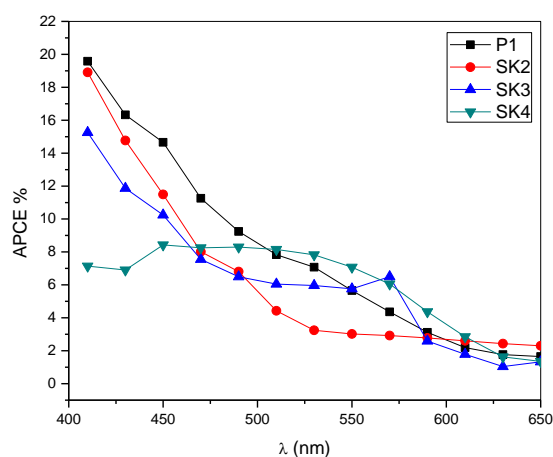
D

Figure 18. Photoelectrochemical and spectral properties of p-type DSSCs in the presence of 1M LiI and 0.1 M I_2 in acetonitrile. A) Current–voltage characteristics; B) Light Harvesting Efficiency (LHE) (LHE(λ) = 1-10$^{-A(\lambda)}$) where A(λ) is the background-subtracted absorbance of the dyed NiO films; C) Photoaction spectra (IPCE vs λ); D) Absorbed photon conversion efficiency spectra (APCE vs λ)

Despite the opacity of the NiO electrodes, causing significant light scattering, and the strong competitive absorption of the iodine based electrolyte, in general the photoconversion appeared to be in a relatively good agreement with the Light Harvesting Efficiency (LHE) (Figure 18B) of the sensitized NiO photoelectrodes, confirming that the excited state of the dye is responsible for the observed photocurrent in the visible region of spectrum.

The LHE plot, with values of 50-60% in the 550-450 nm region, showed that SK4 has here the best light harvesting performance, consistent with its relatively good IPCE response at these wavelengths. The absorbed monochromatic photon-to-current conversion efficiencies (APCE) spectra, obtained by dividing the corresponding IPCE spectra by the LHE of the respective photocathodes, are shown in Figure 4 D. The low energy response of P1 and SK4 are similar, with APCE ~ 10 % at 500 nm. Interestingly, SK4 is able to yield a slightly more efficient conversion for $\lambda \geq$ 550 nm, while P1 prevails below 480 nm. As for the IPCE, the best APCE response is observed in the blue region of the spectrum, with values of ~18-20% for P1 and SK2.

Electrochemical impedance spectroscopy (EIS) was used to further investigate the comparative behaviour of the chromophores in photovoltaic devices. All dyes were stable during potentiostatic measurements, which were performed at potentials between -10 mV and the V_{oc} of the cells. The J/V curves after EIS measurements showed essentially the same performances found before the measurements, which allows to rule out substantial dye or cell degradation affecting the results. The EIS spectra (Figure 19) could be well fitted with the equivalent circuit, comprising the

serial resistance, the counter-electrode interface, the diffusion element accounting for electrolyte transport impedance in a thin layer cell, and the transmission line [66](DX1 in Zview) which describes the transmission network of the NiO, applied by Zhang et al. to p-type DSSCs, comprising both the transport and the charge transfer resistance (R_{ct} (NiO)) (recombination resistance) at the NiO/electrolyte interface.
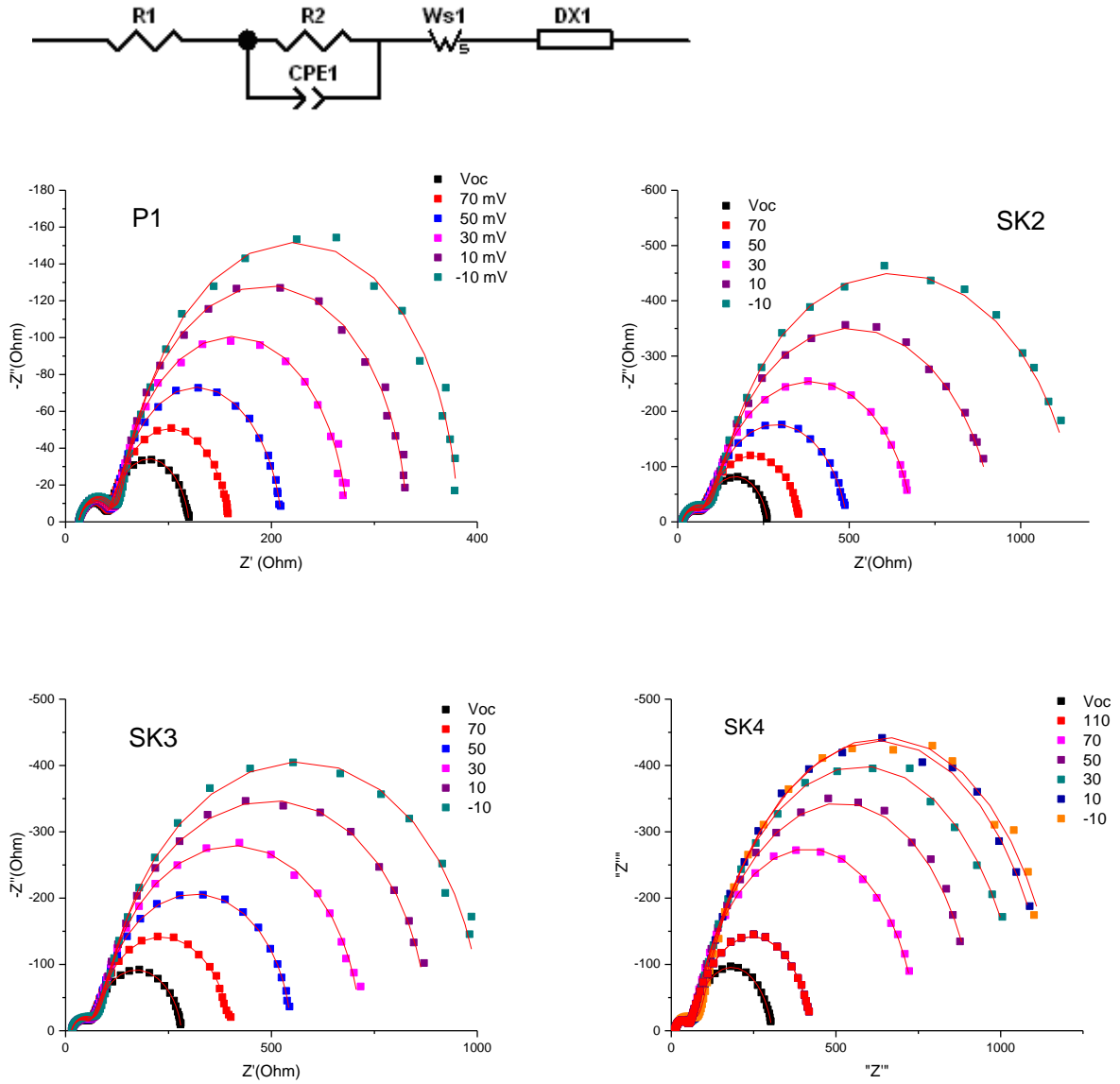
Figure 19. EIS spectra of the SK series of dyes

The impedance response of the NiO based DSSC exhibited similar features, appearing as a small high frequency semicircle, due essentially to the counter-electrode electrochemical interface, followed by a much larger loop at lower frequencies, which bears the main contribution of the NiO/electrolyte interface. Indeed the *J/V* curves are essentially dominated by the charge transfer resistance of

the NiO, as can be appreciated by the comparison of the derivative ($\frac{\partial i}{\partial V}$) of the J/V curves and the inverse of the interfacial charge transfer resistance $(R_{ct}(NiO))^{-1}$ (Figure 20 B). This agreement is particularly good in the case of the SK series, for which the charge transfer resistance was the largely predominant contribution to the total cell resistance at each potential and varied typically between 1000 and 200 Ω depending on the voltage. Obviously, the lowest $R_{ct}(NiO)$ are in all cases found at the open-circuit voltage, due to hole accumulation into the mesoscopic film under open-circuit conditions.

The NiO capacitance (Figure 20 A), calculated according to C = $CPE(\omega)^{n-1}$, where n is the exponent of the CPE admittance from the transmission line, in all cases variable between 0.9 and 0.84, and ω is the frequency at the maximum of the large low frequency loop, was reasonably linear on a logarithmic scale, indicating a chemical capacitance[67] behaviour determined by empty states in the valence bands or in surface states following a Boltzmann distribution near the valence band edge. The inspection of Figure 20 reveals that P1 is the dye which exhibits the lowest charge transfer resistance and highest capacitance, indicating a superior capability of hole injection.

A

B

28
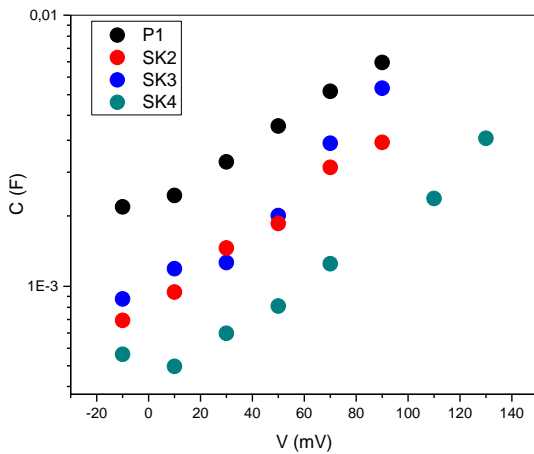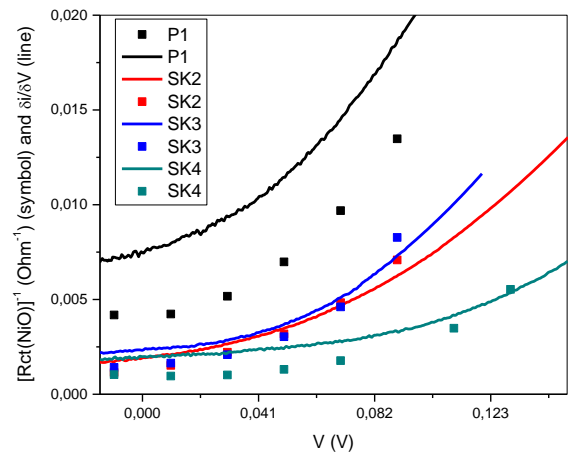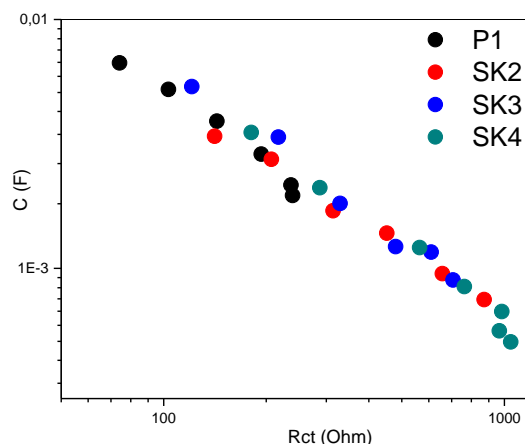
C

Figure 20. A) Capacitance of sensitized NiO films at increasing potentials in the forward direction; B) Reciprocal of the charge transfer resistance at the NiO/electrolyte interface (squares) compared to the derivative of the JV curve (solid lines); C) Chemical capacitance of NiO vs interfacial charge transfer resistance in p-type DSSCs under study.

The representation of R_{ct}(NiO) vs C(NiO) on a logarithmic scale indicates that all the dyes behave intrinsically similarly to each other, as far as recombination kinetics are concerned, when compared at the same chemical capacitance of the NiO. In other terms, the charge loss pathways involving direct dye⁻/h⁺ and hole recapture by I⁻ occurred at comparable rates for all the dyes under investigation. Accordingly, the higher photovoltage observed for the SK4-sensitized device is likely due to a positive shift of the valence band edge of the NiO by ca. 30-40 mV, induced by the adsorption of the dye sensitizer, as can be observed by comparing the different voltages at which the similar capacitances are found, rather than by slower interfacial recombination kinetics.

Figure 21 Dark currents of the sensitized NiO DSCs (SK series)

The voltage shift observed for SK4 in EIS under illumination is quantitatively consistent with the more positive onset of the anodic current observed for this moiety in the dark (Figure 21).

2.7. Summary`

New p-type photosensitizers based on organic linear and di-branched donor-acceptor systems bearing a tryphenylamine group as a donor and strong electron-acceptor Dalton's (SK2) or ben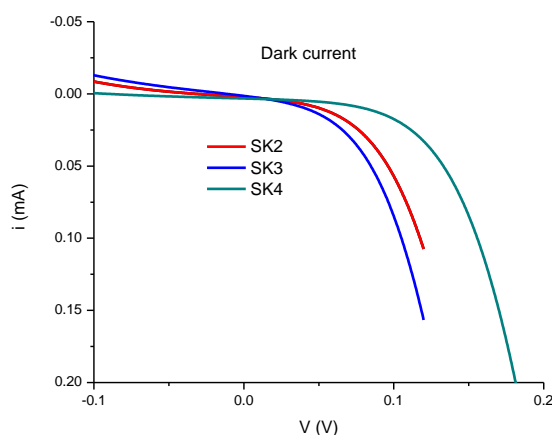zothiadiazole(SK3 and SK4) groups were synthesized and characterized by steady state spectroscopic, electrochemical, and computational studies. All the dyes under investigation exhibited strong charge transfer bands in the visible regions with ground and excited state energetic which are favourable to the sensitization of NiO electrodes. The computational investigation revealed a clear directionality of the lowest excited state exhibiting a marked charge transfer character, shifting the electron density from the donor core to the acceptor branches, an electronic situation which is favourable to the hole injection in p-type semiconductors such as NiO. However, the exciton binding energy, i.e. the energy of the bound electron-hole pair, is about twice as large as that of a known literature standard (P1), suggesting that a more difficult charge separation in the new dyes might occur.

When tested as photosensitizers in p-type DSSCs the SK series was able to successfully sensitize NiO electrodes, resulting in photocurrents which are about half that of P1-based cells. The charge recombination kinetics, probed by considering the charge transfer resistance at the NiO/electrolyte interface at a comparable chemical capacitance, showed that the dyes behaved similarly under this respect and that the higher photovoltage observed for the device based on SK4 dye is seemingly due to a positive shift of the valence band edge, consistent with the shift in the anodic threshold measured in the dark. The fact that similar recombination resistances were found at a comparable photohole density in the NiO corroborates the indication, gained by DFT studies, that the superior performance, particularly in photocurrent, of P1 may be ascribed to a superior charge separation capability originating by its smaller exciton binding energy. Future designs of dyes for p-type sensitization will take this parameter into consideration for achieving a more effective charge separation.

External Internship

School of Biological and Chemical Sciences
Queen Mary University of London
United Kingdom

Supervisors:

Dr. P.B.Wyatt
Prof. W. Gillin

3. Fully halogenated organic luminescent sensitizers

3.1 Introduction

Since all electronically excited lanthanides in organic environment suffer from vibrational quenching due to proximity with O-H, C-H and other hydrogen bonds, substitution of the hydrogen atoms (or preferably even all hydrogen atoms) in high proximity with Ln^{3+} ion is essential for obtaining material with high photoluminescence and long lifetime of the excited state.[68-69] Therefore materials for organic amplifiers are usually operating on halogenated compounds. Highly and fully halogenated and, particularly, fluorinated materials give an opportunity to avoid vibrational quenching and tend to lower the HOMO-LUMO molecular orbitals. [70-72] Another benefit of using halogenated materials to sensitize Ln^{3+} is enhanced singlet-triplet mixing due to a higher molecular weight of halogen comparing to hydrogen which forces formation of a long lived excited state.

Two main approaches towards application of the organic chromophores for Ln^{3+} sensitization are known in the-state-of-the-art. The first one operates on direct bonding of the organic ligands to the lanthanide core[76], whereas the second method is operating on mechanical mixture of organic material with lanthanide compounds.[77]

Fully fluorinated imidodiphosphinate ligand (FTPIP) (Figure 22) [73-74] has shown one of the best results among lanthanide complexes with organic sensitizers. It forms a shell structure around the atom of Er, therefore, protecting the whole molecule from coordination with molecules of solvent or water, an effect which causes a sharp decrease in photoluminescent properties of the resulting material. Good photophysical parameters have been also shown by complexes of this ligand with neodinium Nd(III) and ytterbium Yb (III). The lifetime of the excited state of lanthanide complexes with FTPIP sensitizer was in the range of 1 ms.

A novel organic antenna sensitizer based on the highly fluorinated carboxylate ligand 3,5-bis(perfluorobenzyloxy)benzoic acid (Figure 22) showed an efficient photosensitization of Tb^{3+}. [78] This new complex features considerably long lifetime of the excited state of up to 1.15 ms in solid state (though it was significantly lower when measured in thin film). The influence of the hydrogen atoms which are still present in this system was minimal probably due to the fact that they were shielded by benzene rings close to the Tb^{3+} atom. Polymer films doped with the Tb(III)–3,5-bis(perfluorobenzyloxy) benzoate complex displayed bright green luminescence and slightly increased lifetime values comparing to precursor compound, thus making these approach very promising for application in photonics.
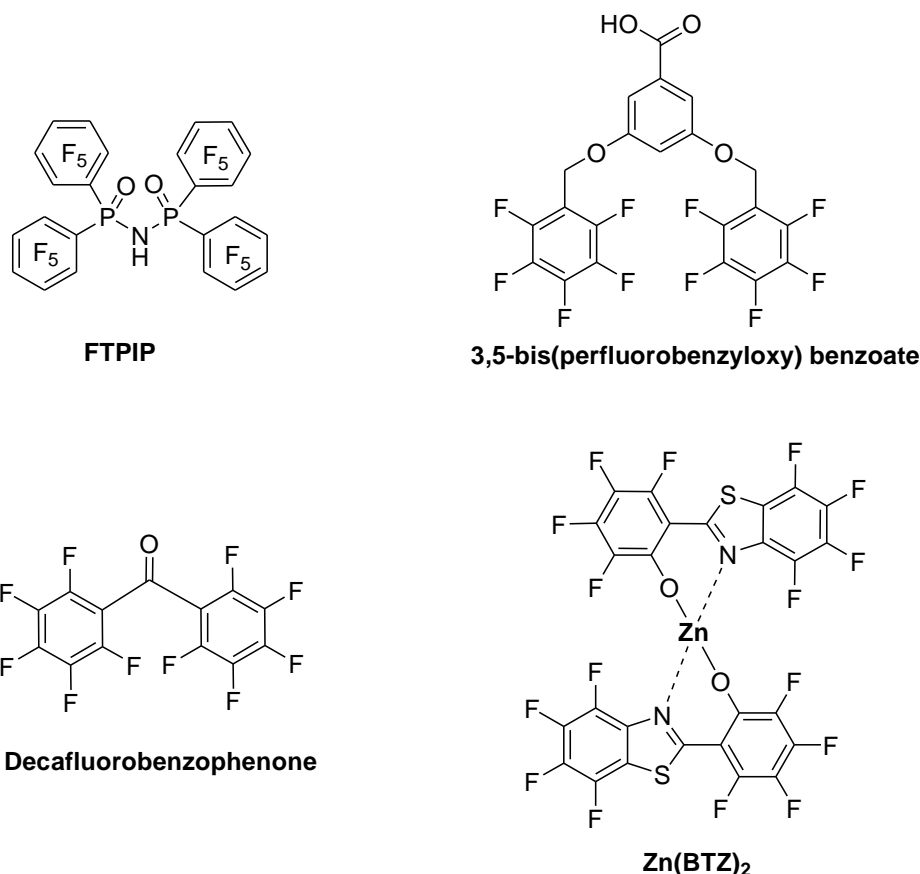
Figure 22. Fluorinated compounds used for Ln^{3+} sensitazation.

A successful attempt to get efficient sensitization and a long lifetime of the whole system's excited state by mechanical mixtures of lanthanide and organic compound was recently performed by Mech and all.[79] Organic framework was designed in from of a nanochanel loaded with molecules of decafluorobenzophenone (Figure 22) and Er^{3+} ions. Under the excitation conditions direct energy transfer from the organic molecule to erbium was taking place resulting in the overall excited state lifetime of 0.21 ms.

However, the best currently known result for mechanical mixtures of the photoluminescent materials was achieved by the group of Dr. P.B.Wyatt and prof. W. Gillin.[77] The Zn (II) complex with perfluorinated 2-(2-hydroxy-3,4,5,6-tetrafluorophenyl)-4,5,6,7-tetrafluorobenzothiazole ligand ($Zn(BTZ)_2$) was co-sublimed with $Er(FTPIP)_3$ to form a nicely blended film. Under the excitation conditions, the film showed significantly strong sensitisation over broad band of 350-480 nm wavelengths compatible with high power LEDs. The pure $Er(FTPIP)_3$ film though didn't have any visible absorption at this wavelengths. Most probably the energy transfer from $Zn(BTZ)_2$ to the Er^{3+} ions occurred due to the matching of the excitation bands between fully fluorinated zinc complex and fully fluorinated erbium

complex. Lifetime of the Er^{3+} excited state in the film doped with Zn(II) complex was around 0.8 ms being a new record for the erbium sensitization.

3.2. Aim of the study

This work is very much inspired by the result obtained for the fully fluorinated organic $Zn(BTZ)_2$ and focuses on investigating organic chemistry-based approaches for tuning material properties of luminescent synthesizers towards formation of prolonged exciting state.
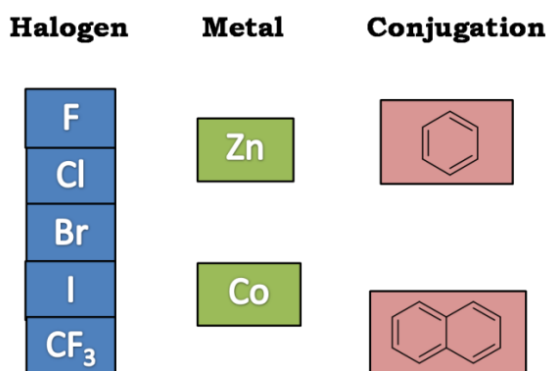
Figure 23. Building blocks of the designed materials

To this end, we aim to design a series of ligands based on benzothiazole connected to the benzene or naphtaline ring (Figure 23). All hydrogen bonds in to-be-developed chromophores are planned to be substituted with either fluorine or any other halogen or CF_3 group (Figure 24). As dictated by the concept, the triplet excited state formations relies significantly on the intersystem crossing, different atomic structure and electro negativity of substitute groups, whereas halogens have been proved to endorse photoluminescence and promote formation of the long lived triplet state.

Moreover, we aim to distinguish the influence of conjugation on the physical properties of resulting sensitizer. The electron tunnel effect enhanced by prolonged conjugation was beneficial when applied in materials for field effect transistors (FETs), whereas OLEDs inspired us to try it in our target materials.[80,81]

Finally, we aim to compare influence of the complexing metal on energy transfer from the fully halogenated complex to the Ln^{3+} ion. Zn (II) and Co (II) have been selected for this purpose for the following reasons: Co(II) attracted our attention because its sensitization properties, while look quite promising, have never been applied in organic amplifying materials, whereas Zn(II) complex has already proved its efficiency in lanthanide sensitization.
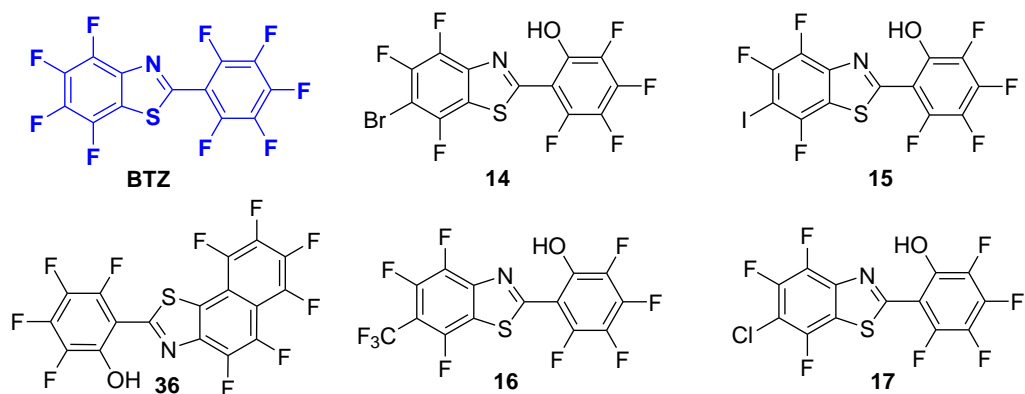
Figure 24. Designed fully halogenated ligands.

3.3. Synthesis

Following on from our recent experience in the synthesis of fully fluorinated BTZ ligand,[77] we've developed a new series of compounds by substituting the F-atom in position *6* of the benzothiazole ring with Cl, Br and I halogen atoms as well as CF$_3$ group. Ligands were obtained according to the synthetic way depicted in Scheme 4.

3,4,5-tetrafluoro-6-methoxybenzoyl chloride **20** was synthesised *via* the methilation reaction of pentafluoro benzoic acid with magnium methoxylate.[82] It was used as a starting material for the target compounds **14-17** and **36** (Figure 24). Afterwards resulting intermediate reacted with thionyl chloride and obtained product **20** was used without further purification.
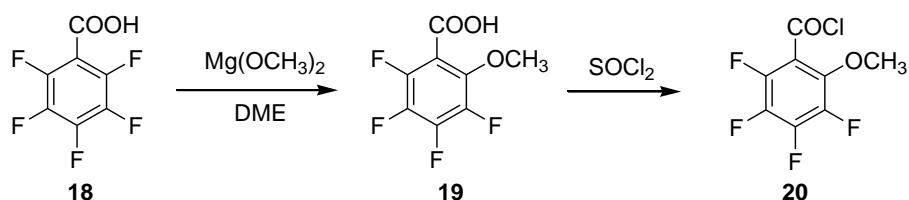
Scheme 4. Synthesis of starting benzoyl chloride

We tend to work with widely commercially available amine compounds used as a starting material on the first step of synthesis, because such approach favours the further possible industrial application of the obtained sensitizers. Therefore 4-bromo-2,3,5,6-tetrafluorobenzenamine was chosen for the synthesis of the bromine substituted ligand **14** and 2,3,5,6-tetrafluoro-4-(trifluoromethyl)benzenamine – for the synthesis of ligand **16**.

As 4-iodo-2,3,5,6-tetrafluorobenzenamine **22** and 4-chloro-2,3,5,6-tetrafluorobenzenamine **23** were not commercial available at that time, benzamine **22** was synthesised using updated literature procedure (Scheme 5).[83-84] 2,3,5,6-tetrafluorobenzenamine **21** reacted with iodine in presence of yellow Hg(II) oxide in

the media ethanol. Reaction resulted in rather good yields of the crude product which was further purified by column chromatography to obtain pure material as yellowish solid in 85% yield.
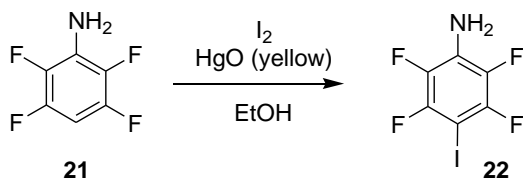
While amine **22** was easily synthesised using a known literature procedure, it was rather challenging to find an effective and high yielding strategy towards the synthesis of chlorinated benzamine **23** (Scheme 6). Nevertheless, after numerous attempts, amination of pentafluorochloro benzene [85] resulted in a mixture of target compound **23** (80%) and byproduct amines substituted with chlorine in 2- and 3- position (20%). Unfortunately we didn't find sufficient way to separate the crude mixture, what pushed us to try a chlorination of 2,3,5,6-tetrafluorobenzenamine with *N*-chlorosuccinimide. Although this reaction hasn't been published before, bromination with *N*-bromosuccinimide in the same conditions usually worked good for different substrates.[86-87] Indeed chlorination with NCS was successfully performed yielding 90% of desired chloro-substituted benzamine. The purity of the compound was high enough to use it in the next synthetic step without additional purification.
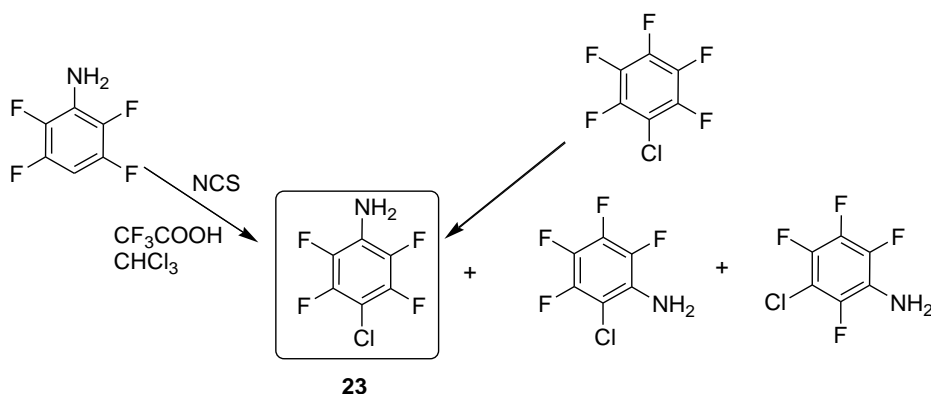
Scheme 6. Synthesis of chlorobenzamine **23**.

Obtained benzoamines subsequently reacted with acyl chloride (**20**) to give amide derivatives **24-27** with 65-80% yields. It should be mentioned that with exception of the trifluorobenzamine, all halogene-substituted compounds easily reacted with acyl derivative at room temperature. Probably due to the strong electronegativity of the CF_3- group and bulkiness of the three fluorine substituents at

one carbon atom, reaction towards amide **27** required to be catalysed. While carried out with 1 molar equivalent of pyridine and at reflux in toluene, 65% of target compound **27** was obtained.
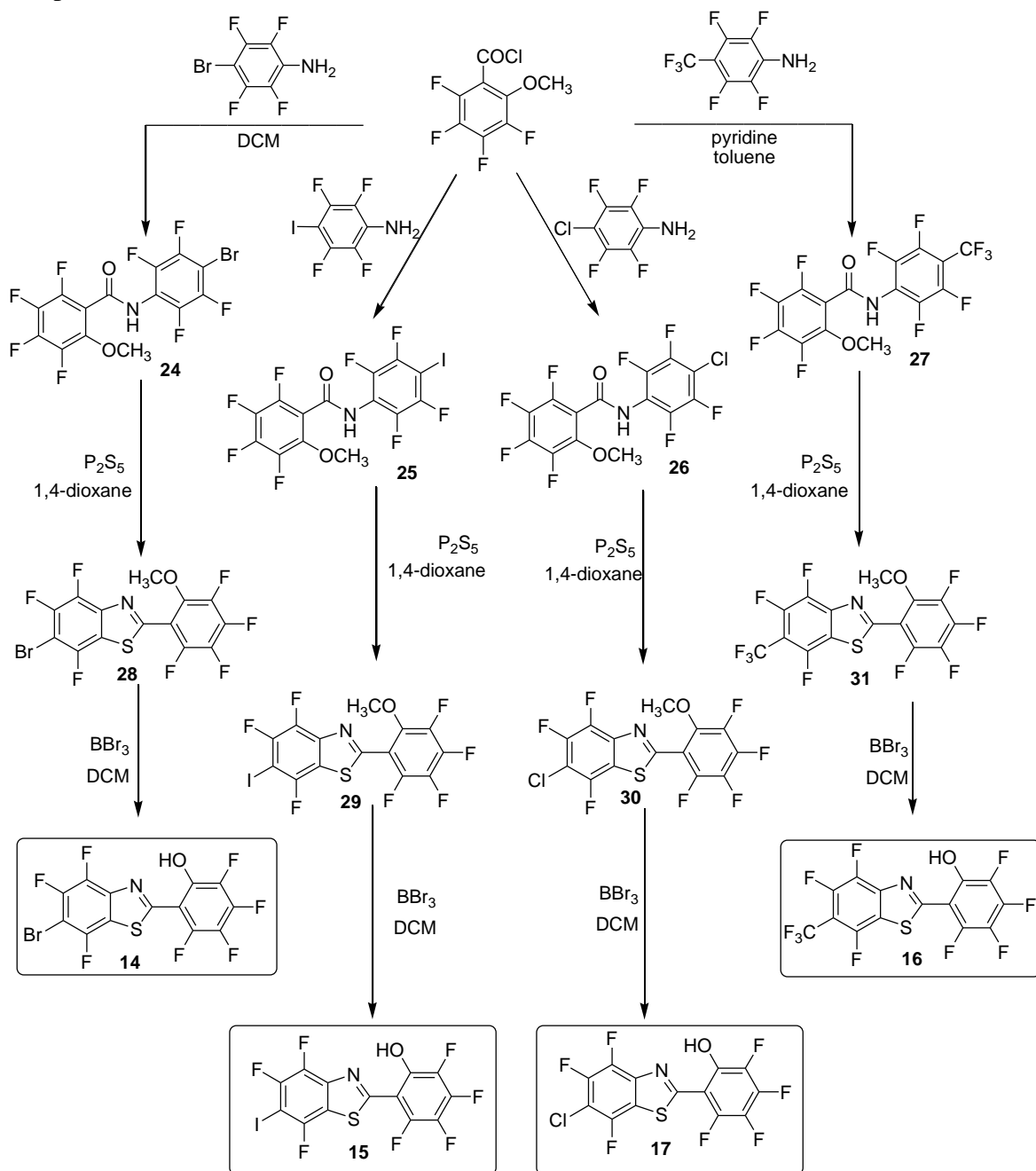
Scheme 7. Synthetic path towards ligands **14-17**

Resulting crude products **24-27** were subjected to the column chromatography to obtain products in 65-85% yield. This was followed by their cyclisation carried in the dry dioxane and catalyzed with phosphorus pentasulfide P_2S_5. Cyclasation reaction is going according to the mechanism showed in Scheme 8 and can be generally described as Paal-Knorr reaction.
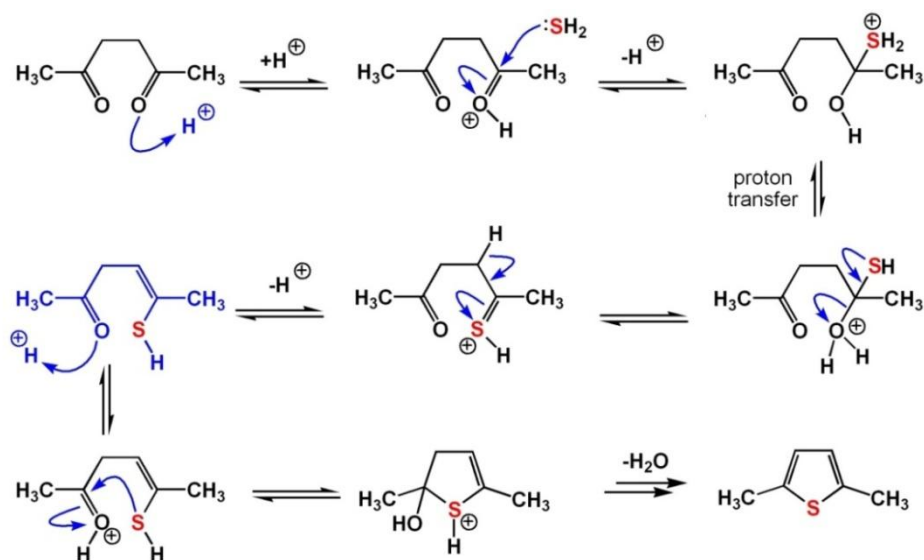
Scheme 8. Paal-Knorr reaction mechanism .

Benzothiazole derivatives **28-31** were obtained with 60-75% yields and then subjected to the demethylation reaction with boron tribromide in the anhydrous DCM. Demethylations in these conditions were very high yielding providing the desired ligands **14-17** with 90-95% yields and high enough purity to be used at the next step.

In order to obtain naphtaline based ligad **36**, we tried synthetic approaches similar to those described for halogenated ligands **14-17** (Scheme 9). Amination of **32** was previously reported by Vaganova *et al*. and ran with good selectivity to give amine **33** with 75% yield.[88]
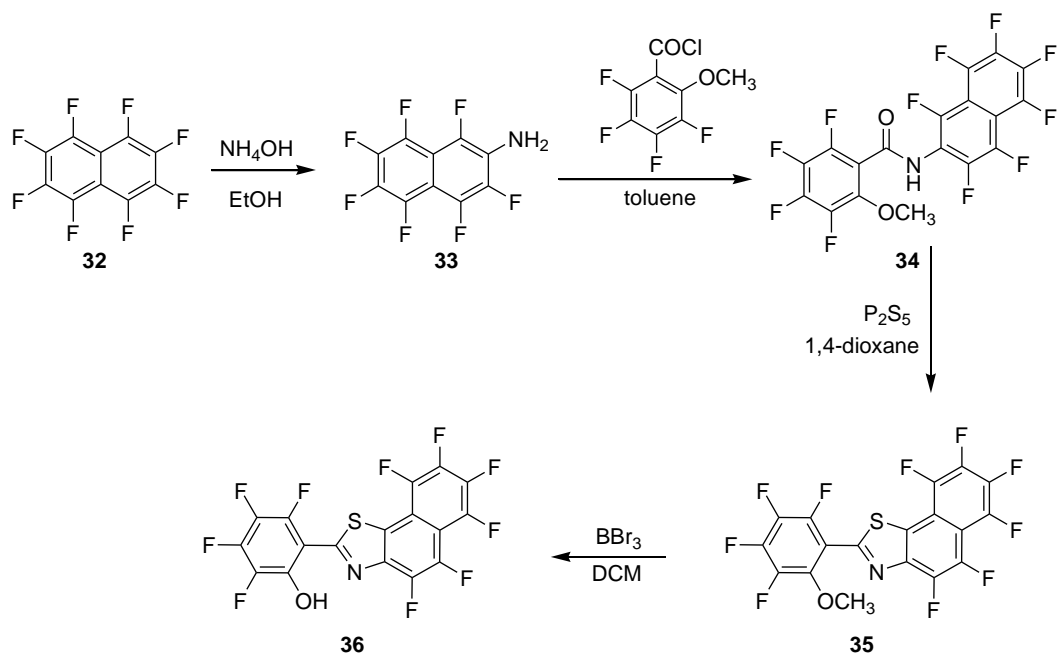
Scheme 9. Synthesis of naphthaline ligand **36**

Obtained ligands were used for the synthesis of corresponding Zn(II) and Co(II) complexes following the common synthetic path depicted on the Scheme 10. Due to the full halogenation, the ligands were not as reactive as their hydrogenated analogues.
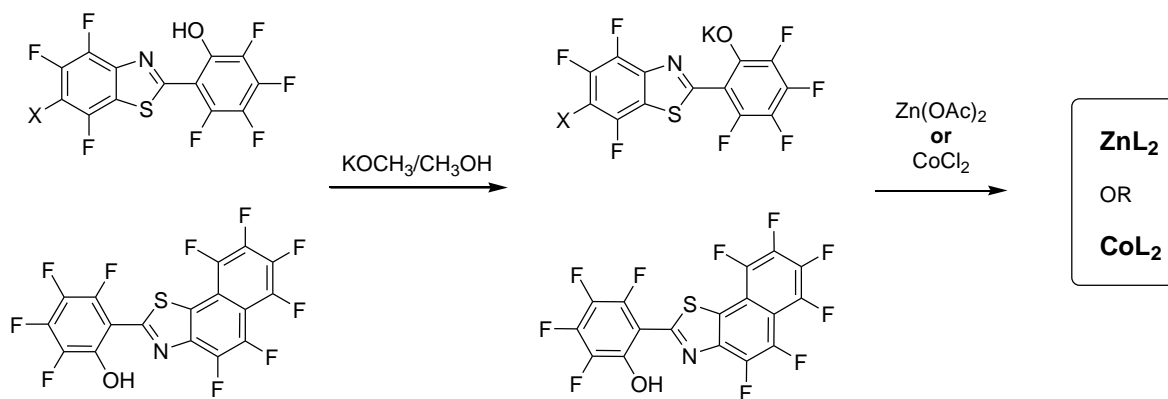
Scheme 10. Synthesis of the CoL_2 and ZnL_2 complexes.

Therefore straightforward complex formation was not an option in the case of such fully halogenated systems. Instead, desired complexes were achieved through the formation of the potassium salt of the corresponding chromophore and it's subsequent reaction with either Zn(II)acetate ($Zn(OAc)_2$) or $CoCl_2$ which resulted in target ZnL_2 and CoL_2 series of materials.
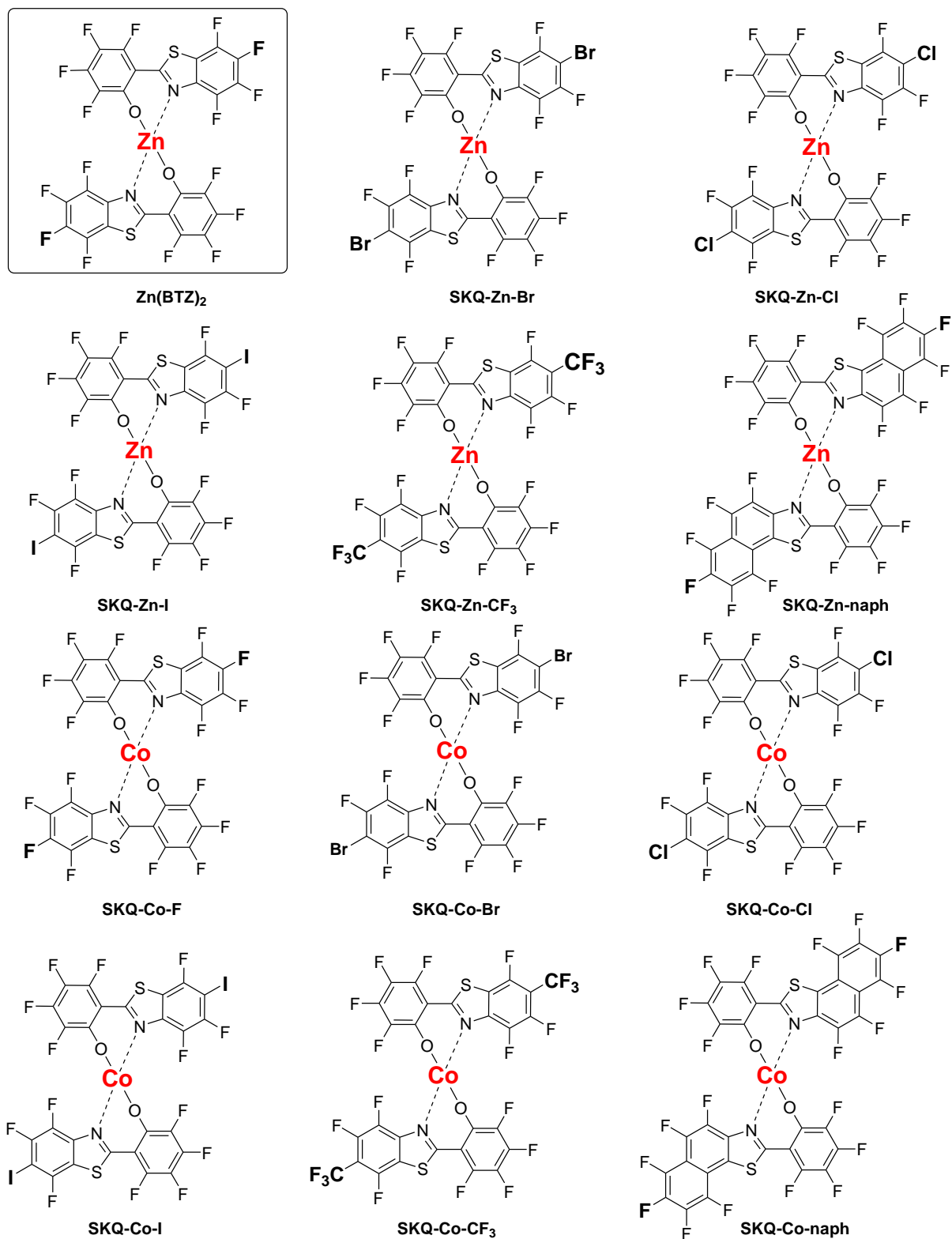
Figure 25. Zn(II) and Co(II) series of organic sensitizers.

3.4 Materials, instruments and methods

Unless otherwise stated, all commercially available solvents and reagents were used without further purification. Dry DCM was collected from the MBraun SPS-800 solvent purification system. TLC was done using Merck silica gel 60 F254 plates. Flash chromatography was performed on Zeochem ZEOprep 60 silica gel (40–63 μm).

Melting points were measured using capillary tubes in a Gallenkamp melting point instrument. IR spectra were obtained by attenuated total reflection (ATR), using a PerkinElmer Spectrum 65 FT-IR spectrometer. NMR spectra were determined at 400MHz for 1H, 376 MHz for 19F and with a Bruker AVIII 400 spectrometer. 19F NMR spectra were recorded with proton decoupling. Emission in solution was recorded by a Horiba FluoroMax-3 fluorometer. Mass spectra were obtained by the EPSRC NMSF, Swansea.

X-ray quality crystals of zinc and cobalt complexes were grown by vacuum sublimation in a sealed glass pipette (with a pressure below 10^{-5} mbar, temperature between 230 °C and 280 °C). Single crystal X-ray diffraction was carried out at Queen Mary University of London using the KAPPA APEX ii DUO diffractometer, with MoKα radiation ($\lambda = 0.71073$ Å). X-ray crystal structures were solved and refined using the Bruker SHELXTL software package.

Experimental calculations on the SKQ-Zn-Br structure were carried out at the DFT and TDDFT level with a LANL2DZ basis set by using Gaussian 09 A02 on the pre-optimized structure at the the semi-empirical PM6 level. All calculation were carried out in the presence of DMSO treated within the PCM (Polarizable continuum) model. The output isodensity surface and optimized equilibrium geometries at the ground, first excited singlet state and first excited triplet state were generated and visualized with Gaussview 5.0. Electron density difference maps of the lowest transitions were generated using Gausssum 2.2

Photoluminescent properties of the sublimed materials were measured using the setup of the home-built photoluminescence measurement systems shown in Figures 26-27.

The setup for powerful beaming of the sample operated on Panther *optical parametric oscillator* (OPO) is shown in Figure 26. The polariser is used to remove the polarised so-called idler beam, and the intensity of the signal pulse is measured using a multifunction optical meter. The laser beam is collimated and reflected onto the sample after a 385 nm absorbing filter is positioned for removing leaked 355 nm light. The sample is positioned on a home-made sample stage. The luminescence from the sample is collimated into the entrance slit of the detector Triax 550 spectrometer. The probed photoelectric signals are magnified by specific photomultiplier tube (PMT) (Hamamatsu R5509-72). The spectra of output signals are displayed on an oscilloscope (LeCroy waverunner LT372) and the spectra data are collected by PC.
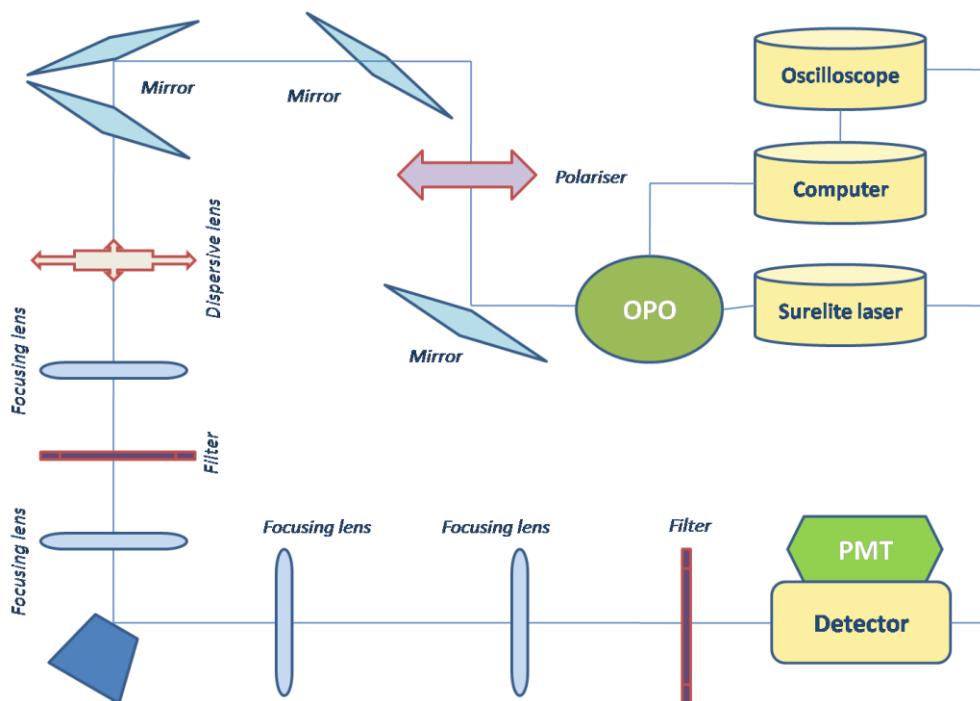
Figure 26. Setup for measuring photoluminiscence using OPO light source

For ligand-centred photoluminescence measurements in the visible light range, the light path setup looks similar (Figure 27).
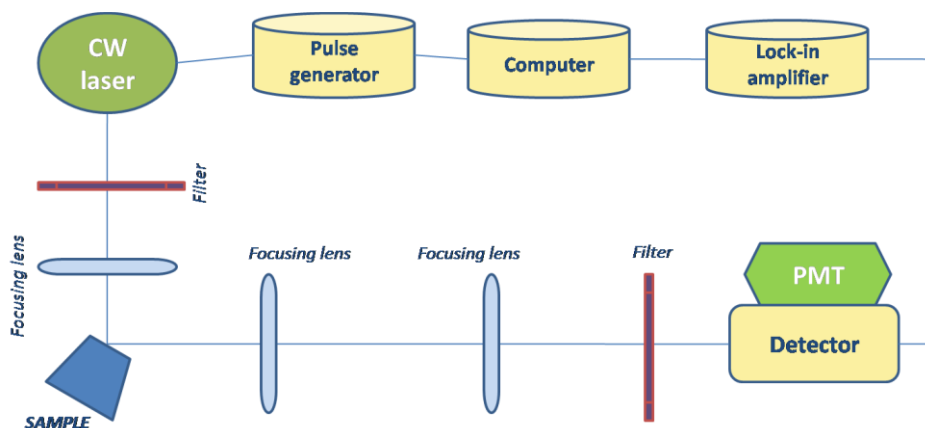
Figure 27. Setup for measuring photoluminiscence using CW laser

As the light source part is used 405 nm CW laser from which the beam is going to the focusing lense through the filter and then directly shines on the sample. The focusing lense could be omitted, however it helps to get maximum possible signal when the emission of the material is not bright enough. The pulse frequency of the laser is controlled by a Function, Arbitrary and Pulse generatorTG251xA. The signal is processed by a lock-in amplifier to collect steady state emission intensity.

3.5. Optical characterization

Uv-vis absorbance of the synthesised complexes was measured in DMSO solution. Zn^{2+} complexes with bromo-, chloro-, and iodo-substituted ligands showed qualitatively similar behaviour featuring two absorption peaks at around 410 nm and 275 nm with difference in their maximums of 2-5 nm (Figure 28). All of the results are 25-30 nm shifted comparing to the reference $Zn(BTZ)_2$ complex and show slightly broader absorption bands.
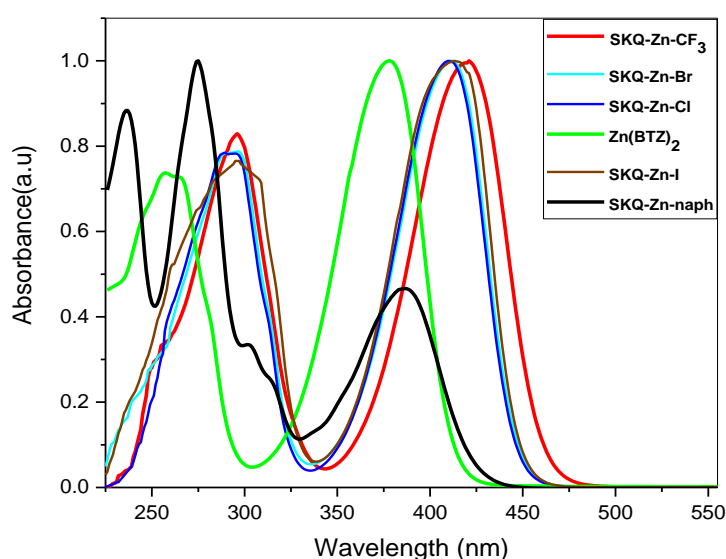
Figure 28. Uv-vis absorption spectra of the Zn^{2+} series

In contrast to halogenated sensitizers and the reference complex, fully fluorinated SKQ-Zn-naph had more intense absorption at 225-275 nm band with two maximums at 262 nm and 238 nm. Double peak in the blue region could be explained by $\pi-\pi^*$ transitions taking place in conjugated naphtaline fragment. More narrower and less intense absorption peak of SKQ-Zn-naph at 396 nm was only 8 nm red shifted than the $Zn(BTZ)_2$ unlike the complex with CF_3-substituent which showed batochromic shift of 50 nm with absorption maximum at 423 nm.
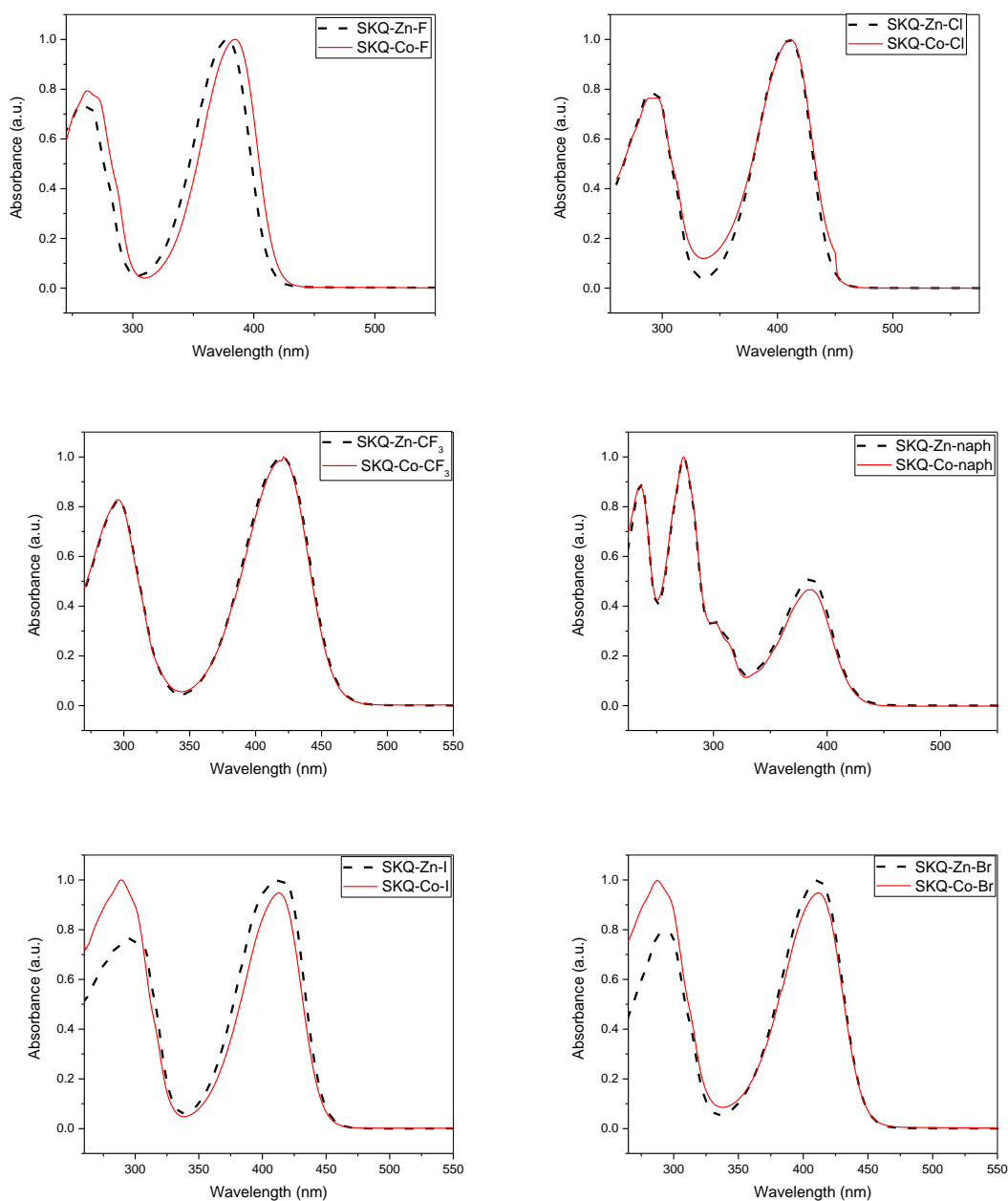
Figure 29. Uv-vis absorption spectra of Zn^{2+}

The absorption bands off both Co(II) and Zn(II) series lied in the same wavelengths with slight 1-3 nm variation in absorption maximums. However SKQ-Zn-Br and SKQ-Zn-I presented increased absorption intesity in the blue region which is probably due to the overlapping of the halogen and cobalt molecular orbitals and therefore increased intraligand $\pi-\pi^*$ transitions.

More detailed explanation of the patterns in behaviour of obtained series of complexes is discussed in the part 3.6.

3.6. Crystal structures and computational characterization

Crystals suitable for the X-ray diffraction analysis were obtained using sublimation method. Series of materials formed translucent, either shard- or block - like crystals, light yellow in case of the Zn^{2+} family of compounds or dark orange for Co^{2+}. Similar structural parameters were present within the whole zinc and cobalt family of the sensitizers, which are shown on an exemplar of complexes with brominated ligand SKQ-Zn-Br and SKQ-Co-Br (Figure).

SKQ-Zn-Br packing   SKQ-Co-Br packing
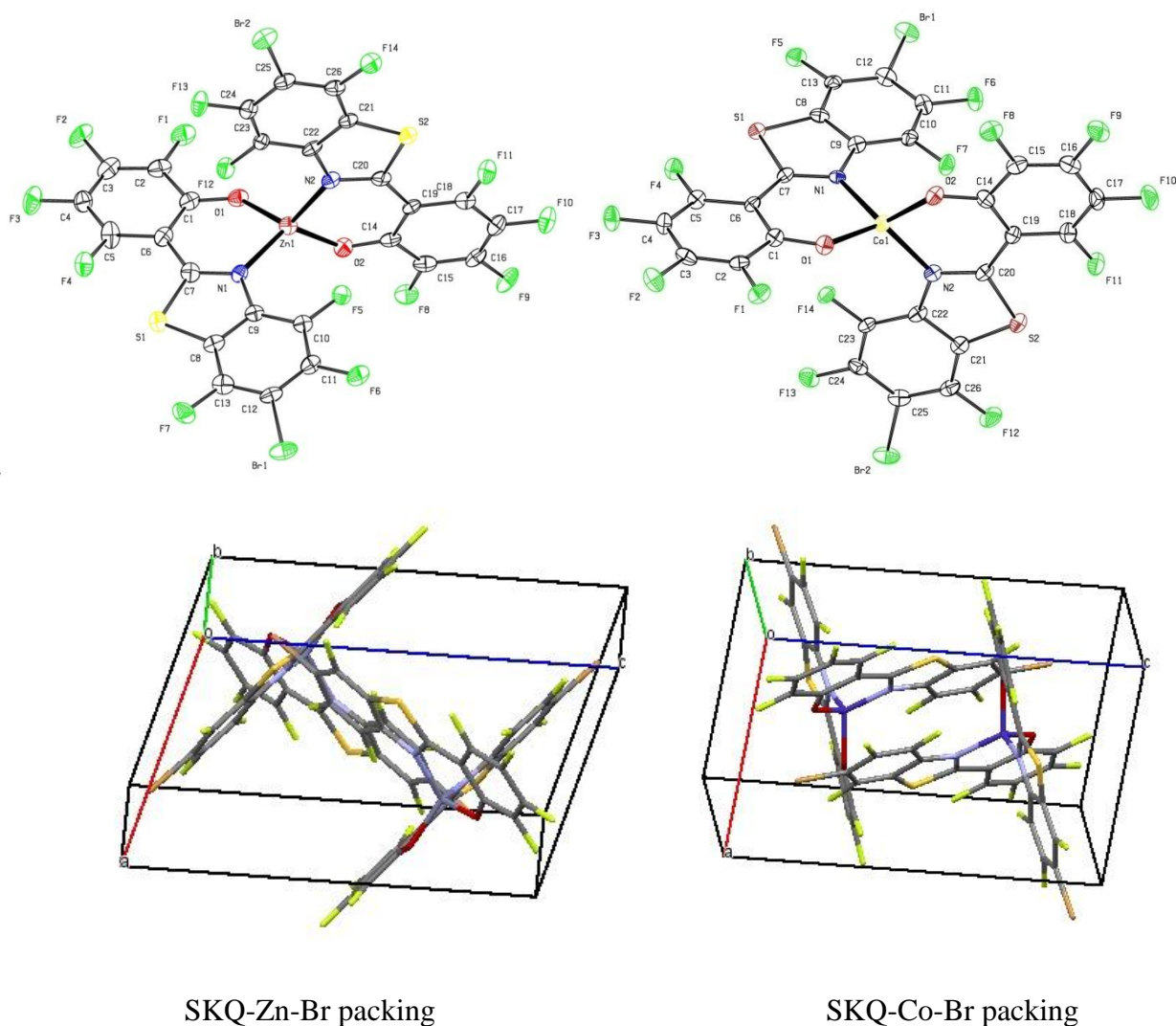
Figure 30. Crystal structure and packing of Co^{2+} and Zn^{2+} complexes

Metal ion is tetracoordinated by two atoms of nitrogen and two atoms of oxygen, forming a tetrahydral structure. The coordination bond distances of N-Zn (N-Co) and O-Zn (O-Co) were lying in range of 2.12-2.13 and 1.95 Ấ, correspondingly. The ligands of the materials are substantially planar and orient almost orthogonally with respect to each other, with bond angles of 121 - 122° between two ligands(N1-

Zn-O2 or N1-Co-O2) and 93-94°in the same ligand (N1-Zn-O1 or N1-Co-O1). The dihedral angles, defined by N-Zn-O plane of one ligand with the respective O and N atoms of the other, were 134-135° (O2-Co(or Zn)-O1-C1) and around 114° (N2-Co(or Zn)-O1-C1), correspondingly. The fluorinated benzothiazole rings are essentially planar, whereas due to coordination the phenol ring of the ligand is slightly distorted. Zn^{2+} and Co^{2+} lie out of plane defined by each ligand with an angle of approximately 17°.

Figure 31. Ground state geometry of SKQZnBr and SKQZnCl.

The ground state geometry of SKQZnBr and SKQZnCl were taken as a model for the Zn complexes and are shown in Figure 31. A distorted tetrahedral geometry of molecules could be clearly observed. Computational calculations are in a good agreement with experimentally measured crystal structures.
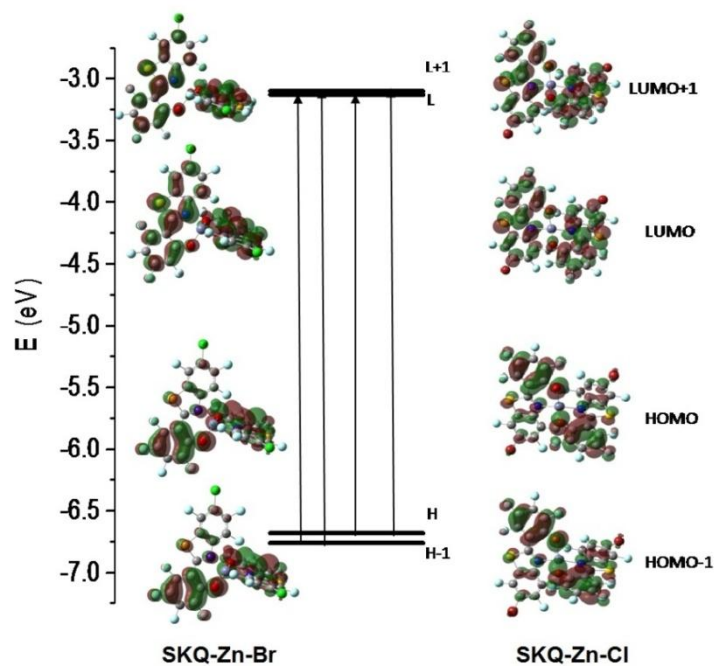
Figure 32. Frontier Kohn Sham Molecular Orbitals

The energy of the frontier orbitals (HOMO-1, HOMO, LUMO, LUMO+1) involved in the low energy absorption is represented in Figure 32, together with the isodensity surface of the selected orbitals (isovalue 0.02).

As expected, metal plays essentially a structural role with negligible contributions to the frontier orbitals which are centered on the ligands. The frontier orbitals consist of two pairs of nearly degenerate orbitals. HOMO and HOMO-1, while being widely delocalized on the organic ligands, show larger lobes on the fluorinated phenol ring and on the oxygen atoms coordinating the metal, whereas a node is present on the bridging carbon atom of the benzothiazole ring, between nitrogen and sulfur. Small lobes of π symmetry are also observed on the bromine substituents. The first two unoccupied orbitals show an increased number of nodes, consistent with their antibonding nature, with an increased density on the benzothiazole ring and on the nitrogen atoms coordinating Zn^{2+}.

The lowest transitions calculated at the TDDFT level (Figure 33) are in good agreement with the experimental spectrum, showing two distinct groups of transitions giving a rise to the two main structure-less bands observed experimentally in DMSO solution. In particular, the four lowest energy transitions constituting the lowest energy absorption band, around 400 nm, are relevant to the photochemical and photophysical properties of the excited state and are significant for the application of these complexes in luminescent devices. These transitions could be described by single excitations of the type HOMO$\rightarrow$LUMO (402.2 nm); HOMO $\rightarrow$ LUMO +1 (397 nm); HOMO-1$\rightarrow$ LUMO (393 nm) and HOMO-1$\rightarrow$LUMO +1 (386 nm) (in case of SKQ-Zn-Br complex). The other remaining high energy transitions are grouped around 315 nm. The Cl substituted Zn complex showed also good agreement with the experimental spectrum with two main bands centered around 400 and 310 nm, with a forbidden gap around 350 nm. With respect to the experimental values the calculation predicts a slight blue shift (ca. 10 nm, 0.055 eV) of the group of low energy transitions and red shift of the higher energy band, grouped at 310 nm (4 eV), with respect to the experimental band located at ca 300 nm (4.13 eV). In complete analogy with the case of the Br substituted complex, the 4 lowest transitions which are of relevance for the Visible-Near UV are characterized by single orbital contributions on the Kohn-Sham basis, involving nearly degenerate frontier orbitals HOMO-1, HOMO, LUMO, LUMO+1 according to the Figure33.

The optical properties are thus dominated by ligand localized π-π* transitions, as it is illustrated by the associated EDDM maps of SKQ-Zn-Br complex, displaying the change in electronic density occurring during a given optical transitions (violet surfaces correspond to depleted electron density and light blue to increased electron density).

SKQ-Zn-Br   SKQ-Zn-Cl
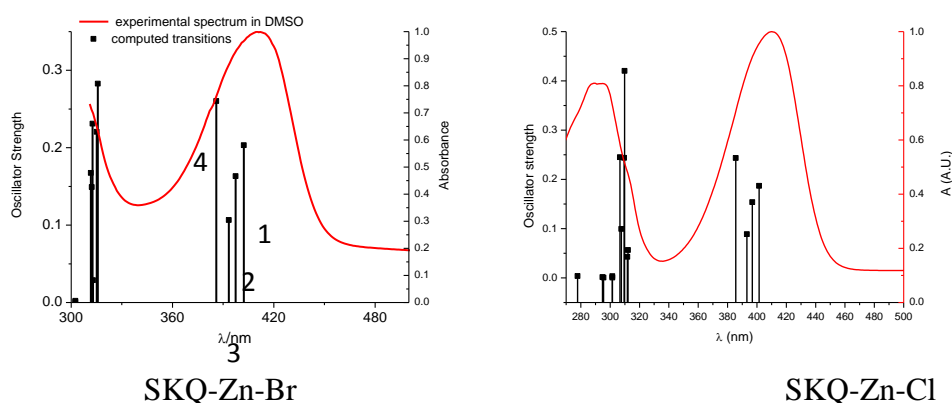
Figure 33. Electronic transitions compared to the experimental spectrum in DMSO.

EDDMS of the lowest transitions are consistent with the molecular orbital picture, where the phenol ring is depleted by electron density and the benzothiazole is enriched. The equilibrium geometry of the first excited singlet (A,B) and triplet (C,D) states are reported in Figure 5.
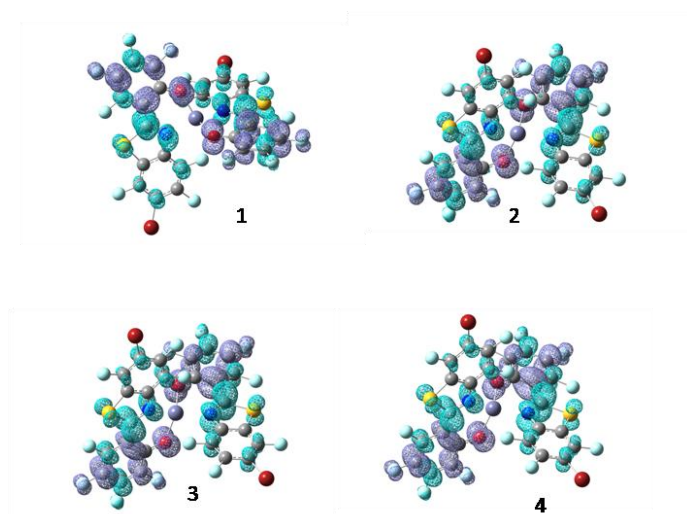
Figure 34. Electron density difference maps of the first lowest 4 transitions.
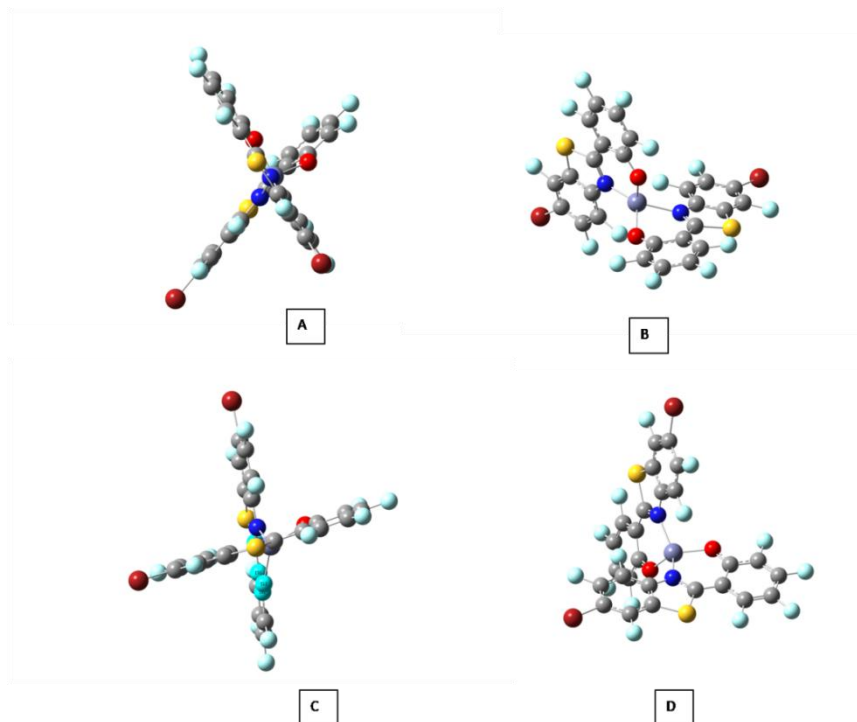
Figure 35 Equilibrium geometry of the singlet and triplet excited states

In the singlet state there is a significant tetragonal distortion of the coordination sphere of Zn^{2+} where one the Zn-O bond become substantially longer (2.1 Å). In addition one of the O-Zn-N bond angles becomes substantially larger and the other comparatively smaller than those found at the ground state (50° and 41°correspondingly). In the triplet state the tetrahedral environment is restored, with a geometry similar to the ground state. However smaller degree of ligands distortion is observed, which are now significantly planarized. This is consistent with the frontier SOMOs (Singly Occupied Molecular Orbitals) showing a large degree of delocalization accompanied by the disappearance of the node in correspondence to the bridging carbon atom in alpha to nitrogen.

The spin density map of the lowest triplet is again consistent with a delocalized ligand centered excited state. Bromine and chlorine atoms are involved in the triplet delocalization and should cause increase in the triplet population via heavy atoms effects.

In view of the calculations, the spectral properties of these emitters are dominated by excited states centered on the ligands. Zn has mainly a structural role in guaranteeing a sufficiently rigid geometry to emphasize the radiative decay over vibrational decay. Distortion in the singlet state indeed involves mainly the coordination environment of Zn, rather than normal modes of the ligands. However, the effect of the substituents on spin orbit should induce triplet population.

SOMO 175   SOMO 176
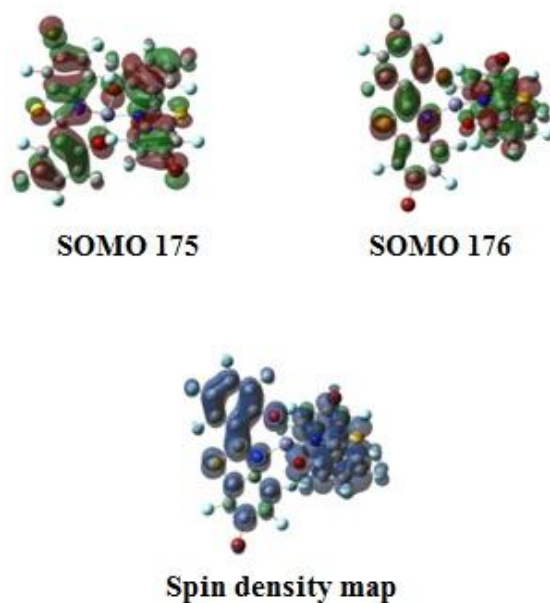
Spin density map

Figure 36. SOMOs and spin density of the lowest triplet state.

Indeed, the calculated first triplet excited state of SKQ-Zn-Br is located at ca. 0.54 eV below the lowest singlet excited state, corresponding to a theoretical vertical emission wavelength of 488 nm, allowing to conclude that the emission arising from the SKQ-Zn family is originated by their triplet excited state (Figure 37).
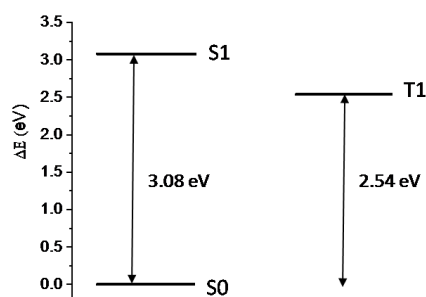
Figure 37. Lowest excited states in SKQ-Zn-Br

Rather different results of computational analysis showed SKQ-Co-Cl emitter. It also possesses a distorted tetrahedral geometry which is in good agreement with the experimental X-ray structure. However, its set of the three highest singly occupied molecular orbitals (177-179 in Figure 38) shows a significant amplitude on the ligands with contributions from d orbitals of cobalt, consistent with a small degree of back bonding from cobalt to π-orbital of the ligands, while the chlorine atoms participates with strong orbital contributions to the SOMO 177. Nearly degenerate lowest virtual orbital 180 (as well as 181) ($\Delta E = 0.03$ eV) is delocalized on both ligands with very minor contributions from both the cobalt center and the chlorine atoms.
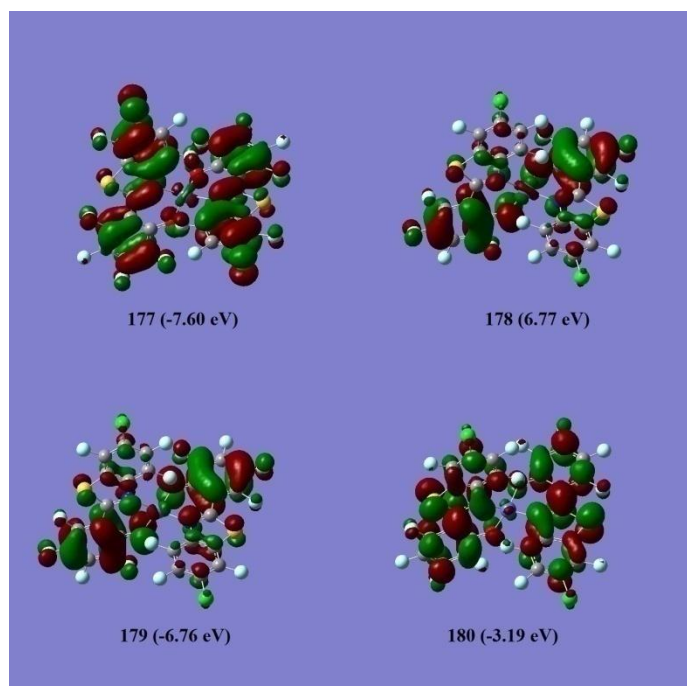
Figure 38. SOMOs of the SKQ-Co-Cl complex

The frontier orbital energy gap between unoccupied orbitals 180-181 and the highest SOMOs 178 and 179 is 3.6 eV, corresponding to an excitation energy for the optical transition at 344 nm, which is clearly an upper estimate to the lowest excited state.

Contrary to the case of Zn complexes, orbitals contributions from the T2 orbitals of cobalt are expected, moreover the small overlap between the d-orbitals of cobalt and the π-orbitals of the ligands are producing transitions. The presence of orbitalic transitions characterized by a small degree of electron density on cobalt may favor spin orbit coupling population with respect to the Zn^{2+} complexes and the population of the triplet state could be feasible. However based on the electron configuration of cobalt, the excited doublet state could be also formed. The planar ligands also favor intermolecular π-interaction at the excited states and the formation of excimers, which will be demonstrated in the next chapter.

3.7. Photoluminescence of the sensitizers in powder

Photoluminescence of the synthesised materials was measured in powder to eliminate possibility of complexes solvation, additional coordination or dissociation in the solvent. Since physical parameters of the light source used in such measurements had significant influence on the population of the triplet states, two different setups operating on OPO and CW lasers were used for data collection.
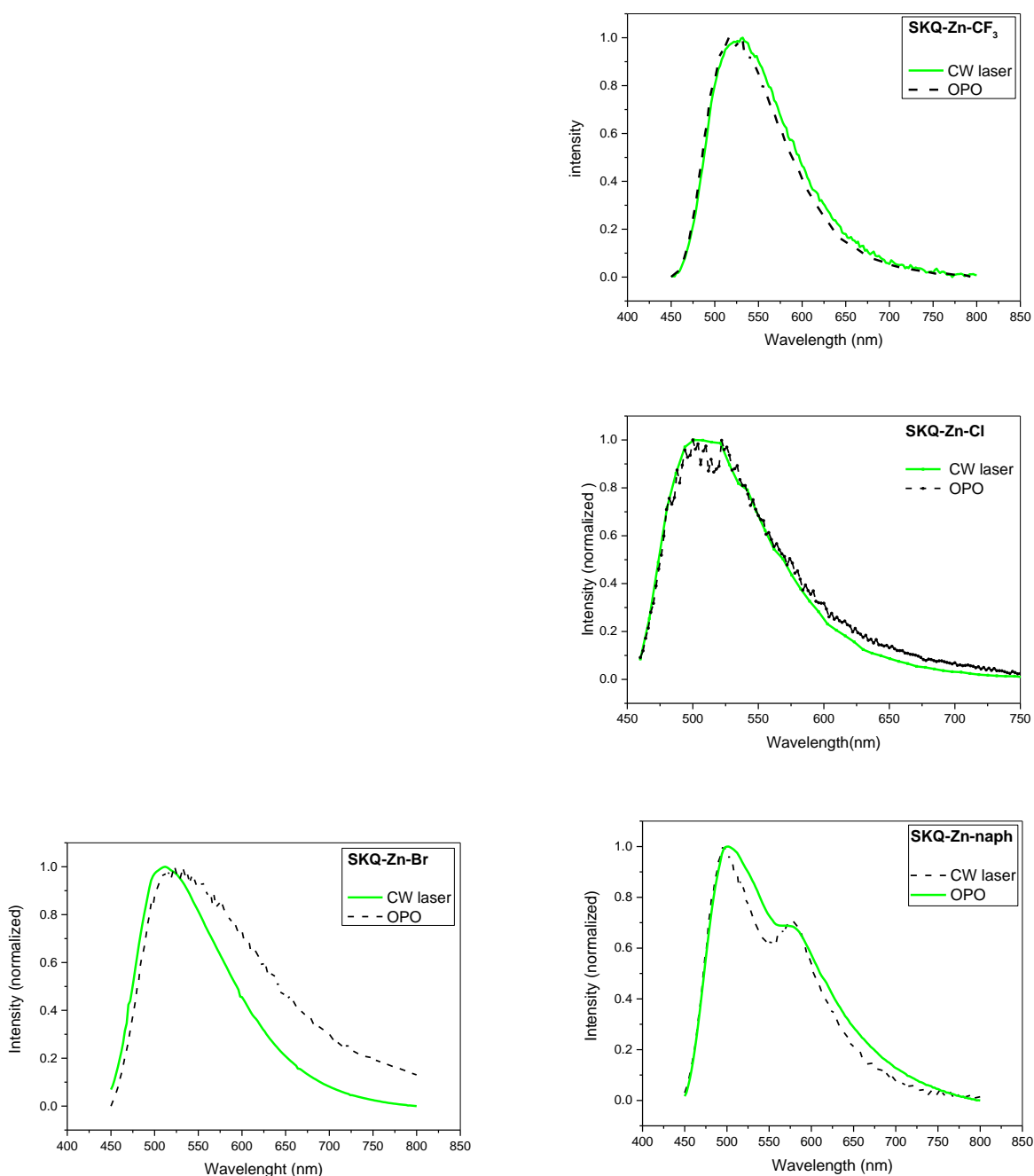
Figure 39. Dependencies in photoluminescence of Zn (II) series

On the one hand, the OPO excited the tested sample with powerful beam of light, therefore, it was expected that generated population of triplets would be large for enough for detection and collection using the setup described in Figure 26. On the other hand, the low power CW laser (Figure 27) has proven to be more efficient in singlet excitation.

Figure 39 presents emission spectra of the designed Zn(II) series of materials tested in both setups. The synthesised SKQ-Zn-CF$_3$ complex and the reference

Zn(BTZ)$_2$ complex show similar behaviour under different excitation conditions. However, with an increase of the substituting halogen atomic weight, the difference between emission spectra became apparent. A particularly vivid pattern was observed in case of Zn (II) complexes with Br-substituted and naphtaline fully fluorinated ligand. Thus, the emission maximum of SKQ-Zn-Br was shifted by 30 nm when excited with a high power source and featured a considerable broadening of the peak and long decay time suggesting formation of a large population of triplet excited states. The SKQ-Zn-naph material under low power excitation conditions had two peaks of the emission (with the maximums at 490 and 570 nm, correspondingly), whereas after excitation with OPO the peak differences have been smoothed forming a single emission peak with much longer decay period.

Another surprising result was observed when experimenting with the Co(II) series of materials. Under the excitation conditions with low power laser and optical oscillator, emission of this series was significantly less bright comparing to the Zn^{2+} compounds. However, the corresponding emission spectra (Figure 40) revealed an interesting pattern in emission peak band. While the Co(II) sensitizer with fully fluorinated BTZ ligand had a maximum at around 490 nm, the next member of the SKQ-Co-Cl series showed a batochromic shift of around 200 nm for the first excitation peak and the second significantly broader excitation peak with the maximum at around 700 nm. It worth noting, that the SKQ-Co-Br series showed a pattern similar to Cl-substituted Co^{2+} complex featuring a broad luminescence with a maximum at around the same 700 nm wavelengths.
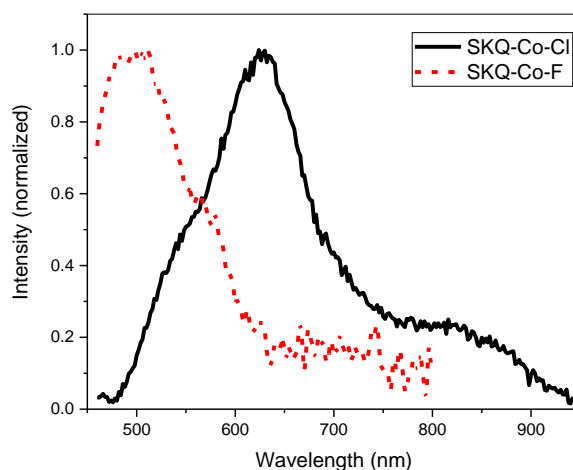
Figure 40. Photoluminescence of SKQ-Co-Cl and SKQ-Co-F complexes

Digging deeper into the cause of this, we hypothesized that the peaks at 700 nm may refer to the signal of triplet. To check this hypothesis, we have conducted a phase modulated experiment for both, the SKQ-Co-Cl and the SKQ series, as follows. If we sinusoidally modulate the excitation intensity, the signal from singlet's and

triplet's excited states also becomes a sinusoid wave. This approach could be described as smooth repetitive oscillation:

$$y(t) = A\sin(2\pi f t + \varphi) = A\sin(\omega t + \varphi),$$

where:

- A is the amplitude.
- F is frequency as the number of oscillations per second of time
- ω the angular frequency
- φ the phase, where the oscillation is at t = 0.

By manual adjusting the phase of the lock-in amplifier during the experiment, we could separately measure a singlet's or triplet's signal. Indeed, by setting up an experiment at 90° to the expected phase of the singlet we obtained a clear signal of the triplet, and vice versa, an experiment with the phase fixed at 90° to the triplet's signal revealed the singlet's peak (Figure 41).
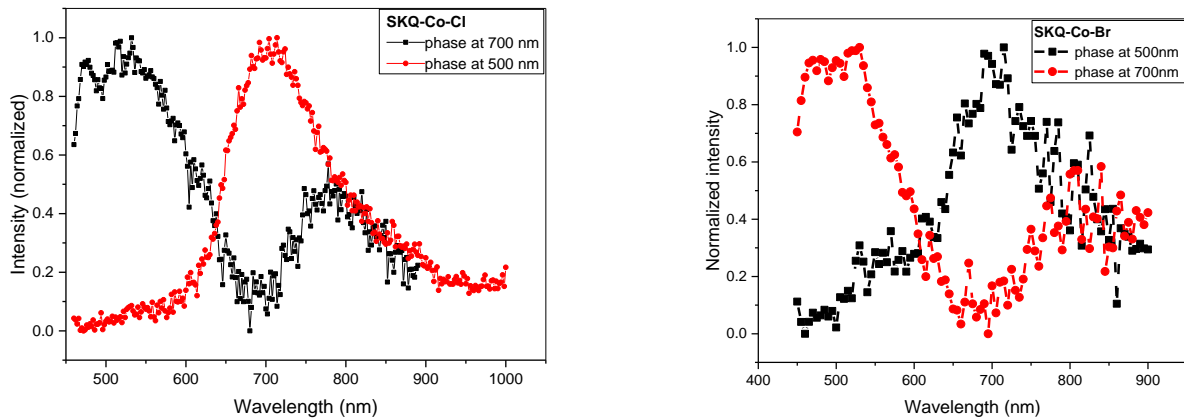
Figure 41. Singlet and triplet excited states of SKQ-Co-Cl and SKQ-Co-Br.

Next, the luminescence lifetime of the synthesised materials was measured in comparison to the instrument response function (RF) which is much faster than the one of the sample. The obtained spectra were further fitted to a bi-exponential decay (Equation (1)) to give the desired lifetime values. The percentage (*w*) of each component was calculated with Equation (2) and (3), whereas the average lifetime τ with Equation (4).

$$\text{1} \qquad I = I_0 + A_1 e^{-[(t-t_0)/\tau_1]} + A_2 e^{-[(t-t_0)/\tau_2]}$$

$$\text{2} \qquad w_1 = \frac{A_1 \tau_1}{A_1 \tau_1 + A_2 \tau_2}$$

$$\text{3} \qquad w_2 = 1 - w_1$$

$$\text{4} \qquad \tau = w_1 \tau_1 + w_2 \tau_2 = \frac{A_1 \tau_1^2 + A_2 \tau_2^2}{A_1 \tau_1 + A_2 \tau_2}$$
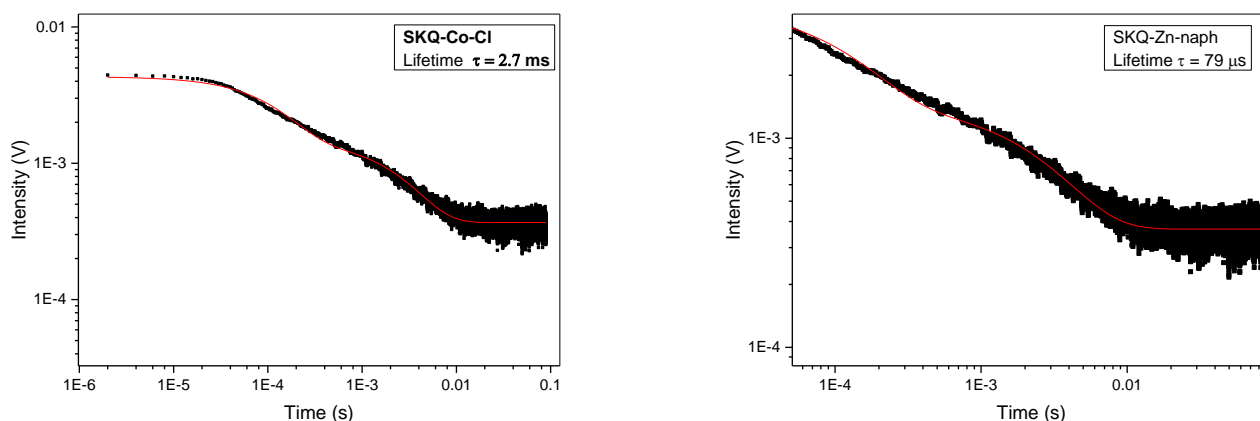
Figure 42. Lifetime of some Co(II) and Zn(II) sensitizers

For efficient lanthanide ion sensitization, the triplet states of the ligand must be closely matched to, or slightly above, the metal ion's emitting resonance levels [15]. The energy could then be transferred from the triplet flows through non-radiative excited states of the metal until it reaches the emissive levels and the metal centred emission occurs. Particularly, Zn(II) series of complexes, which showed the luminescent peak at 500-530 nm, are good candidates to sensitized Er^{3+} ions as their resonance levels match (Figure 43). The SKQ-Co-Cl and SKQ-Co-Br, however, demonstrated the excitation peak at around 700 nm making them potentialsensitizers for Nd^{3+}, Tm^{3+} and Pm^{3+}.
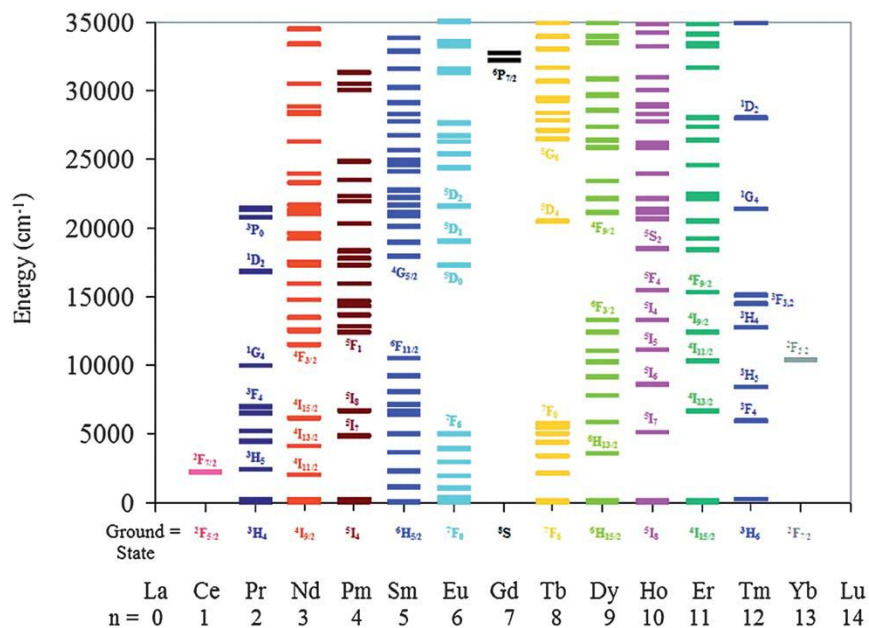
Figure 43. Energy diagrams for Ln^{3+}

3.8. Summary

As a result of the current study, a series of the target ligands with different halogene substituents and conjugation has been synthesised and two series of zinc(II) and cobalt (II) complexes have been successfully prepared and characterised with steady state spectroscopic, crystallographic, and computational analysis.

Further, an X-ray analysis revealed that both Co^{2+} and Zn^{2+} compounds have tetrahedral geometry. The ligands of the materials are substantially planar and orient orthogonally to each other, while metal ion lies out of ligands planes. The UV-visible spectra of Zn^{2+} and Co^{2+} compounds bonding to the same type of ligand were also similar featuring two absorption peaks at 395-425 nm and 225-275 nm wavelengths. However, a 8-40 nm red shift of the absorption band was observed for all newly designed materials in comparison to the reference Zn(BTZ)$_2$ complex.

Despite their similar crystal structures and absorbance in solution, computational calculations revealed differences in HOMO-LUMO levels between Co^{2+} and Zn^{2+} families. In contrast to negligible contributions to the frontier orbitals from zinc atom, cobalt contributions from d orbitals cause strong amplitude on the ligands, whereas the substituent halogen atom participates with strong orbital contributions to singly occupied molecular orbitals resulting in an overall improvement of the spin-orbit mixing and favoring formation of the triplet exciting state under excitation conditions.

Finally, a study of the photoluminescent properties of materials in powder proved the results obtained from calculations. A significant increase in triplet excited

state was observed within Zn^{2+} series of compounds where the biggest triplet population was generated by materials with heavy halogen substituents or prolonged conjugation. In its turn, Co^{2+} series showed photoluminescent maximum at around 700 nm and prolonged lifetime of the triplet excited state of up to 2.7 ms.

These findings bring us to the following conclusion: since Zn(II) series of complexes show a maximum of the photoluminiscene at 500-530 nm they are potentially good candidates to sensitized Er^{3+} ions, whereas SKQ-Co-Cl and SKQ-Co-Br with their excitation peak at around 700 nm are potential sensitizers for Nd^{3+}, Tm^{3+} and Pm^{3+}.

4. Conclusions and future work

1. A series of novel organic dyes for p-type DSSCs was designed, synthesized and characterised using spectroscopic, electrochemical, and computational methods.
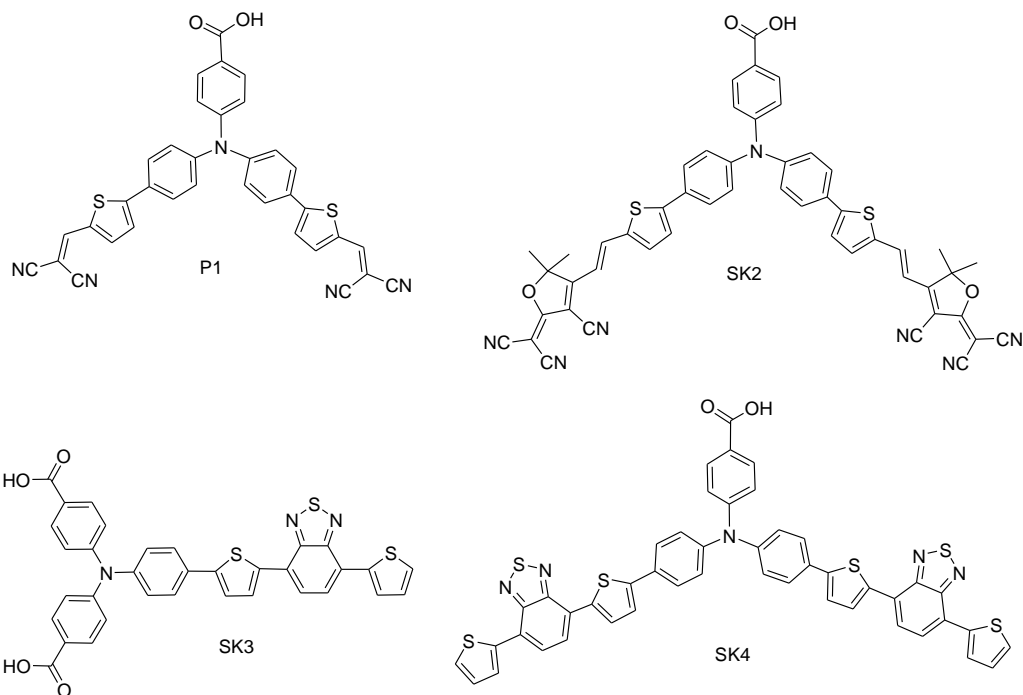
2. All investigated sensitizers showed favourable charge transfer properties for the sensitization of NiO semiconductor. A significant shift of their electron density from the donor core to the acceptor branches allows to promote hole injection in p-type semiconductors such as NiO.

3. The designed organic compounds were used in fabrication of p-type DSSCs. All of the compounds have been successfully applied in sensitized NiO electrodes and provided sufficient photocurrent. Additionally, the SK4 dye has showed increased photovoltage values with respect to the reference dye (P1).

4. A family of fully halogenated ligands and two series of their complexes with Co^{2+} and Zn^{2+} were carefully designed and successfully synthesized.
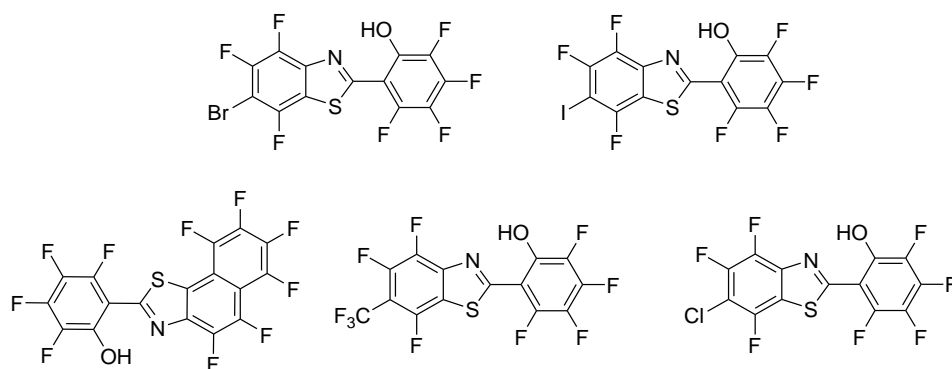
5. The obtained Zn^{2+} complexes featured patterns in crystals structure, absorption in solution etc. similar to the corresponding patterns of the Co^{2+} complexes with the same ligand. A computational study, however, revealed significant differences in contributions to the frontier orbitals and HOMO-LUMO states between zinc and cobalt materials.

6. In photophysical study Zn^{2+} compounds show a maximum of the photoluminescence at 500-530 nm. The excitation becomes broader with increase of the substituent halogen molecular weight, which indicates growth in population of the triplet excited state. Unlike zinc, Co^{2+} materials were emitting at 700 nm and showing prolonged decay of the excited state. Such photo-physical properties make Zn(II) series potentially good candidates to sensitize Er^{3+} ions, whereas Co(II) series can be used to sensitize Nd^{3+}, Tm^{3+} and Pm^{3+} .

7. Since the obtained organic complexes tend to form large population of the triplet excited state, which is very much appreciated for the prolonged sensitization on lanthanide (III) ions, as a future work we plan to grow thin films of suitable fully fluorinated Ln^{3+} complex together with Zn^{2+} or Co^{2+} emitter. This way we aim to get lifetime of the lanthanide excited state on the level of 1-3 ms and further incorporate the best performing material in an organic waveguide.

8. As the results of the current work suggested, substituent groups on the beng manzothiadiazole part of the ligand influence photophysical properties of the resulting material. Therefore, another promising direction for future work we see in developing an alternative series of fully halogenated ligands by putting the substituent groups in the phenoxide ring.
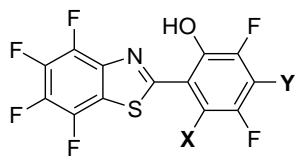
This way we hope to increase the spin-orbital mixing induced by substantial overlapping between molecular orbitals of substituent group and metal and, thus, to endorse formation of the triplet excited state under the excitation conditions.

9. Finally, and motivated by similar considerations, we are planning to design complexes of obtained ligands with heavy trivalent metal, e.g., iridium Ir^{3+} which is known for advanced photoluminescent properties.

List of publications

1. S. Karamshuk, S. Caramori, N. Manfredi, M. Salamone, R. Ruffo, S. Carli, C. A. Bignozzi and A. Abbotto **"Molecular level factors affecting the efficiency of organic chromophores for p-type dye sensitised solar cells"** – in submission to "Dyes and Pigments" journal.

2. S. Karamshuk. J. Hu, S. Caramori, M. Motevalli, P.B. Wyatt and W.P. Gillin, **"Fully halogenated systems for optical amplification of Er^{3+}-Based Infrared Emission at telecommunications wavelengths"** – in preparation.

3. S. Karamshuk. J. Hu, S. Caramori, M. Motevalli, P.B. Wyatt and W.P. Gillin, "Efficient sensitization of lanthanide (III) ions with fully halogenated organic complexes of cobalt (II)" – work in progress.

References

1. Y. Shirota, *J. Mater. Chem.*, 2000, **10**, 1-25.
2. Stephen R. Forrest, *Chem. Rev.* 1997**, 97**, 1793−1896.
3. M. Bass, *HANDBOOK OF OPTICS, Volume I*,1994.
4. B. O'Regan and M. Grätzel, *Nature,*1991, **353**, 737–740.
5. IEA International Energy Agency*, Potential for building integrated photovoltaics*, Report IEA PVPS Task 7, NET Ltd., St. Ursen, Switzerland, 2002.
6. C. Cornaro, S. Bartocci, D. Musella, C. Strati, A. Lanuti, S. Mastroianni, S. Penna, A. Guidobaldi, F. Giordano, E. Petrolati, T. M. Brown, A. Reale, A. D. Carlo,*Prog. Photovolt*: Res. Appl., 2013.
7. S. Mathew, A. Yella, P. Gao, R. Humphry-Baker, F. E. CurchodBasile, N. Ashari-Astani, I. Tavernelli, U. Rothlisberger, M. K. Nazeeruddinand M. Grätzel, *Nature Chem.*, 2014, **6**, 242.
8. E. Mosconi, J.-H. Yum, F. Kessler, C. J. Gomez García, C. Zuccaccia, A. Cinti, M. K. Nazeeruddin, M. Gratzel, F. De Angelis, *J. Am. Chem. Soc.* 2012, **134**, 19438−19453.
9. Y. Ooyama, Y. Harima, *Eur. J. Org. Chem.* 2009, 2903–2934.
10. K. Hara, T. Sato, R. Katoh, A. Furube, Y. Ohga, A. Shinpo, S. Suga, K. Sayama, H. Sugihara, H. Arakawa, *J. Phys. Chem. B*, 2003; **107**, 597.

11. S. Ito, H. Miura, S. Uchida, M. Takata, K. Sumioka, P. Liska, P. Comte, P. Pechy, M. Graetzel, *Chem. Commun.*, 2008, **41**, 5194–5196.
12. D. Kim, J. K. Lee, S. O. Kang, J. Ko, *Tetrahedron*, 2007; **63**, 1913-1922.
13. C. Qin, W. Peng, K. Zhang, A. Islam and L. Han, *Org. Lett.,* 2012; **14**, 2532–2535.
14. Y. Numata, I. Ashraful, Y. Shirai and L. Han, *Chem. Commun.*, 2011; **47**, 6159–6161.
15. S. Y. Qu, C. J. Qin, A. Islam, Y. Z. Wu, W. H. Zhu, J. L. Hua, H. Tian and L. Y. Han, *Chem. Commun.*, 2012; **48**, 6972–6974.
16. M. A. Green, *Third Generation Photovoltaics: Advanced Solar Energy Conversion*; Springer-Verlag: Berlin, Heidelberg, 2003.
17. A. Hagfeldt, G. Boschloo, L. Sun, L. Kloo and H. Peterssen, *Chem. Rev.* 2011, **110**, 6595.
18. D.R. Lide, *Handbook of Chemistry and Physics*, 90th ed., C. Press, 2010.
19. F. Odobel, Y. Pellegrin, E.A. Gibson, A. Hagfeldt, A. L. Smeigh and L. Hammarstrom, *Coord. Chem. Rev.,*2012, **256**, 2414.
20. M. Radziwon, A.L.F. Cauduro, M. Madsen, H.-G. Rubahn, *Journal of Nanomaterials*, vol. 2014, **6**.

21. Kim, S.; Lee, J. K.; Kang, S. O.; Ko, J.; Yum, J. -H.; Fantacci, S.; Angelis, F. D.; Di Censo, D.; Nazeeruddin, M. K.; Grätzel, M. *J. Am. Chem. Soc.* **2006**, *128*, 16701–16707.

22. Qin, H.; Wenger, S.; Xu, M.; Gao, F.; Jing, X.; Wang, P.; Zakeeruddin, S. M.; Grätzel, M. *J. Am. Chem. Soc.* **2008**, *130*, 9202–9203.

23. Shirota, Y. *J. Mater. Chem.* **2000**, *10*, 1–25..

24. M.J. Connolly, *Semiconductor Optical Amplifiers, Boston*, MA Springer-Verlag, 2002

25. R. H. Stolen and E. P. Ippen, *Appl. Phys. Lett.*, 22, **276** (1973)

26. Curry, R. J.; Gillin, W. P. *Appl. Phys. Lett.* 1999, **75,** 1380.

27. Bünzli, J.-C. G. *Accounts Chem. Res.* 2005, **39,** 53.

28. Kido, J; Okamoto, Y. *Chem. Rev.*, 2002, **102**, 2357.

29. Crosby, GA; Whan, RE; Alire, RM. *J. Chem. Phys.*, 1961, **34**, 743.

30. Bhaumik, ML; El-Sayed, MA. *J. Phys. Chem.*,1965, **69**, 275.

31. Van der Meer, BW; Coker, G; Chen, SYS. *Resonance Energy Transfer Theory and Data*, Wiley-VCH, New York, 1994.

32. Dexter, DL. *J. Chem. Phys.*, 1953, **21**, 836.

33. Forster, T. *Discuss. Faraday Soc.*, 1959, **27**, 7; Forster, T. *Annalen der Physik 2,* 1948 55, English translation (1993).

34. Chen, B; Yang, Y; Zapata, F; Qian, G; Luo, Y; Zhang, J; Lobkovsky, EB. *Inorganic Chemistry*, 2006, **45**(22), 8882.

35. H. Zhu, A. Hagfeldt and G. Boschloo, *J. Phys. Chem. C*, 2007, **111**, 17455.

36. M. Borgstrom, E. Blart, G. Boschloo, E. Mukhtar, A. Hagfeldt, L.Hammarstromand, and F.Odobel, *J. Phys.Chem.B*, 2005, **109**, 22928.

37. E. A. Gibson, A. L. Smeigh, L. Le Pleux, J. Fortage, G. Boschloo, E. Blart, Y. Pellegrin, F. Odobel, A. Hagfeldt and L. Hammarström, *Angew. Chem., Int. Ed.*, 2009, **48**, 4402.

38. A. Morandeira, G. Boschloo, A. Hagfeldt and L. Hammarstrom, *J. Phys. Chem. C*, 2008, **112**, 9530.

39. Nattestad, A.; Mozer, A. J.; Fischer, M. K. R.; Cheng, Y.-B.; Mishra, A.; Bäuerle, P.; Bach, U. *Nature. Mater.* 2010, **9**, 31–35.

40. P. Qin, H. Zhu, T. Edvinsson, G. Boschloo, A. Hagfeldt and L. Sun, *J. Am. Chem. Soc.,* 2008, **130**, 8570.

41. A. Abbotto, N. Manfredi, C. Marinzi, F. De Angelis, E. Mosconi, J. H. Yum, X. X. Zhang, M. K. Nazeeruddin and M. Gratzel, *Energy Environ. Sci.*, 2009, **2**, 109.4

42. A. Abbotto, V. Leandri, N. Manfredi, F. De Angelis, M. Pastore, J. H. Yum, M. K. Nazeeruddin and M. Gratzel, *Eur. J. Org. Chem.*, 2011, **6195**.

43. N. Manfredi, B. Cecconi and A. Abbotto, *Eur. J. Org. Chem.*, 2014, **7069**.

44. A. Nattestad, A. J. Mozer, M. K. R. Fischer, Y.-B. Cheng, A. Mishra, P. Bäuerle and U. BachNature Mater.,2010, **9**, 31.

45. b) X.L. Zhang, Z. Zhang, D. Chen, P. Bäuerle, U. Bach and Y.-B. Cheng, *Chem. Commun.*, 2012, **48**, 9885.

46. A. Baheti, P. Tyagi, K. R. J. Thomas, Y. C. Hsu and J. T. Lin, J. *Phys. Chem. C*, 2009, **113**, 8541–8547.

47. L. Cai, H. N. Tsao, W. Zhang, L. Wang, Z. Xue, M. Graetzel, B. Liu, *Adv. Energy Mater.,* 2012, **3**, 200–205.

48. I. Jung, J. K. Lee, K. H. Song, K. Song, S. O. Kang, J. Ko, *J. Org. Chem.*, 2007, **72**, 3652–3658.

49. G. Melikian, F. P. Rouessac and C. Alexandre, *Synth. Commun.*, 1995, **25**, 3045.

50. A. Yassara, C. Videlotb and A. Jaafari, *Sol. Energy Mater. Sol,* 2006, **90**, 916–922

51. W.C. Barrette, H.W. Johnson and D.T. Sawyer, *Anal. Chem.,* 1984, **56**, 1890

52. J. O. M. Bockris and S. U. M. Khan, *Surface Electrochemistry.*

53. W. Wu, J. Yang, J. Hua, J. Tang, L. Zhang, Y. Long and H. Tian, *J. Mater. Chem.*, 2010, **20**, 1772.

54. A. Scrascia, M. Pastore, L. Yin, R. A. Picca, M. Manca, Y.-C. Guo, F. De Angelis, F. Della Sala, R. Cingolani, G. Gigli and G. Ciccarella, *Curr. Org.Chem.,* 2011, **15**, 3535.

55. b) M. Mba, M. D'Acunzo, P. Salice, T. Carofiglio, M. Maggini, S. Caramori, A. Campana, A. Aliprandi, R. Argazzi, S. Carli, and C. A. Bignozzi, J. *Phys. Chem. C*, 2013, **117**, 19885.

56. Z. Ji, G. Natu, Z. Huang and Y. Wu, *Energy Environ. Sci.*, 2011, **4**, 2818.

57. X. Qian, Y.-Z. Zhu, J. Song, X.-P. Gao and J.-Y. Zheng, *Org. Lett.,* 2013, **15**, 6034.

58. P. Qin, J. Wiberg, E.A. Gibson, M. Linder, L. Li, T. Brinck, A. Hagfeldt, B. Albinsson and L. Sun, *J. Phys. Chem. C,* 2010, **114**, 4738;

59. A. Nattestad, A. J. Mozer, M. K. R. Fischer, Y.-B. Cheng, A. Mishra, P. Bäuerle and U. Bach *Nature Mater,* 2010, **9**, 31.

60. G.A. Petersson, H. Nakatsuji, M. Caricato, X. Li, H. P. Hratchian, A. F.Izmaylov, J. Bloino, G. Zheng, J. L. Sonnenberg, M. Hada, M. Ehara, K. Toyota, R. Fukuda, J. Hasegawa, M. Ishida, T. Nakajima, Y.Honda, O. Kitao, H. Nakai, T. Vreven, J. A. Montgomery, Jr., J. E.Peralta, F. Ogliaro, M. Bearpark, J. J. Heyd, E. Brothers, K. N.Kudin, V. N. Staroverov, R. Kobayashi, J. Normand, K.Raghavachari, A. Rendell, J. C. Burant, S. S. Iyengar, J. Tomasi, M.Cossi, N. Rega, J. M. Millam, M. Klene, J. E. Knox, J. B. Cross, V.Bakken, C. Adamo, J. Jaramillo, R. Gomperts, R. E. Stratmann, O.Yazyev, A. J. Austin, R. Cammi, C. Pomelli, J. W. Ochterski, R. L.Martin, K. Morokuma, V. G. Zakrzewski, G. A. Voth, P. Salvador, J.J. Dannenberg, S. Dapprich, A. D. Daniels, Ö. Farkas, J. B.Foresman, J. V. Ortiz, J. Cioslowski, and D. J. Fox, *Gaussian, Inc.,* Wallingford CT, revision A.02.,2009.

61. J. Autschbach, *ChemPhysChem,*2009, **10**, 1757.

62. T. Ziegler,M. Seth, M. Krykunov, J. Autschbach and F. Wang, *J. Molec. Struct.: THEOCHEM*, 2009, **14**, 106.

63. A.D. Becke*, J. Chem.Phys.*, 1993, **98**,5648.

64. A.D. Becke, *J. Chem.Phys*, 1993,**98**, 1372.

65. W. Koch and M. Holthausen*, A Chemist's Guide to Density Functional Theory*, 2001, 2nd Volume, Wiley-VCH, Weinheim.

66. B. A. Gregg, *J. Phys. Chem. B,* 2003, **107**, 4688.

67. C.-G. Zhen, U. Becker and J. Kieffer, *J. Phys. Chem. A,*2009, **113,**9707.

68. V. L.Ermolaev, E. B. Sveshnikova, *Russ. Chem. Rev.* **1994**, *63*, 905.

69. Englman, R.; Jortner, J. *Mol. Phys.* **1970**, *18*, 145.

70. Y.-W. Shi, M.-M. Shi, J.-C. Huang, H.-Z. Chen, M. Wang; X.-D. Liu, Y.-G.Ma; H. Xu, B. Yang, *Chemical Communications* **2006**, *0*, 1941.

71. S. K. Lower; M. A. El-Sayed, *Chem. Rev.* **1966**, *66*, 199.

72. H.-Q. Ye, Y. Peng, Z.Li, C.-C. Wang, Y.-X. Zheng, M. Motevalli, P.B. Wyatt, W.P. Gillin and I.Hernández, *J. Phys. Chem. C*, **2013**, *117*(45), pp 23970-23975.

73. B. L. Chen,; Yang, Y.; Zapata, F.; Qian, G. D.; Luo, Y. S.; Zhang, J. H.;Lobkovsky, E. B. Inorg Chem **2006**, 45, 8882.

74. Glover, P. B.; Bassett, A. P.; Nockemann, P.; Kariuki, B. M.; Van Deun, R.;Pikramenou, Z. Chem-Eur J **2007**, 13, 6308.

75. R.V. Deun, P. Fias, K. Driesen, K. Binnemans and C. Gorller-Walrand, Phys. Chem. Chem. Phys., 2003, 5, 2754–2757

76. Y. Peng, H. Ye; Z.Li, M. Motevalli, I. Hernández, W. P. Gillin; P.B Wyatt, .Journal of Physical Chemistry Letters 2014, **5**, 1560-1563.

77. H. Q. Ye, Z. Li, Y. Peng, C. C. Wang, T. Y. Li, Y. X. Zheng; A. Sapelkin, , G Adamopoulos; I. Hernandez, P. B. Wyatt, W.P. Gillin, *Nat. Mater*. 2014, **13**, 382.

78. S. Sivakumar and M. L. P. Reddy, J. Mater. Chem**.**, 2012,**22**, 10852-10859.

79. A. Mech, A. Monguzzi, F.Meinardi; J.Mezyk, G.Macchi; R. Tubino, J.Am. Chem. Soc. 2010, **132**, 4574.

80. J. Zaumseil and H. Sirringhaus, Chem. Rev. 2007, 107, 1296−1323.

81. F. Li, H. Tang, J. Anderegg and J. Shinar, Appl. Phys. Lett., **70**, 1977, 1233.

82. I. T. Bazyl; S. P. Kisil, Y. V. Burgart; V. I. Saloutin, O. N. Chupakhin, *Journal of Fluorine Chemistry***,** 1999, **94**, 11.

83. H. H. Wenk and W. Sander, *Angew. Chem. Int. Ed*. 2002, **41**.

84. O.S. Bushuyev, A. Tomberg, T. Friščič ́, and Christopher J. Barrett* *J. Am. Chem. Soc.*, 2013, **135**.

85. Selivanova; Pokrovskii; Shteingarts, Russian Journal of Organic Chemistry, 2001 **, 37**.

86. K. Rajesh, M. Somasundaram, R. Saiganesh, K. K. Balasubramanian, J. Org. Chem., 2007, **72**.

87. H. Yagi and D.M. Jerina, *J. Am. Chem. Soc.*, 1975, **97**.

88. T.A. Vaganova *et al.*, *Journal of Fluorine Chemistry,* 2008, **129**.

89. D. Voss, *Nature* **407**, 442-444.

90. G. Calogero, , G.D. Marco, *Solar Energy Materials & Solar Cells* ,**92,** 2008.

91. D. M. Yebra, S. Kiil∗, K. Dam-Johansen, *Progress in Organic Coatings* , **50**, 2004.

APPENDIX

ARTICLE TYPE

Molecular level factors affecting the efficiency of organic chromophores for p-type dye sensitised solar cells

Svitlana Karamshuk,[a] Stefano Caramori,[*,b] Norberto Manfredi,[a] Matteo Salamone,[a] Riccardo Ruffo,[a] Stefano Carli,[b] Carlo A. Bignozzi[b] and Alessandro Abbotto[*,a]

A series of mono- and di-branched donor-π-acceptor (D-π-A) charge-separated dyes incorporating a triphenyl-amine core as a donor group and either Dalton or benzothiadiazole fragments as acceptor groups was synthesized and characterized with the aim of understanding their fundamental properties [10] relevant to the sensitization of nanocrystallineNiO. The dyes exhibited an intense visible absorption band with a strong charge transfer character favorable to the sensitization of NiO electrodes, shifting the electron density from the donor core to the acceptor branches. Nevertheless the associated exciton binding energy, evaluated by DFT, was found ca. twice that of a known literature standard (P1) (0.35 eV vs 0.17 eV) suggesting a more difficult charge separation in the new dye architectures. When tested in p-[15] type dye-sensitized solar cells the new dyes were found to successfully sensitize NiO electrodes, resulting in photocurrent densities about half than that of the reference dye. Being recombination kinetics comparable, the larger photocurrent generated by P1 agrees with a superior charge separation capability originating by its smaller exciton binding energy.

Introduction

[20] With the increasing demand of clean, secure, cost-effective, and renewable energy sources, the exploitation of solar light as a major source has clearly emerged as a key strategic priority. Following the first publication of Grätzel and O'Regan in1991,[1] dye-sensitized solar cells (DSSCs) were recognized as a relatively [25] cheap and easy-to-scale approach to direct solar-to-electrical power conversion. Furthermore, their transparency, versatile design and wide colour palette offer unique structural and architectural possibilities in the emerging field of building integration,[2a,b] for example through the realization of [30] photovoltaic windows and façades. The key feature of DSSCs is the sensitization of a porous wide-band-gap semiconductor thin film with a photoactive dye which, following excitation, is able to transfer either electrons (n-type sensitization) or holes (p-type sensitization) to a semiconductor substrate. n-type DSSCs have [35] been intensively investigated over the last two decades, recently reaching optimized power conversion efficiencies up to 13% with a single photoactive junction (dye/n-TiO$_2$).[3] Despite these recent progresses, power conversion efficiencies in n-type DSSCs seem to have reached a plateau urging to look for new viable [40] approaches to further increase DSSCs efficiencies. A particularly promising strategy to produce DSSCs with significantly enhanced power conversion efficiencies is the connection of an n-type photoelectrode (n-dye/TiO$_2$) with a p-type photoelectrode(p-dye/NiO), affording a tandem cell composed by two serially [45] connected photoactive electrodes, each contributing to the total

photovoltage delivered by the cell. Applying such a concept organic-based photovoltaic devices with up to 40% conversion efficiency could be theoretically achievable.[4] Unfortunately, until now, sensitized p-type systems have been so far much less [50] investigated and much lower photocurrents, compared to their n-type counterparts, have been reported.[5] One of the main limitations in p-type systems, commonly based on NiO as a hole semiconductor,[6] arises from the fast charge recombination[7] between the photoinjected hole in NiO and the reduced dye. [55] Therefore, it is essential to develop new p-type chromophores which could produce a long-lived charge separated state and minimize back recombination.

Several families of p-type dyes have been so far synthesised for this purpose. Those based on coumarin, porphyrin and [60] peryleneimide scaffolds showed incident monochromatic photon-to-current conversion efficiencies(IPCE) only up to 4% and overall efficiencies lower than 0.2%.[8a,b,c,d] One of the best examples of improved charge separation through dye design is represented by push-pull systems based on a D-π-A (donor-π-[65] spacer-acceptor) structures, like P1, firstly reported in 2008 by Sun and co-workers.[9] This prototypical p-type dye had a carboxylic anchoring group on the triphenylamine donor part bridged to dicyanovinyl acceptor by thiophene acting as a π-linker. Along the same general and successful principles, more [70] complex dyes based on much more elaborated triphenylamine/oligothiophene dyes have soon followed.[10] Nevertheless, even in the best cases, the power conversion efficiencies obtained by p-type sensitizers are still about one order of magnitude lower than then the average efficiency

delivered by n-type devices.

We were thus triggered to explore new different structures for potentially efficient chromophores for p-type devices, by considering that the intramolecular charge transfer, at the basis of efficient charge separation in donor-acceptor dyes, is strongly dependent on the electron-withdrawing ability of the acceptor. We have therefore designed and investigated new p-type dyes where P1-like structures have been optimized by inserting stronger and more efficient electron-acceptor groups compared to the conventional dicyanovinyl moiety. Firstly, we have designed the SK2 dye, where the dicyanovinyl group of P1 has been replaced by the much stronger 3-cyano-2-(dicyanomethylene)-4,5,5-trimethyl-2,5-dihydrofuran (Dalton's acceptor) group, widely used in other materials science fields.[11] Secondly, mono-

and di-branched dyes (SK3 and SK4) characterized by a D- π-A-π architecture were realized. In the latter dyes, an additional benzothiadiazole-based acceptor-spacer unit was introduced both in linear (SK3) and branched (SK4) geometrical motifs for the manifold purpose of increasing the transition dipole moment, improving the spatial separation between hole and electron, and favouring the electron transfer to the electron mediator (I^-/I_3^-), resulting in improved interfacial charge separation.

Herein, we report the synthesis of the new p-type chromophores as well as their computational, electrochemical and photoelectrochemical properties in comparison with the literature standard P1. We have investigated the new dyes as p-type sensitizers in p-type DSSC and the results were compared with the reference dye P1.
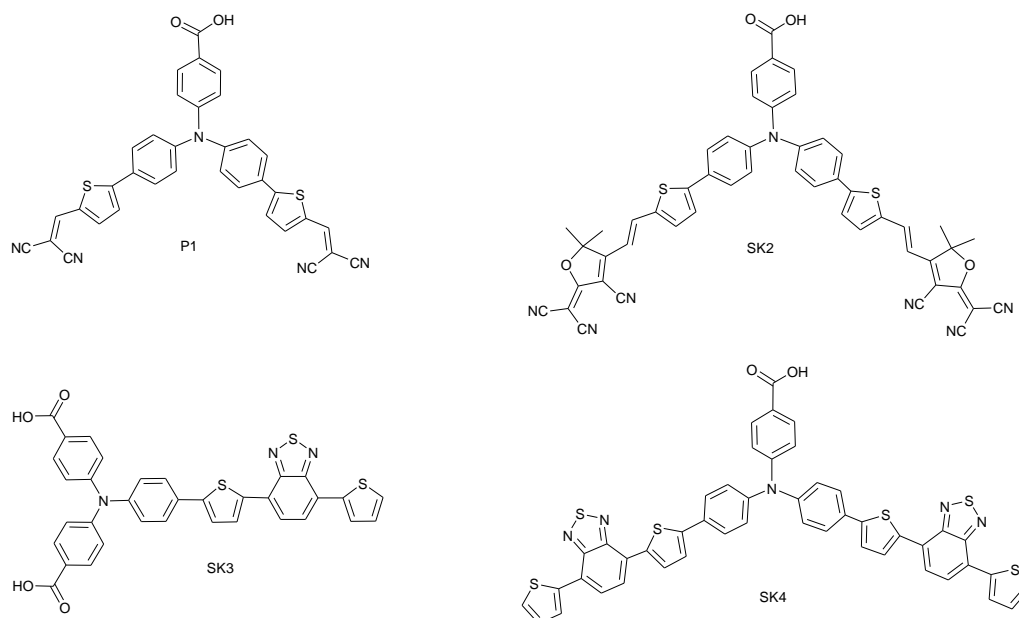
Figure 1. Structure of the investigated and reference (P1) dyes.

Results and discussion

Synthesis

SK2, SK3 and SK4 were obtained following a synthetic pathway shown in Scheme1.4-[Bis-(4-bromophenyl)amino]benzaldehyde (**1**) was oxidized to the corresponding benzoic acid **2** by standard silver mirror reaction and then submitted to the Suzuki coupling with 5-formyl-2-thienylboronic acid for introducing the two thienyl linkers.[9]Knoevenagel reaction between the resulting bis-aldehyde **3** and 2-(3-cyano-4,5,5-trimethylfuran-2(5*H*)-ylidene)malononitrile afforded the desired chromophore SK2. It should be noted that the Knoevenagel condensation of **3** could be successfully accomplished only in acidic conditions at relatively high temperatures (>75 °C), while the reaction under conventional basic conditions (piperidine/EtOH) did not afford the condensation product, likely for the presence of the terminal COOH substituent on the donor core.

Preparation of SK3 and SK4 started from bromination of 4,7-di(thiophen-2-yl)benzo[c][1,2,5]thiadiazole (**4**) to the mono-bromide **5** using *N*-bromosuccinimide (NBS) in presence of a 1:1 solution of CH_2Cl_2 and acetic acid.[12] Since such reaction gave mono- and di-substituted products possessing close polarities, the separation of these two compounds by column chromatography had to be performed with care in order to afford the mono-derivative in moderate yields. Borination of **5** with bis(pinacolato)diboron resulted in the key intermediate boronic ester **6.** Different reaction conditions (solvent, base, temperature) were investigated for Suzuki condensation between **6** and triphenylamine derivatives. The best choice in both cases was dimethoxyethane (DME) as a solvent and aqueous solution of K_2CO_3 as a base. Under these conditions the coupling reaction started immediately after mixing up the reagents and within a considerably short time afforded the desired targets **7** and **8** with fairly good yields. SK3 and SK4 were then obtained by following the previously described procedure for SK2.
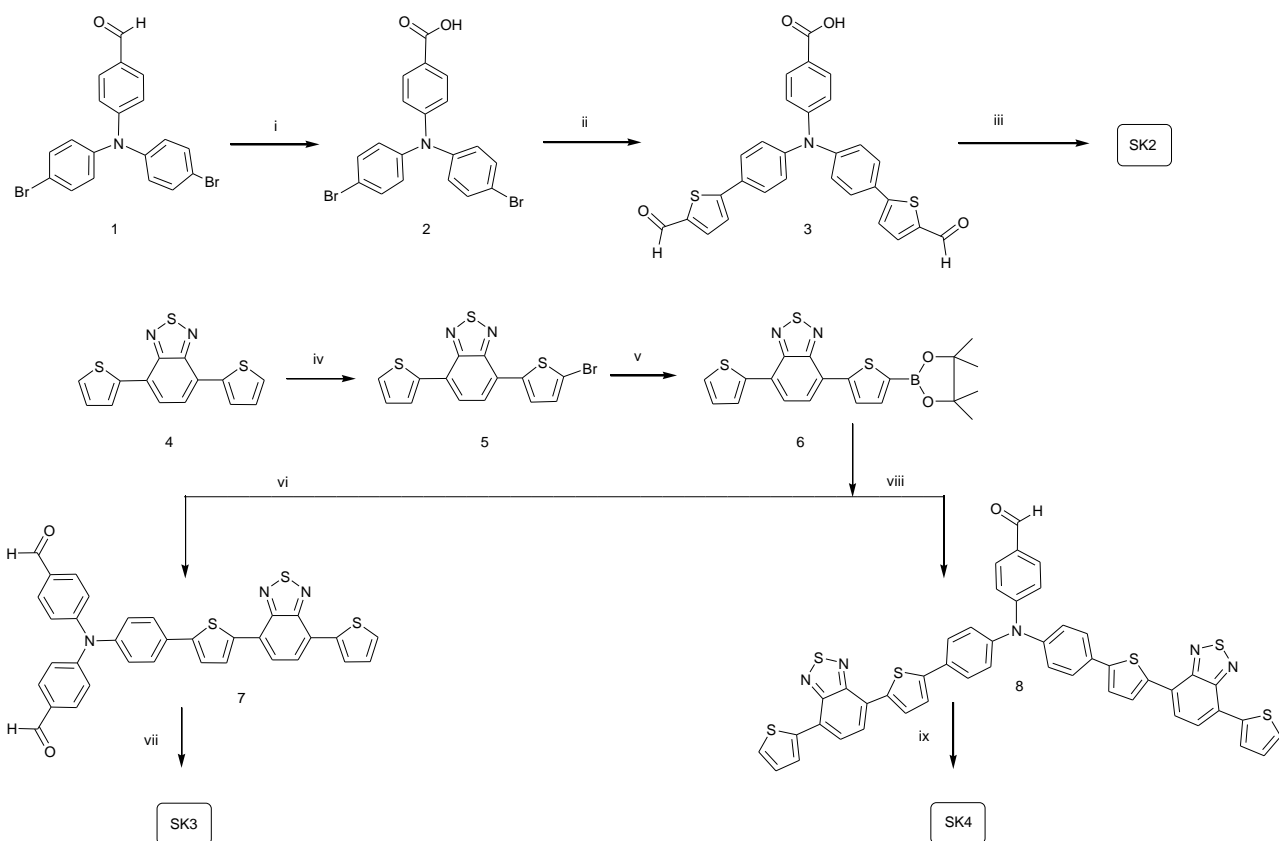
Scheme 1. Synthesis of SK2, SK3 and SK4. Reagents and conditions: (i) Ag$_2$O, EtOH, NaOH, r.t.; (ii) Pd(dppf)Cl$_2$, 5-formyl-2-thienylboronic acid, K$_2$CO$_3$, toluene/MeOH, microwave; (iii) 2-(3-cyano-4,5,5-trimethylfuran-2(5H)-ylidene)malononitrile, NH$_4$OAc/AcOH, EtOH, reflux; (iv) NBS, CH$_2$Cl$_2$/AcOH, r.t.; (v) bis(pinacolato)diboron, Pd(dppf)Cl$_2$, KOAc, dioxane, reflux; (vi) 4-bromo-N,N-bis(4-formylphenyl)aniline, Pd(dppf)Cl$_2$, aq. K$_2$CO$_3$, DME, reflux; (vii) Ag$_2$O, EtOH, NaOH, r.t.; (viii) 4-(bis(4-bromophenyl)amino)benzaldehyde, Pd(dppf)Cl$_2$, aq. K$_2$CO$_3$, DME, reflux; (ix) Ag$_2$O, EtOH, NaOH, r.t.

Spectroscopic and Electrochemical Properties

The absorption spectra of SK2, SK3 and SK4 in DMSO are depicted in the Figure 2 together with that of the reference dye P1. All dyes under investigations exhibited similar general spectral features, summarized by two intense ($\varepsilon > 3 \times 10^4$ M^{-1}cm^{-1}) relatively broad absorption bands extending the light harvesting up to 700 nm in the case of SK2, where the presence of an efficient intramolecular charge transfer to the strong electron-withdrawing groups resulted in a significant bathochromic shift (ca. 70 nm) of the visible absorption maximum.
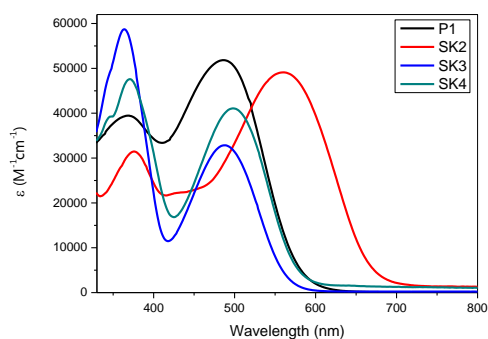
Figure 2. Absorption spectra of P1, SK2, SK3 and SK4 in DMSO.

SK3, SK4, and P1 are ca. 100 nm blue-shifted with respect to SK2, showing a visible absorption maximum at 480-490 nm and an absorption onset at ca. 600 nm. In all cases the second band is located in the UV region, with an absorption peak in the interval 350-370 nm, where SK3 and his di-branched analogue SK4, incorporating the same donor-acceptor side arm, showed the sharpest and most intense band. The main optical and electrochemical parameters together with HOMO/LUMO energies estimated by cyclic voltammetry in 0.1 M TBAClO$_4$ in DMSO are collected in Table 1.

As often observed with organic D-π-A dyes,[16a,b] the electrochemical behaviour (Figure S2, Supporting Information) of the series under investigation is dominated by irreversible processes which complicate a rigorous thermodynamic evaluation of the redox levels relevant to NiO sensitization. At anodic potentials, all chromophores presented a similar oxidation behaviour resulting in an irreversible wave having a peak potential at ca. 0.5 V vs Fc$^{+/0}$ which is related to the oxidation of the electron-rich TPA group.[17] The reductive behaviour is generally more complex and not well defined, showing multiple weak irreversible waves probably originated by electrochemical-chemical processes. Therefore we preferred to estimate the LUMO energy by subtracting the HOMO energy from the spectroscopic energy gap (E^{00}) (Figure S3, Supporting Information).[18] In agreement with the structural similarity of their acceptor group, SK3 and SK4 showed close LUMO energies at -

3.5 eV. This estimate is in reasonable agreement with the quasi-reversible wave observed at -1.55 V vs Fc[+/0]. The reduction of SK2 dye, bearing a stronger acceptor group, is comparatively more anodically shifted with a lower energy LUMO at -3.8eV.Thus, no thermodynamic limitation to hole transfer to NiO are expected: in all cases the HOMO energies are similar to the P1 dye and sufficiently lower than the upper valence band edge of NiO, located at 0.5 – 0.6 V vs NHE.[19a,b]Electron transfer to I_3^-, relevant to dye regeneration, is significantly exoergic, with ΔG^0 values > 1.2 eV, allowing to predict fast kinetics.

Table 1.Optical and electrochemical parameters of the dyes.[a]

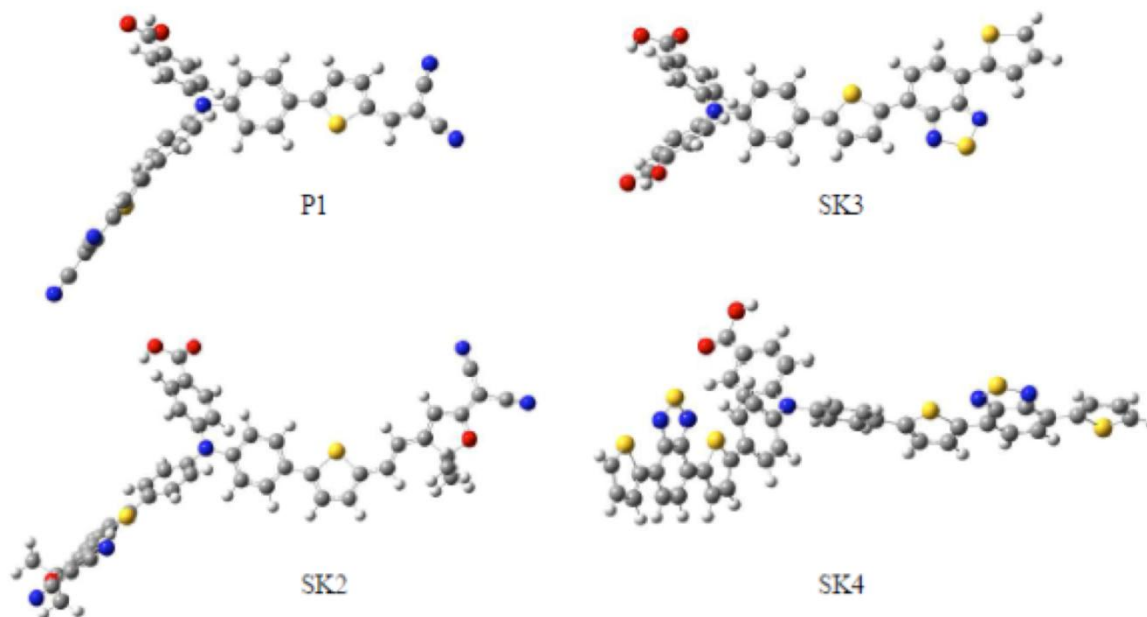| Dye	λ_{abs}(nm) $(\varepsilon)(10^4 \text{ M}^{-1}\text{cm}^{-1})$	λem (nm)	E^{00}(eV)[b]	$E_{(HOMO)}$vs NHE(V) (vs vacuum) (eV)[c]	$E_{(LUMO)}$vs NHE (V) (vs vacuum) (eV) [d]
P1	372 (3.97) 489 (5.17)	611	1.91	1.16(-5.8)	-0.75(-3.8)
SK2	373 (3.12) 559 (4.90)	674	1.94	1.19(-5.8)	-0.75(-3.8)
SK3	357 (5.87) 488 (3.28)	609	2.25	1.14(-5.7)	-1.11(-3.5)
SK4	365 (4.76) 498 (4.11)	621	2.18	1.13(-5.7)	-1.05(-3.5)

[a] in DMSO. [b] Calculated from the intercept of the normalized absorption and emission spectra of the dyes. [c] Evaluated from the oxidation peak potential from cyclic voltammetry in the presence of ferrocene as an internal reference ($E_{1/2}$ Fc[+]/Fc = 0.68 V vs NHE)[13] and using a potential value of -4.6 eV for NHE vs. vacuum.[14][c] Obtained from $E^{00} - E_{HOMO}$.[15]

Computational Investigation

To gain insights into the electronic and optical properties of the investigated sensitizers, we performed Density Functional Theory (DFT) calculations. All the calculations have been performed using the GAUSSIAN 09 program package.[20]The dye structures at the ground state were optimized at the B3LYP level employing the 6-31G* basis set, starting from a semi-empirical PM3 pre-optimized geometry. Similar structural features were observed throughout the whole series. The nitrogen atom of the triphenylamine core gives rise to a distorted tetrahedral motif, resulting in a dihedral angle between the branches of the order of 40°. The π-A unit, constituted by thienylene bridges and dicyanovinly groups in P1 and SK2 and benzothiadiazole fragments in SK3 and SK4, is essentially planar in agreement with the presence of an extended π-electron delocalization. Each branch is linked to the electron donating group via a benzene ring, with a dihedral angle of about 20-27°. Such twisting angle is expected to be beneficial for decoupling holes and electrons, once the initial charge separation is achieved.

Figure 3. Equilibrium geometries of the p-type dyes under investigation calculated at the DFTB3LYP6-31G* level.

It is notoriously difficult for Time-Dependent DFT (TDDFT) methods to reliably describe charge transfer states, particularly those involving spatially separated orbitals and long range excitations as in the case of our p-type systems.[21a,b] Therefore, in the attempt to drive reasonable insights on the electronic structure and excited state energetics of the dye series under investigation, the excitation energies (Table 2), resulting from calculations with B3LYP[22] and BH&H (Half and Half)[23a,b]functionals were compared. Frontier orbitals isodensity maps (isovalue of 0.02) of the selected dyes are reported on Figure S5 (Supporting Information).

ARTICLE TYPE
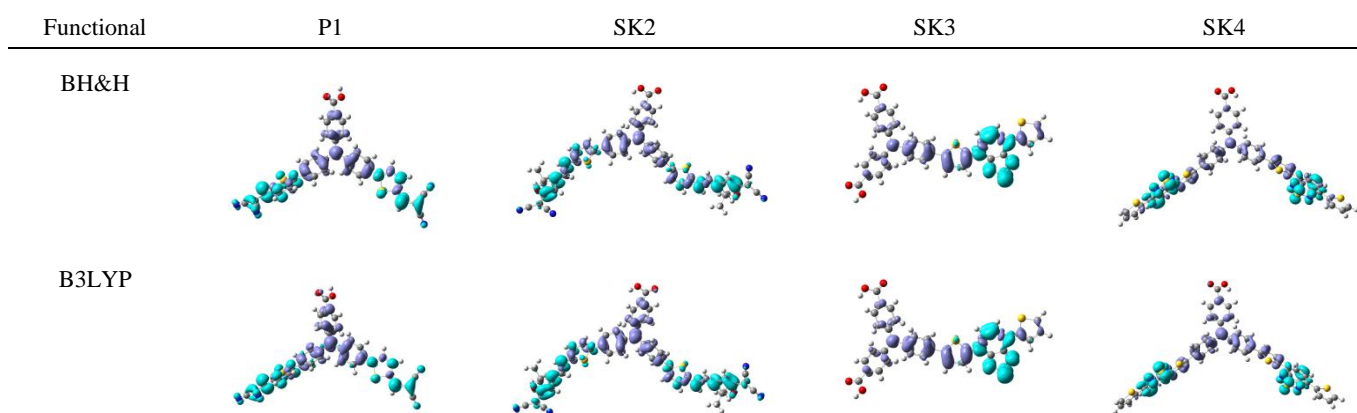
Table 2.Comparison of experimental and calculated lowest absorption maximum of the investigated dyes in DMSO.

Dye	E_{exp}(eV) [λ_{max}(nm)]	$E^{op}_{BH\&H}$(eV) [λ_{max}(nm)]	E^{op}_{B3LYP} (eV) [λ_{max}(nm)]	$|\Delta E_{BH\&H}|$(eV)	$|\Delta E_{B3LYP}|$(eV)
P1	2.53 [489]	2.79 [443]	2.30 [540]	0.26	0.23
SK2	2.22 [559]	2.86 [433]	2.08 [595]	0.64	0.14
SK3	2.54 [488]	2.62 [473]	2.14 [580]	0.08	0.40
SK4	2.49 [498]	2.48 [501]	1.92 [614]	0.01	0.57

The BH&H is considerably successful in predicting the optical transition energies of dyes SK3 and SK4, where deviations from the experimentally measured spectrum are as low as 0.08 and 0.01 eV, but less successful with dyes P1 and SK2, where the calculated E^{op} is higher than the experimental value by 0.26 and 0.64 eV respectively. The lowest transition has, in all cases, a major HOMO-LUMO component (55-87%) in the Kohn-Sham basis, with minor components arising from higher energy excitations, typically HOMO-1→LUMO, HOMO-1→LUMO+1 and HOMO→LUMO+2. The description of the lowest singlet state (S1) by the B3LYP calculation is roughly similar to that of the BH&H, although the HOMO-LUMO component to the excitation is largely predominating (> 93%). The lowest transition in P1 and SK2 is identified by B3LYP with a lower absolute error (0.21 and 0.11 eV) than the BH&H functional, whereas larger errors are found with SK3 and, particularly, with SK4, which shows long range charge transfers with a high degree of spatial charge separation, as indicated by Electron Density Difference Maps (EDDM) (Scheme 2). Both the B3LYP and BH&H functional agree in the description of the EDDMs, showing a shift in electron density from the triphenylamine core to the electron acceptor branches, where the maximum density is localized in the proximity of the cyano groups (P1 and SK2) or on the benzothiadiazole acceptor (SK3 and SK4). It can be also appreciated that in branched dyes (P1, SK2, and SK4), the electronic excitation involves the two acceptor branches simultaneously. Thus, the electronic distribution resulting from the lowest, and usually most intense, electronic transition is favourable to a successful charge separation. The hole density is localized in the immediate proximity of the surface interacting with NiO via COOH groups. This causes photoexcitation of the electron to occur predominantly on the farthest from the NiO part of the molecule where scavenging of the electron by $I_3^-$is more favourable.

Functional	P1	SK2	SK3	SK4
BH&H				
B3LYP				

Scheme 2. Electron Density Difference Maps (EDDMs) (isovalue = 0.001) of the main transition in the visible region calculated with a 6311 G,d,+ basis set obtained with the BH&H (top row) and B3LYP (bottom row) functionals. DMSO solvent was described as a polarisable continuum model (PCM). Light blue and violet indicate an increased and a depleted electron density respectively.

The exciton binding energy (EBE)[24] was calculated[25] from the B3LYP data set, since BH&H was found to give unrealistically high HOMO-LUMO gaps (Figure S4, Supporting Information) as well as binding energies (>1eV). For the SK dyes, similar binding energies of the order of 0.33-0.38 eV are found, being comparable to that of some efficient n-type push pull charge separators[26] recently reported in the literature. P1 displays the smallest EBE within the series with a value as small as 0.17 eV,

comparable to some of the best n-type charge separators reported.[27] Smaller EBE favour separation of the electron-hole pair, and, consequently, charge injection into the semiconductor. The largest binding energy value of 0.38 eV is found for the dye SK3, which means that a higher energy, usually provided by the local electric potential at the semiconductor/dye interface, or by collision with phonons, is needed in order to promote charge injection. The larger EBE of the SK series may constitute a disadvantage compared to the reference dye P1 for obtaining hole injection with high quantum yields.

Photoelectrochemical Investigation in DSSCs

The SK dyes together with reference compound P1 were tested as photosensitizers in p-type DSSCs. NiO photocathodes were fabricated by blading a NiO colloidal paste, obtained by dispersing commercial 25-nm NiO nanoparticles in terpineol, with ethylcellulose as an organic binder/densificating agent, followed by high temperature sintering on FTO (Fluorine-doped Tin Oxide) coated glass. The resulting photocurrent (J)/photovoltage (V) curves under AM 1.5 illumination (1 sun) are shown in Figure 4A and their main efficiency parameters are listed in Table 3.

Table 3. Photovoltaic parameters of investigated chromophores in p-type DSSC

Dye	J_{sc} (mA/cm^2)	V_{oc} (mV)	FF	PCE (%)
P1	1.14	95	0.32	0.035
SK2	0.51	81	0.33	0.014
SK3	0.54	82	0.33	0.015
SK4	0.43	134	0.32	0.018

Several series of iodine-based I^-/I_3^- and Co (III)/(II) electrolytes with different concentration ratio were tested for the cells fabrication. However, the best average power conversion efficiencies were observed when using the iodide/triiodide redox couple (solution of 1.0 M LiI and 0.1 M I$_2$ in CH$_3$CN). Dye SK4 produces the highest open circuit voltage (133 mV), that is ca. 40 mV higher than that of device sensitized by the other reference and novel dyes. The SK2 and 3 molecules produced comparable J_{sc} (ca. 0.5 mA/cm^2), which was however approximately half that of the reference P1 (ca. 1.1 mA/cm^2). In all cases the sloped J/V characteristic at reverse (negative) bias is consistent with a small shunt resistance of the NiO films, causing charge leaks and losses by recombination. For instance, in the case of P1 the photoinjected charge extracted from the photocathode under short circuit conditions (0 V) is roughly one half that available at -0.2 V. Such a photocurrent loss upon moving from negative to positive potential is less marked for the SK series, which, giving rise to a smaller extent of hole injection, result in fewer charge leaks to the electrolyte. The overall PCE of P1-sensitized cells is about twice as large as that of the SK-based devices, mainly due to their lower photocurrents. In general, although not optimized, the efficiencies of the NiO sensitized solar cells recorded in this work are in agreement with the average performances reported so far in the literature for similar types of sensitized p-type electrodes.

Figure 4.Photoelectrochemical and spectral properties of p-type DSSCs in the presence of 1M LiI and 0.1 M I$_2$ in acetonitrile. A) Current–voltage characteristics; B) Light Harvesting Efficiency (LHE) (LHE(λ) = 1-10$^{-A(\lambda)}$) whereA(λ) is the background-subtracted absorbance of the dyed NiO films; C)Photoaction spectra (IPCE vs λ); D) Absorbed photon conversion efficiency spectra (APCE vs λ)

To understand the nature of photocathodic current, the IPCE spectra of the p-type cells, under short circuit conditions were measured (Figure 4 C). Consistent with their spectral properties, all dyes displayed a strongest response in the blue region of the spectrum for λ< 450 nm, reaching the best values of ca. 12-14% for P1 and SK2. The photoconversion then decreases by moving

from the blue to the red region of the visible spectrum, showing a shoulder the 500-600 nm region, with values of 4-5% in the case of P1 and SK4. Despite the opacity of the NiO electrodes, causing significant light scattering, and the strong competitive absorption of the iodine based electrolyte, in general the photoconversion appeared to be in a relatively good agreement with the Light Harvesting Efficiency (LHE) (Figure 4B) of the sensitized NiOphotoelectrodes, confirming that the excited state of the dye is responsible for the observed photocurrent in the visible region of spectrum.

The LHE plot, with values of 50-60% in the 550-450 nm region, showed that SK4 has here the best light harvesting performance, consistent with its relatively good IPCE response at these wavelengths. The absorbed monochromatic photon-to-current conversion efficiencies (APCE) spectra, obtained by dividing the corresponding IPCE spectra by the LHE of the respective photocathodes, are shown in Figure 4 D. The low energy response of P1 and SK4 are similar, with APCE ~ 10 % at 500 nm. Interestingly, SK4 is able to yield a slightly more efficient conversion for $\lambda \geq 550$ nm, while P1 prevails below 480 nm. As for the IPCE, the best APCE response is observed in the blue region of the spectrum, with values of ~18-20% for P1 and SK2. Electrochemical impedance spectroscopy (EIS) was used to further investigate the comparative behaviour of the chromophores in photovoltaic devices. All dyes were stable during potentiostatic measurements, which were performed at potentials between -10 mV and the V_{oc} of the cells. The J/V curves after EIS measurements showed essentially the same performances found before the measurements, which allows to rule out substantial dye or cell degradation affecting the results. The EIS spectra (Figure S7, Supporting Information) could be well fitted with the equivalent circuit, comprising the serial resistance, the counter-electrode interface, the diffusion element accounting for electrolyte transport impedance in a thin layer cell, and the transmission line[28](DX1 in Zview) which describes the transmission network of the NiO, applied by Zhang et al.[10] to p-type DSSCs, comprising both the transport and the charge transfer resistance (R_{ct} (NiO)) (recombination resistance) at the NiO/electrolyte interface.

The impedance response of the NiO based DSSC exhibited similar features, appearing as a small high frequency semicircle, due essentially to the counter-electrode electrochemical interface, followed by a much larger loop at lower frequencies, which bears the main contribution of the NiO/electrolyte interface. Indeed the J/V curves are ∂i ntially dominated by the charge transfer resistance of the $\frac{\partial i}{\partial V}$ as can be appreciated by the comparison of the derivative ($\frac{\partial i}{\partial V}$) of the J/V curves and the inverse of the interfacial charge transfer resistance ($R_{ct}(NiO))^{-1}$ (Figure 5 B). This agreement is particularly good in the case of the SK series, for which the charge transfer resistance was the largely predominant contribution to the total cell resistance at each potential and varied typically between 1000 and 200 Ω depending on the voltage. Obviously, the lowest $R_{ct}(NiO)$ are in all cases found at the open-circuit voltage, due to hole accumulation into the mesoscopic film under open-circuit conditions.

The NiO capacitance (Figure 8A), calculated according to C = $CPE(\omega)^{n-1}$, where n is the exponent of the CPE admittance from the transmission line, in all cases variable between 0.9 and 0.84,

and ω is the frequency at the maximum of the large low frequency loop, was reasonably linear on a logarithmic scale, indicating a chemical capacitance[29] behaviour determined by empty states in the valence bands or in surface states following a Boltzmann distribution near the valence band edge. The inspection of Figure 5 reveals that P1 is the dye which exhibits the lowest charge transfer resistance and highest capacitance, indicating a superior capability of hole injection.
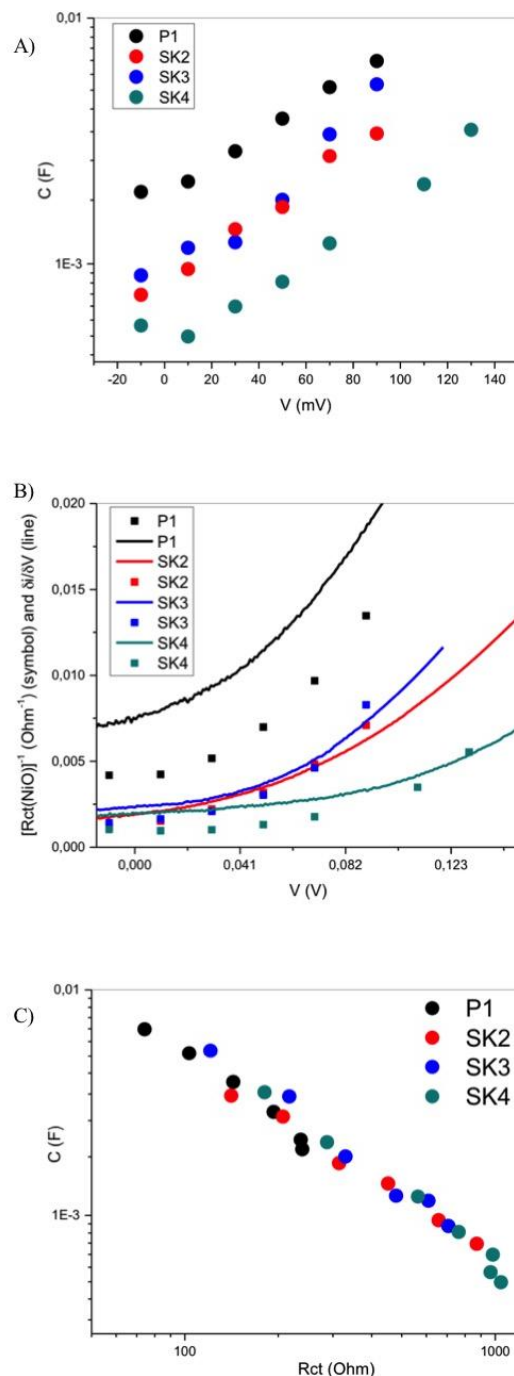

Figure.5 A) Capacitance of sensitized NiO films at increasing potentials in the forward direction; B) Reciprocal of the charge transfer resistance at the NiO/electrolyte interface (squares) compared to the derivative of the

JV curve (solid lines); C)Chemical capacitance of NiO vs interfacial charge transfer resistance in p-type DSSCs under study.

The representation of R_{ct}(NiO) vs C(NiO) on a logarithmic scale indicates that all the dyes behave intrinsically similarly to each other, as far as recombination kinetics are concerned, when compared at the same chemical capacitance of the NiO. In other terms, the charge loss pathways involving direct dye$^-$/h$^+$ and hole recapture by I$^-$occurred at comparable rates for all the dyes under investigation. Accordingly, the higher photovoltage observed for the SK4-sensitized device is likely due to a positive shift of the valence band edge of the NiO by ca. 30-40 mV, induced by the adsorption of the dye sensitizer, as can be observed by comparing the different voltages at which the similar capacitances are found, rather than by slower interfacial recombination kinetics. The voltage shift observed for SK4 in EIS under illumination is quantitatively consistent with the more positive onset of the anodic current observed for this moiety in the dark (Figure S6).

Conclusion

New p-type photosensitizers based on organic linear and di-branched donor-acceptor systems bearing a tryphenylamine group as a donor and strong electron-acceptor Dalton's (SK2) or benzothiadiazole(SK3 and SK4) groups were synthesized and characterized by steady state spectroscopic, electrochemical, and computational studies. All the dyes under investigation exhibited strong charge transfer bands in the visible regions with ground and excited state energetic which are favourable to the sensitization of NiO electrodes. The computational investigation revealed a clear directionality of the lowest excited state exhibiting a marked charge transfer character, shifting the electron density from the donor core to the acceptor branches, an electronic situation which is favourable to the hole injection in p-type semiconductors such as NiO. However, the exciton binding energy, i.e. the energy of the bound electron-hole pair, is about twice as large as that of a known literature standard (P1), suggesting that a more difficult charge separation in the new dyes might occur.

When tested as photosensitizers in p-type DSSCs the SK series was able to successfully sensitize NiO electrodes, resulting in photocurrents which are about half that of P1-based cells. The charge recombination kinetics, probed by considering the charge transfer resistance at the NiO/electrolyte interface at a comparable chemical capacitance, showed that the dyes behaved similarly under this respect and that the higher photovoltage observed for the device based on SK4 dye is seemingly due to a positive shift of the valence band edge, consistent with the shift in the anodic threshold measured in the dark. The fact that similar recombination resistances were found at a comparable photohole density in the NiO corroborates the indication, gained by DFT studies, that the superior performance, particularly in photocurrent, of P1 may be ascribed to a superior charge separation capability originating by its smaller exciton binding energy. Future designs of dyes for p-type sensitization will take this parameter into consideration for achieving a more effective charge separation.

Experimental section

General

NMR spectra were recorded with an instrument operating at 500.13 (^{1}H) and 125.77 MHz (^{13}C). Flash chromatography was performed with silica gel 230–400 mesh (60 Å). Reactions conducted under a nitrogen atmosphere were performed in oven-dried glassware and monitored by thin-layer chromatography by using UV light (254 and 365 nm) as a visualizing agent. 4-[Bis-(4-bromo-phenyl)-amino]-benzaldehyde and 4,4'-(4-bromophenylazanediyl)dibenzaldehyde were synthesised following procedure known in literature.[30a,b]All other reagents were obtained from commercial suppliers at the highest purity and used without further purification. Anhydrous solvents were purchased from commercial suppliers and used as received. Extracts were dried with anhydrous Na$_2$SO$_4$ and filtered before removal of the solvent by evaporation.

Synthesis of the p-type sensitizers

4-[Bis-(4-bromo-phenyl)-amino]-benzoic acid (2)
A procedure reported in the literature was adapted with some modifications.[9] The suspension of sodium hydroxide (62 mmol, 2.5 g) in 45 mL of ethanol was vigorously stirred for 20 min and then silver (I) oxide (9.5 mmol, 2.19 g). Resulting mixture was stirred for another 20 min before 4-[Bis-(4-bromo-phenyl)-amino]-benzaldehyde(1) (1.2 mmol, 550 mg) in 4 mL of toluene was slowly added. The resulting suspension was stirred at room temperature for 24h and then neutralized with HCl (15%, 25 mL) until formation of grey silver chloride precipitate was observed. The resulting solution was decanted and extracted with ethyl acetate (3 × 40 mL). The organic phase was washed with water and dried. Thereafter the solvent was removed by rotary evaporation giving the desired acid **2** (0.8 g, 78%) as white solid, which was used without further purification.^{1}H NMR (500 MHz, DMSO-d_6, ppm): δ 6.90 (d, J = 8.5 Hz, 2H), 6.93 (d, J = 8.8 Hz, 4H), 7.44 (d, J = 8.8 Hz, 4H), 7.79 (d, J = 8.5 Hz, 2H).

4-{Bis-[4-(5-formyl-thiophen-2-yl)-phenyl]-amino}-benzoic acid (3)
The solution of benzoic acid **2** (0.4 mmol, 200.0 mg) and Pd(dppf)Cl$_2$ (0.1 mmol, 79 mg) in toluene (5 mL) was mixed with the solution of 5-formyl-2-thienylboronic acid (1.2 mmol, 187 mg) and K$_2$CO$_3$ (2.5 mmol, 355 mg) in methanol (5 mL). The resulting mixture was irradiated in the microwave oven at 80°C for 20 min and then poured into a saturated solution of ammonium chloride (60 mL). After extraction with ethyl acetate (3 × 100 mL), the combined organic phases were washed with brine, dried and then filtered over Celite and concentrated under reduced pressure. The crude residue was purified by column chromatography over silica gel using dichloromethane (DCM)/methanol 1:9 mixture as the eluent to give the product (145 mg, 62%) in form of yellow solid. M.p. 137-139°C,^{1}H NMR (500 MHz, acetone-d_6, ppm): δ 7.21 (d, J = 8.8 Hz, 2H), 7.28 (d, J = 8.7 Hz, 4H), 7.66 (d, J = 4.0 Hz, 2H), 7.83 (d, J = 8.7 Hz, 4H), 7.98 (d, J = 4.0 Hz, 2H), 8.00 (d, J = 8.8 Hz, 2H), 9.94 (s, 2H), 11.14 (s, 1H).

4-(bis(4-(5-((E)-2-(4-cyano-5-(dicyanomethylene)-2,2-dimethyl-2,5-dihydrofuran-3-yl)vinyl)thiophen-2-yl)phenyl)amino)benzoic acid (SK2)
To a solution of the intermediate **4** (100 mg, 0.2 mmol) and 2-(3-

cyano-4,5,5-trimethylfuran-2(5H)-ylidene)malononitrile (77.2 mg, 0.4 mmol) in ethanol (20 ml) was added catalytic amount of ammonium acetate (8 mg, 0.1 mmol) in 2 ml of acetic acid. Reaction mixture was refluxed under nitrogen atmosphere for 100 hours. Afterwards organic solvent was evaporated under reduced pressure and resulted crude product was washed with ethyl acetate to give the desired dye SK2 (75 mg, 74 %) in form of dark violet solid. m.p. 252–253 °C. ^{1}H NMR (500 MHz, DMSO-d_6, ppm): δ 12.75 (s, 1H), 8.17 (d, J = 16 Hz, 2H), 7.92 (d, J = 8 Hz, 2H), 7.87 (d, J = 4 Hz, 2H), 7.84 (d, J = 8.0 Hz, 4H), 7.73 (d, J = 4 Hz, 2H), 7.2 (d, J = 9 Hz, 4H), 7.16 (d, J = 9 Hz, 2H), 6.83 (d, J = 16 Hz, 2H), 1.81 (s, 12 H). ^{13}C NMR (acetone-$d6$, ppm): δ 26.7, 54.9, 98.3, 99.2, 100.2, 112.4, 113.4, 114.2, 114.3, 123.9, 126.5, 127.2, 129, 129.6, 132.5, 139.5, 140.3, 141.7, 148.2, 151.3, 152.2, 168.1, 175.9, 178.2. vmax/cm^{-1} 3583, 3476, 3007, 2310, 1738, 1590, 1373, 1217.

$C_{51}H_{33}N_7O_4S_2$(871.98) calcd.: C, 70.25; H, 3.81; N, 11.24; found: C, 70.11; H, 4.19; N, 11.60.

4-(5-Bromothiophen-2-yl)-7-(thiophen-2-yl)benzo[1,2,5]thiadiazole (5)

To a solution of 4,7-di-2-thienyl-2,1,3-benzothiadiazole (4)[31] (350 mg, 1.17 mmol) in a 100 mL of acetic acid −CH$_2$Cl$_2$ 1:1 mixture, was added N-bromosuccinimide (NBS) (229 mg, 1.28 mmol) in DCM by small portions over 30 min. The resulting reaction mixture was stirred overnight , then poured into water (100 mL) and the separated organic layer was dried , filtered and concentrated in vacuum. Obtained crude product was purified by flash column chromatography on silica gel (DCM−hexane = 1 : 4) giving a target benzothiadiazole derivative (5) in form of bright orange solid with 70% yield (310 mg, 0.8mmol). ^{1}H NMR (500 MHz, CDCl$_3$, ppm): δ 8.12 (d, 1H,), 7.88 (d, 1H), 7.8 (m, 2H), 7.46 (d, 1H), 7.22 (d, 1H), 7.15 (d, 1H).

4-(5-(4,4,5,5-tetramethyl-1,3,2-dioxaborolan-2-yl)thiophen-2-yl)-7-(thiophen-2-yl)benzo[c][1,2,5]thiadiazole (6)

Schlenk flask was charged with 4,7-di(thiophen-2-yl)benzo[c][1,2,5]thiadiazole (5) (550 mg, 1.45 mmol), potassium acetate (440 mg, 4.48 mmol) and bis(pinacolato)diboron (490 mg, 1.93 mmol) together with the catalytic amount of Pd(dppf)Cl$_2$(0.05 mmol, 39 mg) and 15 ml of dry dioxane. Resulting mixture was heated at reflux under argon atmosphere for 24 hours then poured in water, extracted with 3×50 ml ethyl acetate and dried. After organic solvent was evaporated under reduced pressure, crude product was purified on silica gel using CH$_2$Cl$_2$−cyclohexane 1:4 as eluent. Product was obtained in form of brownish orange solid (318 mg, 55% yield).

m.p. 168–170 °C. ^{1}H NMR (500 MHz, CDCl$_3$, ppm): δ = 8.18 (d, J = 4Hz, 1 H) 8.13 (m, 1 H), 7.92 (d, J = 8Hz, 1 H), 7.87 (d, J = 8Hz, 1 H), 7.72 (d, J = 3Hz, 1 H), 7.45 (m, 1 H), 7.21 (m, 1 H), 1.38 (s, 12 H). ^{13}C NMR (CDCl$_3$): δ = 152.66 (CH), 152.63 (CH), 145.89 (CH), 139.32 (CH), 137.89 (C), 128.65 (C), 128.03 (C), 127.67 (C), 126.97 (C), 126.48 (CH), 126.37 (C),125.83 (CH), 125.75 (C), 84.26 (CH3), 24.79 (C) ppm. $C_{20}H_{19}BN_2O_2S_3$ (426.38): calcd: C, 56.34; H, 4.49; N, 6.57; found C, 56.39; H, 4.60; N, 6.29.

4,4'-(4-(5-(7-(thiophen-2-yl)benzo[c][1,2,5]thiadiazol-4-yl)thiophen-2-yl)phenylazanediyl)dibenzaldehyde (7)

4,4'-(4-bromophenylazanediyl)dibenzaldehyde (114 mg, 0.3 mmol), benzothiadaizole derivative 6(130 mg, 0.31 mmol), a catalytic amount of Pd(dppf)Cl$_2$(0.019 mmol, 18 mg) and a solution of K$_2$CO$_3$(400 mg, 2.9 mmol) in water (3 ml) were charged into Schlenk flask and then dissolved in 15 ml of dry dimethoxyethane (DME). Reaction mixture was refluxed under argon atmosphere for 15 hours and after cooling down to the room temperature it was washed with water , dried and concentrated under vacuum . Crude product was purified by column chromatography on silica gel using ethyl acetate − cyclohexane = 2:7 as the eluent. The pure intermediate 7(55 mg, 30% yield) was obtained in form of bright red solid.

m.p. 173–175 °C. ^{1}H NMR (500 MHz, CDCl$_3$, ppm): δ = 9.91 (s, 2 H), 8.12 (dd, J = 8.0; 15 Hz, 2 H), 7.86 (s, 1 H), 7.81 (d, J = 17.0 Hz, 4 H), 7.68 (d, J = 17.0 Hz, 2 H), 7.45 (d, J = 8.0 Hz, 1 H), 7.39 (d, J = 8.0 Hz, 1 H), 7.24 (d, J = 17.0 Hz, 4 H), 7.21 (d, J = 8.0 Hz, 1 H), 7.17 (d, J = 17.0 Hz, 2 H). ^{13}C NMR (CDCl$_3$): δ= 191.4, 153.5, 153.4, 152.6, 145.8, 140.18, 139.9, 132.7, 132.4, 132.2, 129.5, 128.9, 128.5, 128.2, 127.89, 127.83, 126.9, 126.6, 126.5, 126.3, 125.2, 123.9 ppm.

$C_{34}H_{21}N_3O_2S_3$ (599.74): calcd.: C, 68.09; H, 3.53; N, 7.01; found: C, 67.84; H, 3.63; N, 7.33.

4-(bis(4-(5-(7-(thiophen-2-yl)benzo[c][1,2,5]thiadiazol-4-yl)thiophen-2-yl)phenyl)amino)benzaldehyde (8)

4-[Bis-(4-bromo-phenyl)-amino]-benzaldehyde(1) (100 mg, 0.232 mmol) and benzothiadaizole derivative 6 (213 mg, 0.5 mmol) and K$_2$CO$_3$(691 mg, 5 mmol)were dissolved in 5 ml of water and charged into Schlenkflasktogether with the catalytic amount of Pd(dppf)Cl$_2$(0.02 mmol, 19 mg) and then dissolved in 15 ml of dry DME. Reaction mixture was refluxed under argon atmosphere for 15 hours. After cooling to the room temperature it was washed with water, dried and concentrated under vacuum. Crude product was washed with ethyl acetate and filtered. The desired intermediate 8 was obtained as dark red solid (70mg, yield 45%).

m.p. 189–190°C (decomp.). ^{1}H NMR (500 MHz, CDCl$_3$, ppm)δ = 9.88 (s, 1 H), 8.14 (d, J = 8.0, 4 H), 7.9 (s, 1 H), 7.77 (d, J = 17.0 Hz, 2 H), 7.69 (d, J = 17.0 Hz, 4 H), 7.47 (d, J = 8.0 Hz, 2 H), 7.41 (d, J = 8.0 Hz, 2 H), 7.23 (d, J = 17.0 Hz, 4 H), 7.22 (d, J = 8.0 Hz, 2 H), 7.19 (d, J = 17.0 Hz, 2 H). ^{13}C NMR (CDCl$_3$): δ = 191.4, 153.6, 153.5, 153.4, 146.4, 145.3, 140.2, 139.5, 132.3, 131.7, 130.9, 129.6, 128.9, 128.4, 127.9, 127.8, 127.7, 127.0, 126.8, 126.6, 126.2, 124.9, 121.6 ppm.$C_{47}H_{27}N_5OS_6$ (870.14): calcd.: C, 64.87; H, 3.13; N, 8.05; found C 64.50; H 2.88; N 7.91.

4,4'-(4-(5-(7-(thiophen-2-yl)benzo[c][1,2,5]thiadiazol-4-yl)thiophen-2-yl)phenylazanediyl)dibenzoic acid (SK3)

A suspension of sodium hydroxide (600 mg , 15 mmol) in 10 mL of ethanol was vigorously stirred for 15 min before Ag$_2$O (208 mg, 0.8 mmol) was added. After another 15 min, dibenzaldehyde7 (50 mg, 0.08 mmol) in toluene was added dropwise to the solution. Reaction mixture was stirred overnight at room temperature and quenched by the slow addition of 1M HCl solution, then it was extracted with CH$_2$Cl$_2$ (3 x 75 mL). Combined organic layers were washed with water and dried. After evaporation of solvent under reduced pressure resulting

crude product was washed with diethyl ether to give final compound **SK3** in form of dark red solid (40 mg. 87% yield). m.p. 215–217 °C. ^{1}H NMR (500 MHz,DMSO-*d6,* ppm): δ = 8.20 (t, J = 9 Hz, 2 H), 8.17 (d, J = 8 Hz, 1 H), 8.12 (d, J = 8.0 Hz, 1 H), 7.92 (d, J = 8.7 Hz, 4 H), 7.80 (d, J = 8.5 Hz, 2 H), 7.78 (d, J = 5.1 Hz, 1 H), 7.67 (d, J = 4.0 Hz, 1 H), 7.29 (d, J = 8.7 Hz, 1 H), 7.22 (d, J = 8.5 Hz, 2 H) 7.15 (d, J = 8.7 Hz, 4 H).^{13}C NMR (DMSO-*d6*): δ = 168.1, 153.0, 152.9, 151.4, 146.7, 145.7, 139.8, 138.9, 132.5, 131.4, 130.1, 129.7, 129.5, 128.8, 128.3, 127.7, 127.2, 126.9, 126.4, 126.3, 126.0, 125.9, 124.0 ppm. vmax/cm^{-1}3456, 2970, 2281, 1738, 1494, 1366, 1217.$C_{34}H_{21}N_3O_4S_3$ (631.74): calcd. C, 64.64; H,3.35; N, 6.65; found: C, 64.36; H, 3.74; N, 6.94.

4-(bis(4-(5-(7-(thiophen-2-yl)benzo[c][1,2,5]thiadiazol-4-yl)thiophen-2-yl)phenyl)amino)benzoic acid (SK4).

To the vigorously stirred suspension of NaOH (300 mg, 7.5 mmol) in 10 mL of ethanol was added silver (I) oxide (205 mg, 0.8 mmol). Mixture was stirred for 15 min before adding benzaldehyde**8** (50 mg, 0.057 mmol) in CH_2Cl_2. Reaction mixture was stirred overnight at the room temperature and quenched by the slow addition of 1M HCl solution, extracted with ethyl acetate (3 x 75 mL) and then combined organic layers were washed with water and dried. After evaporation of solvents, crude product was washed with dichloromethane. SK4 dye was obtained in form of black-red solid (40 mg, 90% yield). m.p. > 285 °C (decomp.). ^{1}H NMR (500 MHz, CDCl$_3$, ppm): δ = 8.22 (d, J =3.9 Hz, 2 H), 8.20 (d, J = 3.9 Hz, 2 H), 8.18 (s, 2 H), 8.14 (d, J = 8.3 Hz, 2 H), 7.88 (d, J = 8.7 Hz, 2 H),7.81 (d, J = 8.5 Hz, 4 H), 7.79 (d, J = 5.5 Hz, 2 H), 7.68 (d, J = 4.1 Hz, 2 H), 7.31 (t, J = 8.8 Hz, 2 H), 7.23 (d, J = 8.5 Hz, 4 H), 7.11 (d, J = 8.7 Hz, 2 H). ^{13}C NMR (DMSO-*d6*): δ = 169.07, 153.5, 153.3, 151.8, 151.7, 146.97, 145.8, 142.2, 132.0, 131.5, 130.8, 129.6, 128.9, 128.2, 127.8, 127.7, 126.9, 126.7, 126.6, 126.3, 126.1, 124.6, 122.3 ppm.vmax/cm^{-1}3472, 2976, 2110, 1738, 1546, 1372,1254. $C_{47}H_{27}N_5O_2S_6$ (886.14): calcd. C, 63.70; H, 3.07; N, 7.90;found C 63.88, H 3.44, N 7.68.

Solar Cell Assembly

NiO films were prepared by grounding 7.5 g of NiO nanoparticles (Inframat, nominal size 25 nm) in a mortar in the presence of 200 ìl of acetilacetone. 100 ml of terpineol were then added, followed by 10 g of ethlycellulose dissolved in 110 ml of absolute ethanol. The resulting mixture was homogenized by stirring and sonication in an ultrasonic bath. Ethanol was evaporated under reduced pressure leaving a dense paste constituted by terpineol, ethylcellulose and NiO nanoparticles. The resulting paste could be spread by blading onto well cleaned FTO glass to form, after drying and high temperature sintering, the NiO thin films. The temperature program adopted for drying and sintering in air was the following: 10 minutes at 120 °C, followed by a ramp (15 C°/min) to 450 C° which were maintained for 30 minutes. A subsequent ramp (10 C°/min) brought the temperature from 450 C° to 550 C° which were kept constant for further 20 minutes. Cooling occurred naturally, by interrupting the heating.

Sensitization of the resulting NiO electrodes, having an active surface of 0.25 cm^2, was carried out overnight, by immersion in the DMSO solutions of the selected sensitizers.

Solar cells were fabricated by clamping the sensitized NiO photocathode with a platinum coated FTO counter electrode (Chimet). The electrolyte was 1 M LiI/0.1 M I$_2$ in acetonitrile.

Spectroscopic, Electrochemical, and Photoelectrochemical measurements

UV-Vis spectra of sensitized NiO thin films, collected in transmission mode, were recorded on a JASCO V570 UV-Vis-NIR spectrophotometer. UV-Vis spectra in solution were obtained with a V-570 JASCO spectrophotometer. Emission spectra were recorded FP6200JASCO spectrofluorometer. TBAlClO$_4$ 0.1 DMSO

Cyclic voltammetry of the dye dissolved in 0.1 M solutionof tetrabutylammonium perchlorate (Fluka, electrochemical grade,99.0%) in anhydrous DMSO (Aldrich) as the supporting electrolyte was carried out at a glassy carbon working electrode with a PARSTA2273potentiostat in a two-chamber three-electrodeelectrochemical cell with a scan rate of 50 mVs^{-1}. Potentials are referred to the ferrocenium/ferrocene (Fc$^+$/Fc) couple as internal reference. An Ecochemie PGSTAT 302/N electrochemical workstation equipped with the FRA 2 Frequency Response Analyzer and running under either GPES or Nova software was used for collecting both the JV characteristics and the EIS response of the p-DSSCs. Solar cells were illuminated under simulated solar conditions (Am 1.5 G 100 mW/cm^2) generated by an ABET sun simulator. J/V curves were recorded by linear scan voltammetry, using a scan rate of 5 mV/s. Every cell was left to equilibrate under illumination until a superimposable JV response was obtained upon subsequent scans. Curves reported in this work are those measured after steady state was achieved. Potentiostatic EIS data were collected at various voltages under illumination by applying a 10 mV sinusoidal frequency variable from 10^5 to 10^{-2} Hz. Impedance data were fitted with Zview.

IPCE data were collected under monochromatic illumination, having a band pass of 10 nm, generated by an Applied Photophysicsmonochromator coupled to a 175 W LuxtelXe arc lamp. Short circuit photocurrents were recorded on an Agilent 34401A multimeter. Incident irradiance was measured with a calibrated Centronic OSD 7Q silicon photodiode having an active area of 1 cm^2.

Computational Studies

Optimized ground state geometry of the p-type dyes were obtained at the DFT-B3LYP level by using a 631G* basis set. The DFT calculation was carried out on pre-optimized structures at the PM6 level. Time dependent (TDDFT) calculations in the presence of DMSO solvent, treated as continuum polarisable medium, were carried out on the optimized structures by considering the two different B3LYP and BH&Hfunctionals with the 6311 G* basis set incorporating also diffuse functions (+).

All calculations were carried out with Gaussian 09 A02on multi-core computers. Structures and isodensity surfaces were graphically visualized with Gaussview 5. Electron Density Difference Maps (EDDMs) were generated with Gausssum 2.2

Notes and references

aDepartment of Materials Science and Milano-Bicocca Solar Energy Research Center – MIB-Solar, University of Milano-Bicocca, INSTM Unit,Via Cozzi 55, 20125 Milano, Italy. E-mail: alessandro.abbotto@unimib.it; http://http://www.stc.unimib.it/abbotto/

bDepartment of Chemistry, University of Ferrara, Via L. Borsari 46, 44121 Ferrara, Italy. E-mail: stefano.caramori@unife.it

† Electronic Supplementary Information (ESI) available: CV plot, normalized absorption and emisson spectra, DFT isodensity plots of HOMOs and LUMOs, HOMO-LUMO energy gaps and excition binding energies, dark currents and EIS spectra of p-DSSC, ^{1}H and ^{13}C NMR spectra of intermediates and dyes. See DOI: 10.1039/b000000x/

1 B. O'Regan and M. Grätzel, *Nature,*1991, **353**, 737–740.

2 a) IEA International Energy Agency, *Potential for building integrated photovoltaics*, Report IEA PVPS Task 7, NET Ltd., St. Ursen, Switzerland, 2002; b) C. Cornaro, S. Bartocci, D. Musella, C. Strati, A. Lanuti, S. Mastroianni, S. Penna, A. Guidobaldi, F. Giordano, E. Petrolati, T. M. Brown, A. Reale, A. D. Carlo,*Prog. Photovolt*: Res. Appl., 2013

3 S. Mathew, A. Yella, P. Gao, R. Humphry-Baker, F. E. CurchodBasile, N. Ashari-Astani, I. Tavernelli, U. Rothlisberger, M. K. Nazeeruddinand M. Grätzel, *Nature Chem.*, 2014, **6**, 242.

4 M. A. Green, *Third Generation Photovoltaics: Advanced Solar Energy Conversion*; Springer-Verlag: Berlin, Heidelberg, 2003.

5 A. Hagfeldt, G. Boschloo, L. Sun, L. Kloo and H. Petersssen, *Chem. Rev.* 2011, **110**, 6595.

6 D.R. Lide, *Handbook of Chemistry and Physics*, 90th ed., C. Press, 2010.

7 F. Odobel, Y. Pellegrin, E.A. Gibson, A. Hagfeldt, A. L. Smeigh and L. Hammarstrom, *Coord. Chem. Rev.,*2012, **256**, 2414.

8 a) A. Morandeira, G. Boschloo, A. Hagfeldt and L. Hammarstrom, *J. Phys. Chem. C*, 2008, **112**, 9530; b) H. Zhu, A. Hagfeldt and G. Boschloo, *J. Phys. Chem. C*, 2007, **111**, 17455; c) M. Borgstrom, E. Blart, G. Boschloo, E. Mukhtar, A. Hagfeldt, L.Hammarstromand, and F.Odobel, *J. Phys.Chem.B*,2005, **109**, 22928; d) E. A. Gibson, A. L. Smeigh, L. Le Pleux, J. Fortage, G. Boschloo, E. Blart, Y. Pellegrin, F. Odobel, A. Hagfeldt and L. Hammarström, *Angew. Chem., Int. Ed.*, 2009, **48**, 4402.

9 P. Qin, H. Zhu, T. Edvinsson, G. Boschloo, A. Hagfeldt and L. Sun, *J. Am. Chem. Soc.,* 2008, **130**, 8570.

10 a) A. Nattestad, A. J. Mozer, M. K. R. Fischer, Y.-B. Cheng, A. Mishra, P. Bäuerle and U. BachNature Mater.,2010, **9**, 31; b) X.L. Zhang,Z. Zhang,D. Chen,P. Bäuerle,U. Bach andY.-B. Cheng,*Chem. Commun.*, 2012, **48**, 9885.

11 G. Melikian, F. P. Rouessac and C. Alexandre, *Synth. Commun.*, 1995, **25**, 3045.

12 A. Yassara, C. Videlotb and A. Jaafari, *Sol. Energy Mater. Sol,* 2006, **90**, 916–922

13 W.C. Barrette, H.W. Johnson and D.T. Sawyer, *Anal. Chem.,*1984, **56**, 1890

14 J. O. M. Bockris and S. U. M. Khan, *Surface Electrochemistry – AMolecular Level Approach*, Kluwer Academic/Plenum Publishers, New York,1993.

15 W. Wu, J. Yang, J. Hua, J. Tang, L. Zhang, Y. Long and H. Tian, *J. Mater. Chem.*, 2010, **20**, 1772.

16 a) A. Scrascia, M. Pastore, L. Yin, R. A. Picca, M. Manca, Y.-C. Guo, F. De Angelis, F. Della Sala, R. Cingolani, G. Gigli and G. Ciccarella *Curr. Org.Chem.,* 2011, **15**, 3535; b) M. Mba, M. D'Acunzo, P. Salice, T. Carofiglio, M. Maggini, S. Caramori, A. Campana, A. Aliprandi, R. Argazzi, S. Carli, and C. A. Bignozzi, J. *Phys. Chem. C*, 2013, **117**, 19885.

17 Z. Ji, G. Natu, Z. Huang and Y. Wu, *Energy Environ. Sci.*, 2011, **4**, 2818.

18 X. Qian, Y.-Z. Zhu, J. Song, X.-P. Gao and J.-Y. Zheng, Org. Lett., 2013, **15**, 6034.

19 a) P. Qin, J. Wiberg, E.A. Gibson, M. Linder, L. Li, T. Brinck, A. Hagfeldt, B. Albinsson and L. Sun, *J. Phys. Chem. C*, 2010, **114**, 4738; b) A. Nattestad, A. J. Mozer, M. K. R. Fischer, Y.-B. Cheng, A. Mishra, P. Bäuerle and U. Bach *Nature Mater,* 2010, **9**, 31.

20 G.A. Petersson, H. Nakatsuji, M. Caricato, X. Li, H. P. Hratchian, A. F.Izmaylov, J. Bloino, G. Zheng, J. L. Sonnenberg, M. Hada, M. Ehara,K. Toyota, R. Fukuda, J. Hasegawa, M. Ishida, T. Nakajima, Y.Honda, O. Kitao, H. Nakai, T. Vreven, J. A. Montgomery, Jr., J. E.Peralta, F. Ogliaro, M. Bearpark, J. J. Heyd, E. Brothers, K. N.Kudin, V. N. Staroverov, R. Kobayashi, J. Normand, K.Raghavachari, A. Rendell, J. C. Burant, S. S. Iyengar, J. Tomasi, M.Cossi, N. Rega, J. M. Millam, M. Klene, J. E. Knox, J. B. Cross, V.Bakken, C. Adamo, J. Jaramillo, R. Gomperts, R. E. Stratmann, O.Yazyev, A. J. Austin, R. Cammi, C. Pomelli, J. W. Ochterski, R. L.Martin, K. Morokuma, V. G. Zakrzewski, G. A. Voth, P. Salvador, J.J. Dannenberg, S. Dapprich, A. D. Daniels, Ö. Farkas, J. B.Foresman, J. V. Ortiz, J. Cioslowski, and D. J. Fox, *Gaussian, Inc.,*Wallingford CT, revision A.02.,2009

21 a) J. Autschbach, *ChemPhysChem,*2009, **10**, 1757; b)T. Ziegler,M. Seth, M. Krykunov, J. Autschbach and F. Wang, *J. Molec. Struct.: THEOCHEM*, 2009, **14**, 106.

22 A.D. Becke, *J. Chem.Phys.*, 1993, **98**,5648.

23 a)A.D. Becke, *J. Chem.Phys*, 1993,**98**, 1372; b) W. Koch and M. Holthausen, *A Chemist's Guide to Density Functional Theory*, 2001, 2nd Volume, Wiley-VCH, Weinheim.

24 B. A. Gregg, *J. Phys. Chem. B*, 2003, **107**, 4688.

25 C.-G. Zhen, U. Becker and J. Kieffer, *J. Phys. Chem. A,*2009, **113**,9707.

26 B.-G. Kim, C.-G. Zhen, E.-J. Jeong, J. Kieffer and J. Kim, *Adv. Funct. Mater.* 2012, **22**, 1606.

27 H. Choi, C. Baik, S. O. Kang, J. Ko, M.-S. Kang, M. K. Nazeeruddin, and M. Grätzel, *Angew. Chem. Int. Ed.* 2008 , **47 ,** 327.

28 J. Bisquert, F. Fabregat Santiago, *"Impedance spectroscopy: a general introduction and application to dye-sensitized solar cells"* in *"Dye Sensitized Solar Cells"*, K.Kalyanasundaram Ed, CRC press, 2010.

29 J. Bisquert, *Phys.Chem.Chem.Phys.,*2003, **5**, 5360.

30 a) J.-F. Lefebvre, X.-Z. Sun, J. A. Calladine, M.W. Georgeand E.A. Gibson, *Chem. Commun.*, 2014, **50**, 5258; b) Z. Yang, N. Zhao, Y. Sun, F. Miao, Y. Liu, X. Liu, Y. Zhang, W. Ai, G. Song, X. Shen, X.Yu, J. Sun and W.-Y. Wong, *Chem. Commun.*, 2012, **48**, 3442.

31 D.H. Lee, M.J. Lee, H.M. Song, B.J. Song, K. D. Seo, M. Pastore, C. Anselmi, S. Fantacci, F. De Angelis, M. K. Nazeeruddin, M. Gräetzel and H. K. Kim, *Dyes and Pigments*, 2011, **91**, 192.